Title
THE PHOTOCHEMISTRY OF HNO3 AND ClNO3

Author
Marinelli, W.J.

Publication Date
1981-11-01

LBL-13473

Lawrence Berkeley Laboratory
UNIVERSITY OF CALIFORNIA

Materials & Molecular Research Division

THE PHOTOCHEMISTRY OF HNO_3 AND $ClNO_3$

William Joseph Marinelli
(Ph.D. thesis)

November 1981

Prepared for the U.S. Department of Energy under Contract W-7405-ENG-48

DISCLAIMER

The Photochemistry of HNO_3 and $ClNO_3$

William Joseph Marinelli

Ph.D. Thesis

November 1981

Materials and Molecular Research Division
Lawrence Berkeley Laboratory
and
Department of Chemistry
University of California
Berkeley, California 94720

This work was supported by the U.S. Department of Energy under Contract Number W-7405-ENG-48.

Table of Contents

Abstract. iv

I. Introduction. 1

A. Reaction of HO with HNO_3 and H_2O_2 1

B. Reaction of Cl with HNO_3. 6

C. Photochemistry of $ClONO_2$. 7

D. Absorption Cross Sections and Lineshape for the NO_3 (0,0) Band. 8

II. Experimental. 12

A. Introduction. 12

B. Flash Photolysis/Resonance Fluorescence Experiments . 14

1. Photolysis Source 14

2. Laser Energy Measurements 16

3. Precursor Monitoring. 21

4. Reaction Cells and Product Detection. 23

5. Reactant and Carrier Gas Handling 43

6. Signal Processing and Data Acquisition. 46

7. Experimental Procedures and Methods 47

C. Flash Photolysis/Laser Absorption Experiments 49

1. Photolysis Source 49

2. Energy Measurement. 49

3. Dye Laser Probe System. 53

4. Reaction Cell and Flow System 56

5. Signal Detection and Data Acquisition 59

6. Experimental Procedures 61

D. NO_3 Absorption Cross Section Spectrometer 61

1. Modifications to FP/LA Experiment 62

2. Wavelength Calibration. 63

3. Experimental Methods and Data Acquisition . . . 64

E. Reactants and Gases 65

1. Nitric Acid 68

2. Hydrogen Peroxide 68

3. Chlorine. 69

4. Nitrosyl Chloride 69

5. Ozone 69

6. Di-nitrogen Pentoxide 69

7. Chlorine Monoxide 70

8. Chlorine Nitrate. 70

III. Results. 72

A. Hydroxyl Radical Kinetics 72

1. Interpretation of Data. 72

2. FP/RF Study of the Reaction of HO with HNO_3 . . 81

3. FP/RF Study of the Reaction of HO with H_2O_2 . . 100

4. FP/LA Study of the Reaction of HO with HNO_3 . . 106

B. The Reaction of Cl with HNO_3. 118

1. FP/RF Study 118

2. FP/LA Study 121

C. The NO_3 Photodissociation Quantum Yield from $ClONO_2$ 121

D. Absorption Cross Section and Lineshape for the NO_3 (0,0) Band. 127

IV. Discussion and Conclusions. 136

A. The Reaction of HO with HNO_3. 136

B. The Reaction of HO with H_2O_2. 149

C. The Reaction of Cl with HNO_3. 151

D. The Photochemistry of $ClONO_2$. 156

E. NO_3 Absorption Cross Sections and Lineshape 163

Acknowledgement 178

Appendix A. 180

Appendix B. 182

References. 185

The Photochemistry of HNO_3 and $ClNO_3$

ABSTRACT

The techniques of laser flash photolysis/resonance fluorescence (FP/RF) and flash photolysis/laser absorption (FP/LA) were used to study the reactions

$$HO + HNO_3 \longrightarrow H_2O + NO_3 \quad (2)$$

$$HO + H_2O_2 \longrightarrow H_2O + HO_2 \quad (4)$$

$$Cl + HNO_3 \longrightarrow \text{products} \quad (10)$$

$$ClONO_2 + h\nu \longrightarrow \text{products} \quad (11)$$

and high resolution dye laser spectroscopy was used to measure the absorption cross sections and lineshape of the NO_3 (0,0) band for the A-X transition centered at 619.9 nm. KrF excimer laser photolysis at 248.4 nm was used to produce HO radicals from HNO_3 and H_2O_2 in (2) and (4); and to photolyse $ClONO_2$ in (11). XeF excimer laser photolysis at 350 nm was used to produce Cl atoms in Cl_2/HNO_3 mixtures in (10). Precursor concentrations were determined using UV absorption spectroscopy. Resonance fluorescence was used to follow the psuedo-first order decay of HO and Cl in (2), (4) and (10); while long path laser absorption was used to monitor the NO_3 products in (2) and (11). A flowing mixture of O_3/N_2O_5 was used to generate NO_3 in the cross sections study. The results for reaction (2) are $k_2 = (1.52 \pm 0.43) \times 10^{-14} \exp(644 \pm 79/T)$ cm^3 $molecule^{-1}s^{-1}$ from 218-363K, independent of pressure from 10-50 Torr Ar in the FP/RF experiments; ϕ_{prod} (NO_3 at low fluence) = 1.05 ± 0.26 with k_2 and

ϕ_{prod} (NO_3) found to be pressure, concentration and fluence dependent, having a strong self-correlation in the 298K FP/LA experiments. Rate constants for reactions (4) and (10) were measured to be k_4 = (1.81 ± 0.24) x 10^{-12} cm^3 $molecule^{-1}s^{-1}$ and k_{10} = (6.5 ± 3.4) x 10^{-15} cm^3 $molecule^{-1}s^{-1}$ at 298K and 10 Torr Ar; however, for (10) ϕ_{prod} (NO_3) $\leq$0.05. The FP/LA study of (11) found ϕ_{prod} (NO_3) = $0.55^{+0.3}_{-0.1}$ at pressures from 20-100 Torr of Ar or CH_4, showing the major photodissociation channel to yield Cl and NO_3. The peak absorption cross section for the NO_3 (0,0) band was determined to be 1.9 x 10^{-17} cm^2 $molecule^{-1}$ at 661.9 nm. The high resolution lineshape measured in this study was scaled to match integrated absorption coefficients determined in more direct but lower resolution studies. Under very high resolution ($\leq$200 MHz) the band was structureless and would not fluoresce despite a lack of photodissocation. It was found to fit well to two overlapping Lorentzians in agreement with some theories of intramolecular energy transfer.

THE PHOTOCHEMISTRY OF HNO_3 AND $ClNO_3$

William Marinelli

I. INTRODUCTION

The role of oxides of nitrogen[1] and chlorine[2] in determining overall stratospheric chemistry has been the subject of intense investigation in chemical laboratories and much political debate both in and outside of the scientific community. The economic and public health impacts of projections of anthropogenic pertubations on the stratosphere made on the basis of models, chemistry, and measurements are large enough so as to make it extremely important that these inputs be reliable. Aside from the social necessity to explore this chemistry, the application of new laser techniques to many of the free radicals and metastable molecules found in the stratosphere present new opportunities for the investigation of photochemistry, photophysics and excited state chemistry, as well as spectroscopy. The investigations undertaken here were designed to be relevant and interesting to either the atmospheric or laser chemist.

A. Reaction of HO with HNO_3 and H_2O_2

The odd hydrogen species HO and HOO play an important role in atmospheric chemistry. Hydroxyl radicals influence the ClO_x and NO_x catalytic ozone destruction cycles by acting on the odd chlorine and odd nitrogen reservoir species HCl and HNO_3

$$HO + HCl \longrightarrow H_2O + Cl \qquad (1)$$

$$HO + HNO_3 \longrightarrow H_2O + NO_3 \quad . \qquad (2)$$

The reaction of HO with the odd hydrogen reservoir molecule H_2O_2

$$HO + H_2O_2 \longrightarrow H_2O + HOO \qquad (4)$$

and the reaction

$$HO + HOO \longrightarrow H_2O + O_2 \qquad (5)$$

are also important in removing HO radicals. Model calculations of the rates of reaction and concentrations of stratospheric species[2-5] appear to overestimate the concentration of hydroxyl radicals in the lower stratosphere relative to HO radical concentrations inferred from measurements of ClO and the HNO_3 to NO_2 ratio. This discrepancy has been thought to be a result of the great sensitivity of these models to the rate of reaction (5), which is difficult to measure and highly uncertain.

The recent discovery of a new reservoir molecule peroxynitric acid ($HOONO_2$)[7,8] and measurements of the rate of HO with $HOONO_2$[9] have raised the possibility that two step reaction mechanisms of the type

$$HOO + NO_2 + M \longrightarrow HOONO_2 + M \qquad (6)$$

$$HO + HOONO_2 \longrightarrow H_2O + O_2 + NO_2 \qquad (7)$$

$$\text{net } HOO + HO \longrightarrow H_2O + O_2$$

may be more efficient at removing HOO and HO than the direct reaction. Recent investigations of the rate of reaction of HO radicals with

H_2O_2 and HNO_3 have cast some doubt on previously accepted values for the rate constants for these reactions. The faster rates of reaction measured in these studies, by altering the predicted HO concentrations, alter the estimated anthropogenic perturbation of atmospheric ozone levels through the NO_x, ClO_x, and HO_x catalytic cycles.

The earliest studies of the rate of reaction (2) were indirect measurements at high temperatures[10-12] made in the course of determining the rate of HNO_3 thermal decomposition

$$HNO_3 \xrightarrow{M} HO + NO_2 \qquad (8)$$

which is quickly followed by reaction (2), leading to first order removal of HNO_3. The first measurement of reaction (2) by direct observation of HO was done by Husain and Norrish[13] who used flash photolysis/kinetic spectroscopy and obtained a rate constant of 1.7×10^{-13} cm^3 $molecule^{-1}s^{-1}$ at 295K. They were also able to observe NO_3 as a probable primary product of the reaction. Morley and Smith[14] subsequently used the flash photolysis/resonance absorption technique to measure a rate constant of 1.3×10^{-13} cm^3 $molecule^{-1}s^{-1}$.

This work was followed by a series of two experiments by Smith Zellner[15,16] using flash photolysis/resonance absorption. They determined rate constants of 0.9×10^{-13} cm^3 $molecule^{-1}s^{-1}$ and 0.8×10^{-13} cm^3 $molecule^{-1}s^{-1}$ independent of temperature over the range 240-406K. The discrepancy between these results and previous studies was attributed to the simultaneous occurrence of the reaction

$$HO + NO_2 + M \longrightarrow HNO_3 + M \qquad (9)$$

which had not been accounted for in previous work. Nitrogen dioxide is routinely present in HNO_3 in small ($\leq$2 percent) quantities and later studies measured both NO_2 and HNO_3 by UV absorption in order to determine the magnitude of the correction. Margitan, Kaufman and Anderson[17] also measured k_2 at that time using discharge flow/resonance fluorescence and obtained a value of 0.89×10^{-13} cm^3 molecule^{-1}s^{-1}, independent of temperature from 270–470K in agreement with the later results of Smith and Zellner.[15,16] Reviews of chemical rate constants of stratospheric importance[18-20] recommended an average of these later values for k_2 of 0.85×10^{-13} cm^3 molecule^{-1}s^{-1}.

Recently, Wine et al.[21] measured k_2 to be 1.3×10^{-13} cm^3 molecule^{-1}s^{-1} at 295K using flash photolysis/resonance fluorescence and reported an inverse temperature dependence for the reaction expressed in the Arrhenius form as 1.52×10^{-14} exp(649/T) cm^3 molecule^{-1}s^{-1} over the range 224-336K. These results called into question the identity of the products of this reaction, since simple hydrogen stripping reactions of the type assumed to occur here do not exhibit this type of temperature dependence. At the same time, experiments performed in this laboratory using the same technique[22] determined k_2 to be 0.89×10^{-13} cm^3 molecule^{-1}s^{-1} at 295K and flash photolysis/laser absorption experiments performed concurrently showed NO_3 to be the major product of the reaction.

Since the publication of those two studies, preliminary reports out of several laboratoriss[23-25] continue to show the bimodal distribution of values for k_2, with varying degrees of inverse and non-Arrheius temperature behavior and possible pressure dependences. The continued uncertainty in k_2 has prompted the reexamination of this reaction.

The six previous determinations of the rate constant for the reaction of HO with H_2O_2 (4) also appear to fall into a bimodal distribution. The first measurement by Greiner[26] used flash photolysis/kinetic spectroscopy to obtain a value for k_4 of 9.3×10^{-13} cm^3 $molecule^{-1}s^{-1}$ at 298K. This was followed by determinations by Hack, Hoyermann and Wagner[27] using discharge flow/ESR, and Harris and Pitts[28] who used flash photolysis/resonance fluorescence, resulting in values for k_4 of 8.4×10^{-13} cm^3 $molecule^{-1}s^{-1}$ and 6.8×10^{-13} cm^3 $molecule^{-1}s^{-1}$ respectively. These three determinations led to a recommended value for k_4 of 8×10^{-13} cm^3 $molecule^{-1}s^{-1}$ at 298K.[18-20]

Two later experiments by Keyser[29] using discharge flow/resonance fluorescence, and Sridharan, Reimann and Kaufman[30] using discharge flow/laser induced fluorescence, resulted in values for k_4 of 1.64×10^{-12} cm^3 $molecule^{-1}s^{-1}$ and 1.69×10^{-12} cm^3 $molecule^{-1}s^{-1}$ at 298K. A value for k_4 of 1.57×10^{-12} cm^3 $molecule^{-1}s^{-1}$ at room temperature was measured by Nelson[31] using flash photolysis/resonance fluorescence at a factor of 10 higher pressure than the discharge flow experiments. The reaction is reexamined here as a check on the experimental apparatus and as another independent verification of the rate constant.

B. Reaction of Cl with HNO_3

The reaction of Cl with HNO_3, while not of great atmospheric importance, is interesting in that it is analogous to the reaction of HO with HNO_3. Of the 5 most probable reaction channels:

$$Cl + HNO_3 \longrightarrow HCl + NO_3 \qquad \Delta H_{298} = -1.8 \text{ kcal/mole} \qquad (10a)$$

$$\longrightarrow ClO + HNO_2 \qquad \Delta H_{298} = +8.8 \text{ kcal/mole} \qquad (10b)$$

$$\longrightarrow OClO + HNO \qquad \Delta H_{298} = +51.6 \text{ kcal/mole} \qquad (10c)$$

$$\longrightarrow HOCl + NO_2 \qquad \Delta H_{298} = -4.5 \text{ kcal/mole} \qquad (10d)$$

$$\longrightarrow HO + ClONO \qquad \Delta H_{298} = +15.6 \text{ kcal/mole} \qquad (10e)$$

only reactions (10a) and (10d) are exothermic. There have been two previous disparate studies of this reaction, both employing the discharge flow/mass spectrometric technique. The first study by Leu and DeMore[32] used an excess of Cl atoms and measured the attenuation of HNO_3 at the parent or NO_2^+ peak as a function of sliding injector position and linear flow rate. Approximately 10-20 percent of the HNO_3 was consumed by the reaction. A rate constant of 6.8×10^{-15} cm^3 $molecule^{-1}s^{-1}$ was measured at 295K. No products of the reaction were identified. The study by Poulet, LeBras and

Combourieu[33] used approximately the same Cl atom concentrations (6–9 x 10^{14} atoms cm^{-3}) but a 2–4 fold greater concentration of HNO_3 (1–4 x 10^{15} molecules cm^{-3}) resulting in less than a 2 percent depletion to HNO_3 during the reaction. The rate constant for the reaction was measured to be $1.5 \times 10^{-11}\ e^{-(4378/T)}$ over the range 298–633K. At 298K an upper limit of 2 x 10^{-17} cm^3 $molecule^{-1}s^{-1}$ was placed on the rate constant. The main products observed by mass spectroscopy were HCl, ClO and NO_2, with some traces of HOCl.

The rate constants measured for this reaction at 298K are unusual for a simple hydrogen atom abstraction reaction, thus neither reactions (10a) or (10d) may be discounted as possible product channels.

C. Photochemistry of $ClONO_2$

Chlorine nitrate ($ClONO_2$) is an important reservoir species for both odd chlorine and odd nitrogen. Since the rates of reaction of $ClONO_2$ with other atmospheric components is slow,[34–36] photolysis and thermal decomposition are the major destruction pathways.

There have been three previous investigations of $ClONO_2$ photolysis, all of which have assumed that photolysis may occur along any of four possible channels

$$ClONO_2 + h\nu \longrightarrow ClO + NO_2 \qquad \lambda \lesssim 1100\ nm \qquad (11a)$$

$$\longrightarrow Cl + NO_3 \qquad 700\ nm \qquad (11b)$$

$$\longrightarrow ClONO + O\ (^3P) \qquad 391\ nm \qquad (11c)$$

$$\longrightarrow ClONO + O\ (^1D) \qquad 241\ nm \qquad (11d)$$

The first investigation by Smith, Chou and Rowland[37] used continuous photolysis of $ClONO_2$ at 302.1 nm and end-product analysis to conclude that (11c) was the predominant pathway. A subsequent study by Chang, Barker, Davenport and Golden[38] using a very low pressure photolysis technique determined $\phi_{Cl} = 1.0$, $\phi_{NO_3} \geq 0.5$ and $\phi_O \leq 0.1$ indicating that (11b) was the primary channel.

Most recently, Adler-Golden and Weisenfeld[39] used flash photolysis/resonance absorption of $O(^3P)$ to conclude that (11c) was predominant, while observing no Cl atoms by the same resonance absorption technique. This discrepancy has prompted a reexaminatin of this process.

D. Absorption Cross Sections and Lineshape for the NO_3 (0,0) Band

The visible absorption spectrum of NO_3 was first recorded by Jones and Wulf,[40] subsequently it was reexamined by Schott and Davidson,[41] and Ramsay,[42] and the low resolution absorption cross sections were recently measured by Graham and Johnston[43,44] and Mitchell et al.[45] The spectrum consists of approximately 20 diffuse bands in the region 672 to 400 nm, with the only discernible feature being a short progression in the symmetric stretching vibration ν_1 at a spacing of approximately 930 cm^{-1}. The infrared spectrum of NO_3 has not been observed and thus little is known about its structure or ground state vibrational spacings. The molecule is thought to have a planar configuration in both the ground and excited states (D_{3h} or C_{2v}), with a slight increase in bond length in the excited state.[46]

The channel specific photodissociation quantum yields of NO_3 were determined by Graham and Johnston,[44] and reinvestigated by Magnotta.[47]

They showed the existence of two competing photodissociation channels leading to NO_2 and $O(^3P)$ (400-627 nm) and NO and O_2 (585-623 nm). The (0,0) band was found to be photochemically inactive for single photon processes, however no visible fluorescence was observed when the band was excited by either a CW or pulsed dye laser.[48]

There is some disagreement as to the shape and magnitude of the NO_3 absorption spectrum. The three most recent determinations utilized different techniques, all involving the NO_x/O_3 system under varying experimental conditions. The thermal chemistry of this system is dominated by the reactions

$$N_2O_5 \longrightarrow NO_2 + NO_3 \quad (12)$$

$$NO_2 + NO_3 \longrightarrow N_2O_5 \quad (13)$$

$$NO_2 + O_3 \longrightarrow NO_3 + O_2 \quad (14)$$

$$2NO_3 \longrightarrow 2NO_2 + O_2 \quad (15)$$

$$N_2O_5 + H_2O \text{ (walls)} \longrightarrow 2HNO_3 \quad (16)$$

The first study of Graham and Johnston[43] utilized a flowing mixture of NO_2 in excess O_3 such that the NO_2 was converted to N_2O_5 via reactions (13) and (14). The measured absorption cross sections are directly influenced by changes in the rate constants for (12)-(16), and revisions of the rate constants since the study requires that the reported absorption cross sections be multiplied by 3.68.

The second study of Graham and Johnston[44] did not require a knowledge of the rate constants for the governing reactions, but instead used the molecular modulation technique[49] to directly photolyse the NO_3 radical. A simple relation between the modulation intensities and phase shifts for NO_3 and N_2O_5, to a good first approximation independent of the rate constants for the connecting reactions, can be derived. This can be written as

$$N_2O_5 \underset{k_{15}}{\overset{k_{12}}{\rightleftharpoons}} \overset{k_{14}[O_3]}{\longrightarrow} 2NO_3 \qquad (17)$$

with the phase shifts of N_2O_5 and NO_3 given as -90° and $+90^\circ$ respectively, with reference to the photolysis lamps. The cross sections were determined by alternately monitoring the modulation of NO_3 in the visible and N_2O_5 in the infrared. The measurement gave a peak cross section at the (0,0) band of 1.86×10^{-17} cm^2 $molecule^{-1}$ as compared to a corrected result of 1.48×10^{-17} cm^2 $molecule^{-1}$ in their previous experiment.

The third measurement of the cross sections by Mitchell et al.[45] used direct visible absorption spectroscopy in a double beam short path system. By introducing small amounts of NO_2 into the system containing large excesses (10^5) of O_3, all of the NO_2 introduced is converted to NO_3. In this system the NO_3 concentration is determined by the easily measurable input concentration of NO_2, and determination of the cross sections is very direct. This technique gave a cross section of 1.21×10^{-17} cm^2 at the (0,0) band peak.

The absorption cross sections for NO_3 are important parameters for those interested in determining absolute photodissociation or fluorescence yields, as well as those determining NO_3 concentrations in the atmosphere. This study was designed to characterize the strong absorbtion of the (0-0) band at 662 nm using tunable dye laser spectroscopy.

II. EXPERIMENTAL APPARATUS AND PROCEDURES

A. Introduction

The use of flash photolysis to produce transient free radicals and molecules was first employed by Norrish and Porter.[50] The techniques of kinetic spectroscopy,[13] electron spin resonance,[27] resonance absorption,[14-16] resonance and laser induced fluorescence[52] and laser gain spoiling[53] among others, have been used to characterize the spectra and kinetics of these transients. The earliest flash photolysis devices employed a high energy (10-5000J) electrical discharge through a low pressure inert gas to produce a high intensity semi-continuum burst of photons on the 0.5-10 ms time scale. The advent of high energy tunable and fixed frequency UV-visible pulsed lasers introduced greater wavelength and temporal resolution into the technique and allowed the excitation and production of molecules in specific molecular eigenstates.

The resonance fluorescence technique for the detection of atoms and molecules has been used successfully to observe O, Cl, and H atoms and the NO and HO molecules, both in the laboratory and in atmospheric measurements. The technique has been excellently reviewed by Schofield.[54] The coupling of the flash photolysis technique with in situ resonance fluorescence detection, under conditions where psuedo-first order kinetics dominate, enable the use of simple analytic techniques to extract kinetic and quantum yield information.

The use of CW tunable dye lasers as spectral sources in absorption spectroscopy, when used in conjunction with flash photolysis, is a

simple extension of the kinetic spectroscopy technique. Their low divergence, high spectral brightness, and good frequency and amplitude stability make them ideal sources for multi-pass absorption cells of the White[73] type design. When used in simple absorption spectrometers, the bandwith of these lasers may be narrowed to the point where their effective resolution is many orders of magnitude better than the finest monochromators or spectrographs.

Flash photolysis/resonance fluorescence has been employed here to observe Cl and HO produced and reacting with a variety of precursor molecules. Flash photolysis/laser absorption has been used to observe the NO_3 molecule as a product of reaction (2) and as a primary product in $ClONO_2$ photolysis (11b). A CW tunable dye laser has been used to measure the absorption cross sections, lineshape, fluorescence yield, and examine possible high resolution structure of the NO_3 (0,0) band.

It is the nature of the experimental science that experiments mature and change as levels of understanding change and as an experimental apparatus is asked to perform tasks further away in scope from the purpose for which it was originally designed. The series of flash photolysis/resonance fluorescence (FP/RF) apparatus used here are a good example of this. The experiment was originally designed by Magnotta[47] to study room temperature NO_3 photolysis and subsequently modified by Nelson and myself[31,22] to do HO and Cl kinetics. The experiments on the reaction of Cl with HNO_3 were performed in this device. When it was decided to study the temperature dependence of the HO + HNO_3 reaction, a jacketed version of the Magnotta type

cell was designed in which most of the room temperature HNO_3 and all of the HO + H_2O_2 kinetics were studied. It was later found that this cell was inadequate for doing temperature dependent studies, and an entirely new system was designed in which this work was done. In all cases the transition from device to device was accompanied by experiments showing that results obtained in the old device could be reproduced in its successor.

The flash photolysis/laser absorption (FP/LA) experiment also has similar history. Originally designed as a molecular modulation spectrometer; it was quickly modified when it was decided to do these experiments. The early version of this device, while useful in showing experiments of this type were possible, had many shortcomings and produced erratic results. The redesign of the apparatus eliminated these defects and the results reported here are from the revised version. The experiments done to measure the NO_3 (0,0) band cross sections were performed in a slightly modified version of the FP/LA device.

B. Flash Photolysis/Resonance Fluorescence Experiments

The flash photolysis/resonance fluorescence experiment is shown in Fig. 1 and described below.

1. Photolysis Source

The photolysis source used in all experiments was a Lumonics TE-860-2M rare gas halide excimer laser. The laser was operated on either of two transitions, at 2484 Å (KrF) for HNO_3 and H_2O_2 photolysis, and at 3500 Å (XeF) for Cl_2 photolysis. The typical laser bandwith is approximately 4 Å FWHM and is shown in Fig. 2 as

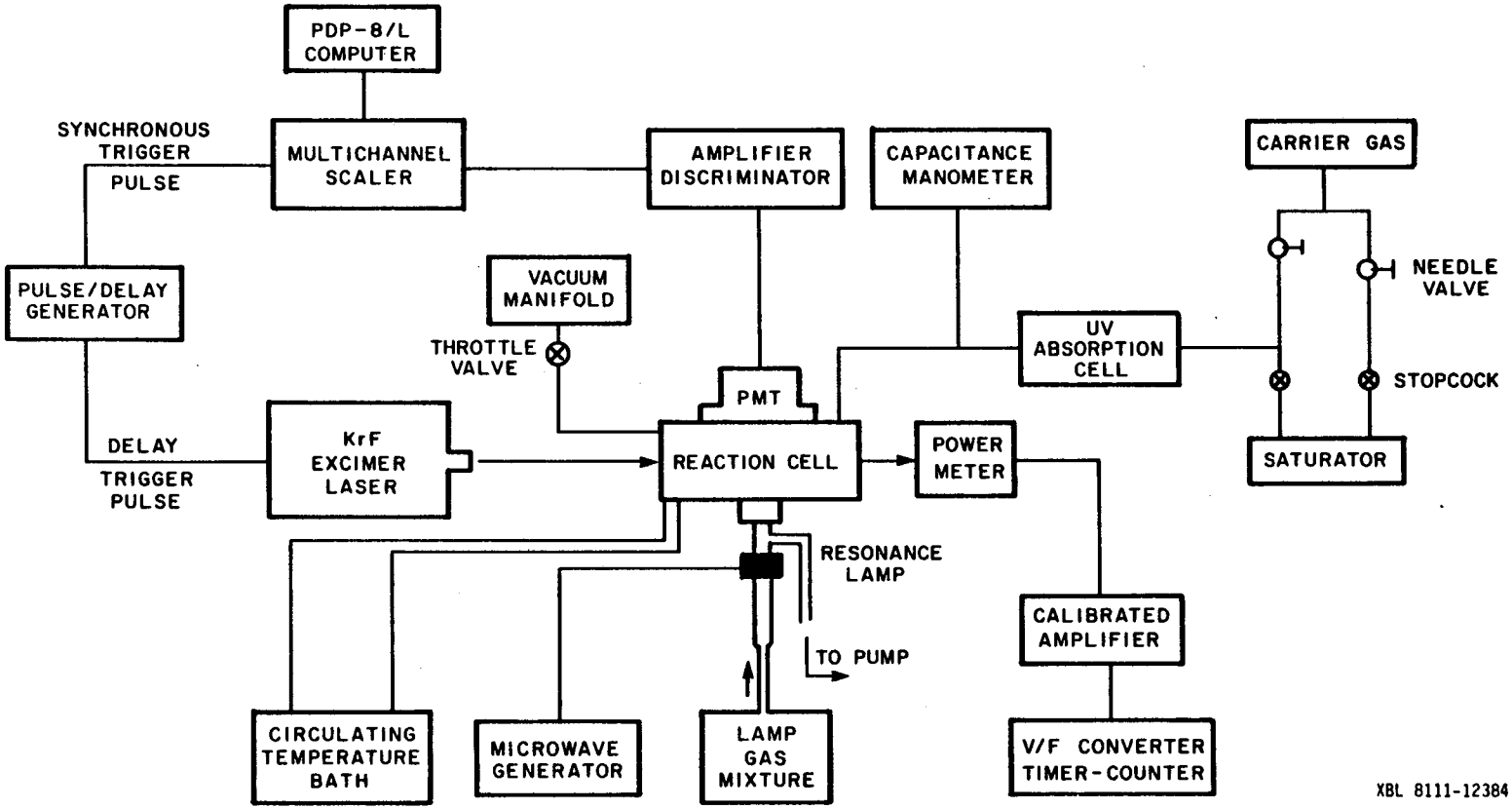

Figure 1. Schematic diagram of FP/RF apparatus. Resonance lamp is shown on PMT axis but actually is perpendicular.

recorded using an optical multichannel analyzer (OMA) (see Section II.C). The manufacturers reported temporal pulse width is 10-20 nsec, much faster than the kinetics of interest that ensue following the pulse, and therefore any chemistry happening during the pulse may be ignored.

The typical pulse from the laser was unpolarized and a rectangular in shape, approximately 7 x 20 mm. The beam had a large divergence and was typicallly 2 x 6 cm by the time it had traveled the 1.5 meters to the cell. The total pulse energy was as high as 250 mJ at KrF and a weak function of discharge energy above the lasing threshold. A circular 1 cm^2 black anodized aluminum aperture, located and centered on the cell entrance window, defined the photolysis beam and reduced the total energy to 10-20 mJ while acting as a beam stop for the beam not passing through the aperture. These pulse energies were sufficient to produce the (1-5) x 10^{11} molecules cm^{-3} of the radical of interest necessary for resonance fluorescence detection. The energy density could be further attenuated by using a series of Vycor plates in the beam path or by varying the age and composition of the laser gas fill.

2. Laser Energy Measurements

If quantum yield information is desired or radical concentrations are to be maintained in a certain range, then accurate pulse energy measurements are required.

The typical laser repetition rate employed in these experiments was 15 Hz. At this repetition rate individual pulse energies could be averaged by measuring average laser power. The laser power was measured by placing a Scientech Model 36-0001 surface absorbing power

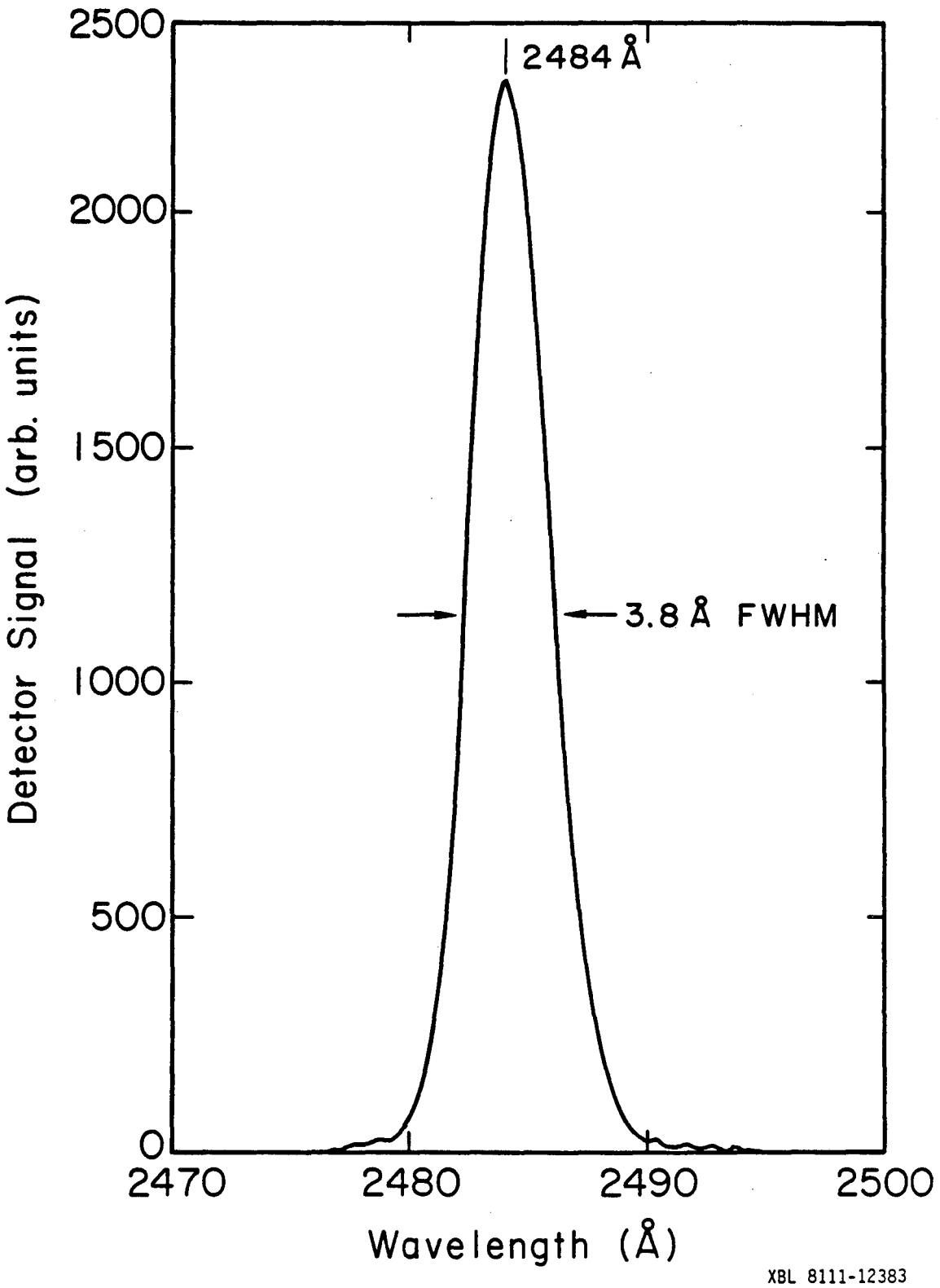

Figure 2. Low resolution (0.4Å) spectrum of KrF excimer laser line.

meter at the photolysis cell exit window. The output from the power meter was sent to an amplifier whose gain was set to be 10X the inverse of the manufacturers calibration such that 1 watt of incident power resulted in 1 volt of amplifier output.

The integrated laser energy during the experiment was measured by sending the amplifier output to a gated voltage to frequency converter and timer having a conversion rate of 1000 Hz $volt^{-1}$. The V/F output was integrated by an events counter and the average laser power was determined from the total counts, elapsed time,and amplifier calibration factor.

The power meter could be calibrated by passing a known current through a resistor of known value placed in the power meter absorbing material by the manufacturer. A Heathkit Model IP-1711 voltage/current source was used in the calibration. The value of the calibration resistor was specified by the manufacturer and confirmed by measurements done in this laboratory. The amplifier output voltages as a function of input power are listed in Table 1 and plotted in Fig. 3. The response is shown to be linear over the range of experimentally employed powers and gives a calibration factor of 1.0422 volts $watt^{-1}$ when corrected for the 98 percent absorbance of the power meter face.

The large thermal mass of the detector face results in approximately a 10-15 second time constant for the detector and therefore the laser was started approximately 1 minute before any power measurements were performed. The short term (10 minutes) stability of the excimer laser was better than 5 percent as measured by the power meter.

Table 1. Power Meter Calibration

Substitution Power (Watts)	Power Meter Output (Volts)
0.004	0.004
0.017	0.017
0.039	0.037
0.069	0.068
0.103	0.105
0.160	0.163
0.268	0.270
0.422	0.427
0.540	0.547
0.750	0.766
0.981	1.004
1.258	1.285
1.636	1.673
1.808	1.848

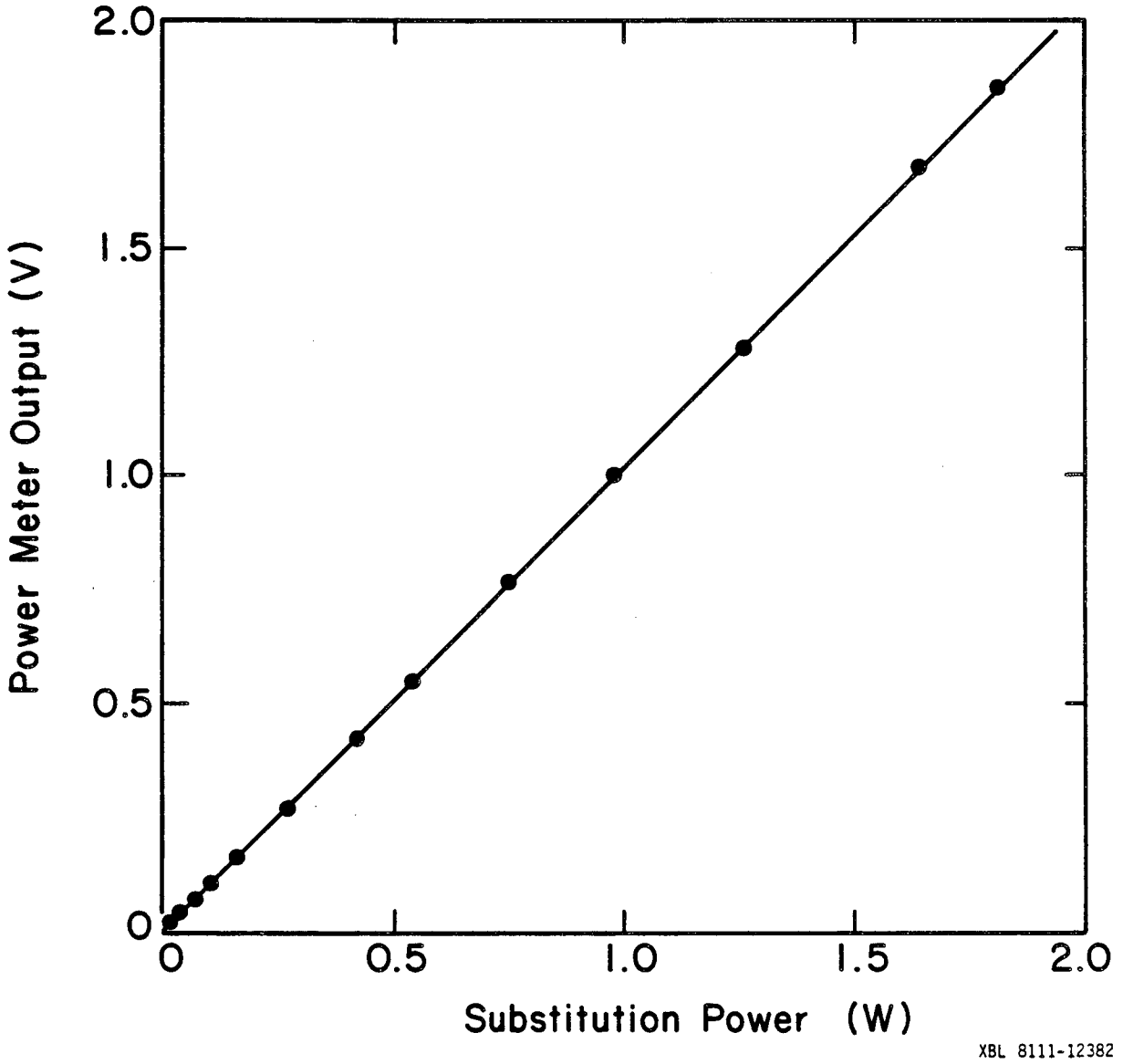

Figure 3. Scientech power meter/amplifier calibration.

3. Precursor Monitoring

Ultraviolet absorption spectroscopy was chosen to measure the precursor/reactant concentrations because of their relatively high absorption cross sections and the ability to distinguish and measure possible impurities. Typical precursor concentrations ranged from (1-20) x 10^{15} molecules cm^{-3} and absorption cross sections in the wavelength range 200-350 nm were sufficient to monitor the concentration of all the desired species.

The ultraviolet absorption cell (Fig. 4) consisted of a deuterium lamp and power supply excised from a Beckman Model DU-2 spectrometer in its original housing. Ultraviolet radiation emerging from a 3.2 mm exit hole in the housing was modulated by an American Time Products 400 Hz tuning fork chopper. The beam was then reflected down a 99.3 cm path length, 2.3 cm I.D. pyrex absorption cell equipped with Suprasil-2 windows. The absorption cell was loosely wrapped in heating tape and could be heated to 50°C to bake out any species absorbed on the cell walls and quickly cooled to room temperature by a muffin fan. An Analog Devices Model AD590 solid state temperature sensor was attached to the cell in order to measure the cell temperature. The radiation then entered a McPherson Model 218 0.3 meter monochromator with a 2400l/mm grating blazed at 1500 Å and an RCA 1P28 photomultiplier tube biased at -950V. A slit setting of 100μm resulted in a resolution of approximately 3 Å. The signal from the PMT was amplified and sent to a lock-in amplifier where the transmission was recorded.

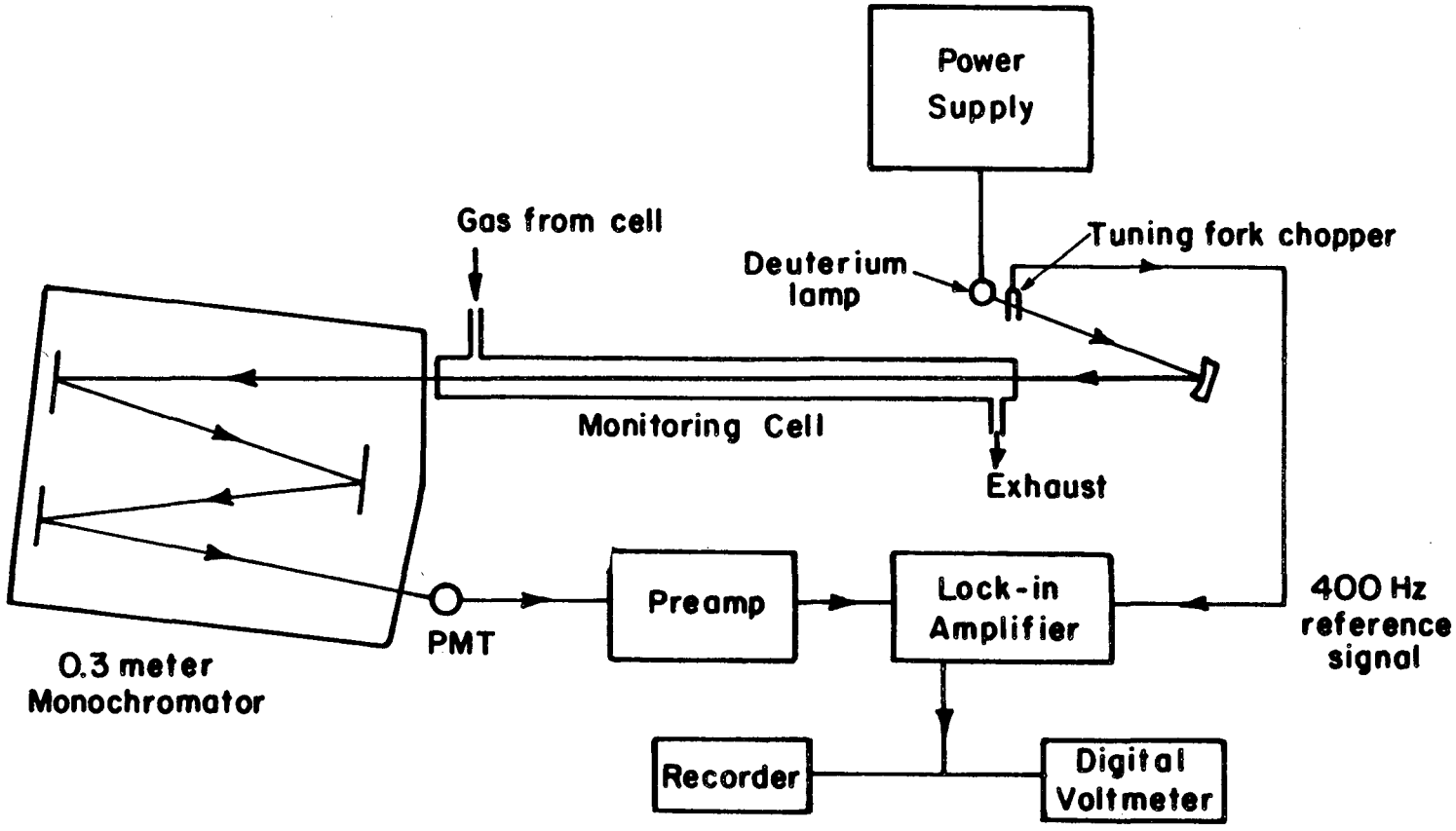

Figure 4. UV absorption monitoring system for precursors and reactants.

The monochromator was calibrated by measuring the position of 6 emission lines from a pen-ray HG lamp[55] between 1849 and 2537 Å. The veracity of the system was checked by measuring the absorption of 3 different NO_2/N_2 mixtures, supplied by Matheson, at 350 nm. In all cases the measurements agreed with the suppliers analysis within 3 percent. The system was found to be stable to within 10 parts in 1500 after 2 hours warm-up.

The spectra of the three major precursor molecules are shown in Figs. 5 an 6. The HNO_3, H_2O_2 and $ClONO_2$ cross sections are those of Molina and Molina.[56,57] The Cl_2O cross sections shown in Fig. 6 are those of Lin.[58] Their significance will be discussed in a later section. Table 2 shows the absorption cross sections employed for all precursor species and their most probable impurities at their photolysis and monitoring wavelength.

4. Reaction Cells and Product Detection

The reaction cell used in early experiments was designed by Magnotta[47] and is shown in Figs. 7 and 8. It consisted of a 3.8 cm diameter, 10 cm long laser path, pyrex tube with two centrally located perpendicular Wood's horns facing the resonance lamp and photomultiplier tube. A No. 9 O-ring joint served as the entrance port for radiation from the resonance lamp and a larger No. 25 O-ring joint acted as the optical exit port to the photomultiplier. Black anodized aluminum baffles were inserted into both O-ring joints to minimize scattered light and eliminate light piping of lamp emission through the cell walls to the PMT. The exterior of the entire cell was spray painted flat black to further eliminate scattered light.

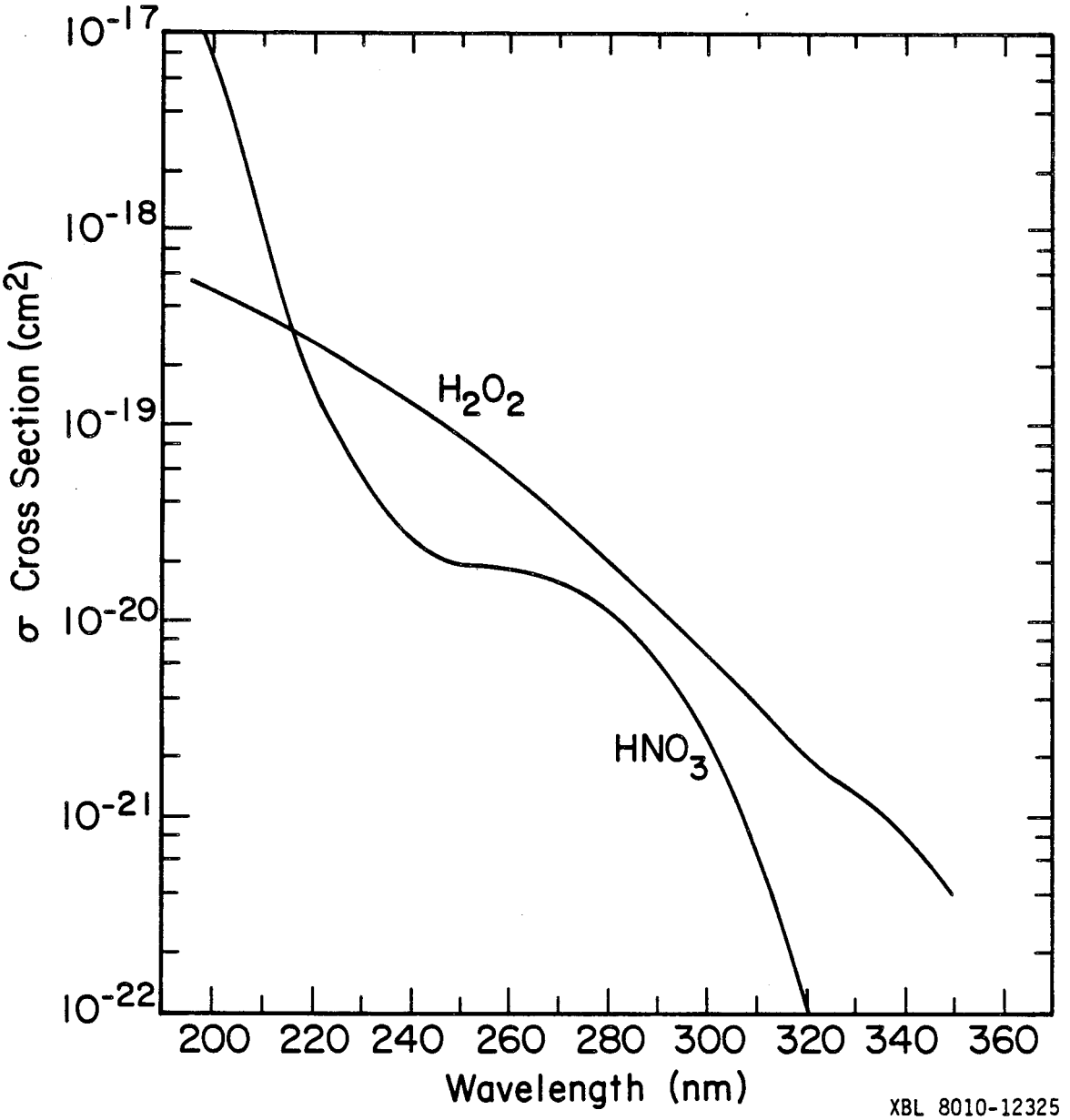

Figure 5. UV absorption coefficients for H_2O_2 and HNO_3.

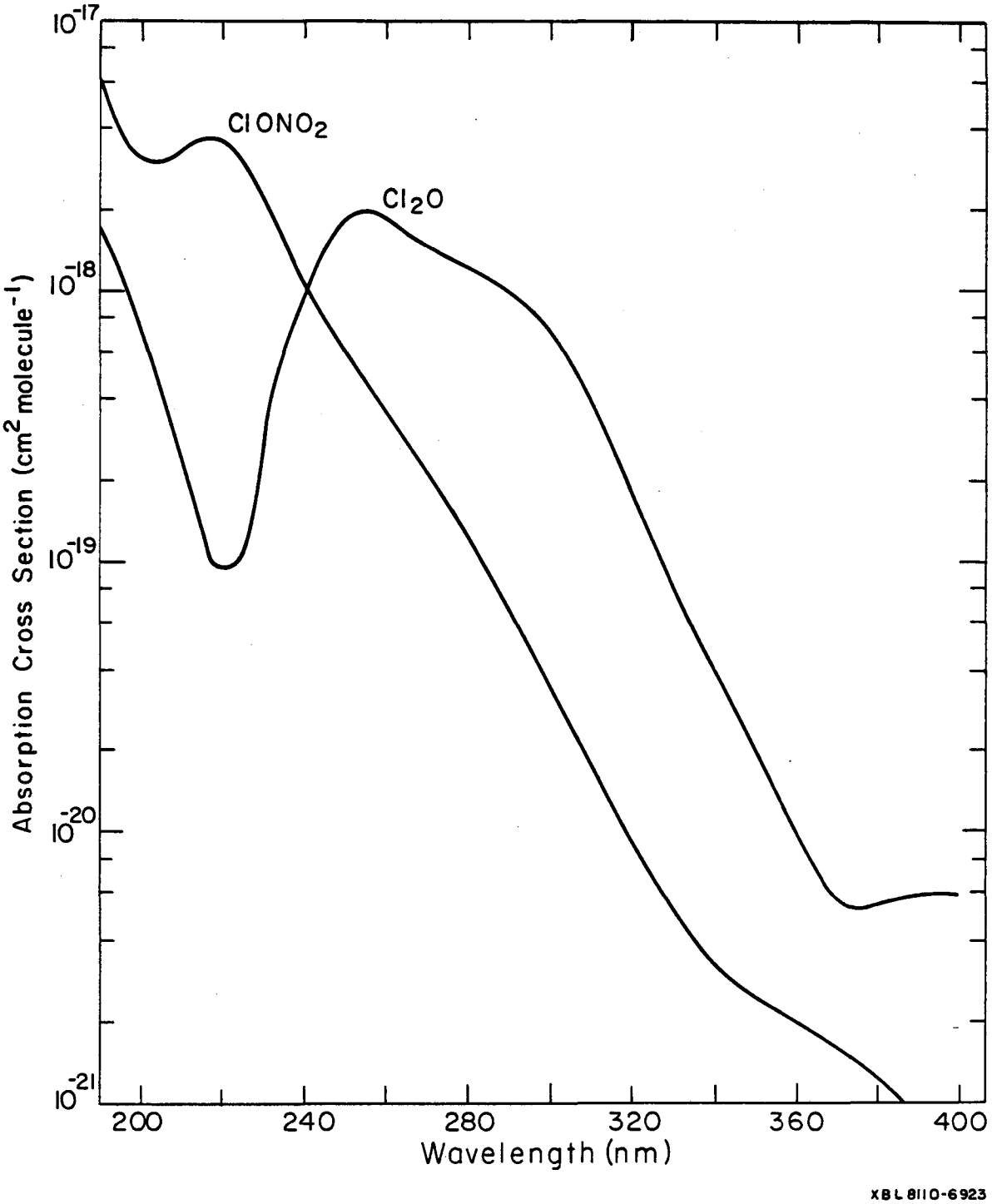

Figure 6. UV spectra of $ClONO_2$ and Cl_2O from Molina and Molina[56,57] and Lin.[58]

Table 2. Absorption cross sections for important species at monitoring and photolysis wavelengths (cm^2/molecule x 10^{20})

	Wavelength (nm)			
Molecule	200	215	248.4	350
HNO_3	661	35.6	1.93	—
H_2O_2	46.7	38.7	8.24	0.03
$ClONO_2$	307	360	63.9	0.25
Cl_2	—	—	0.11	18.9
NO_2	25.0	40.2	1.29	41.0
Cl_2O	66.9	10.0	170	2.00

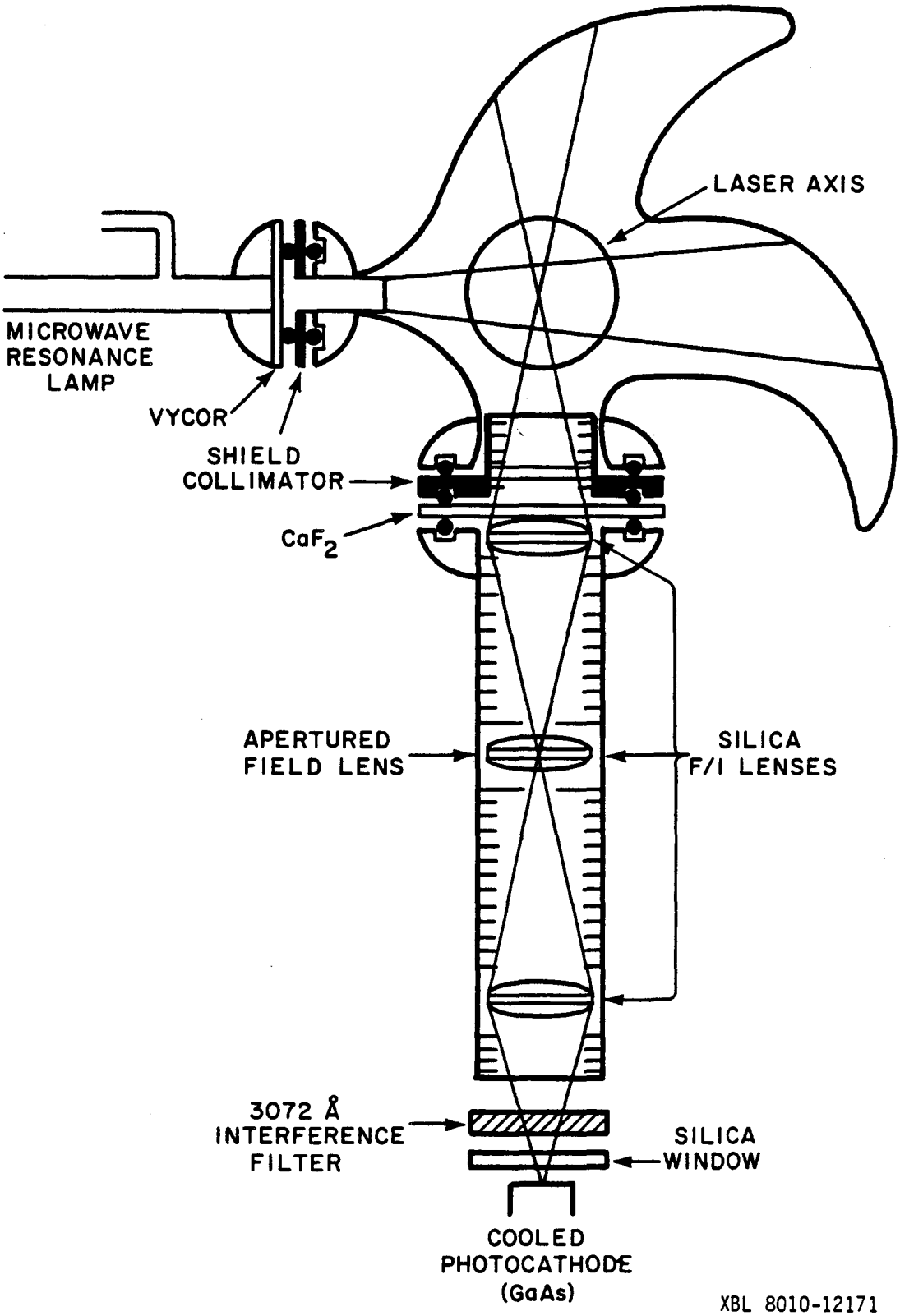

Figure 7. First and second generation HO radical resonance fluorescence detection system from Nelson.[31]

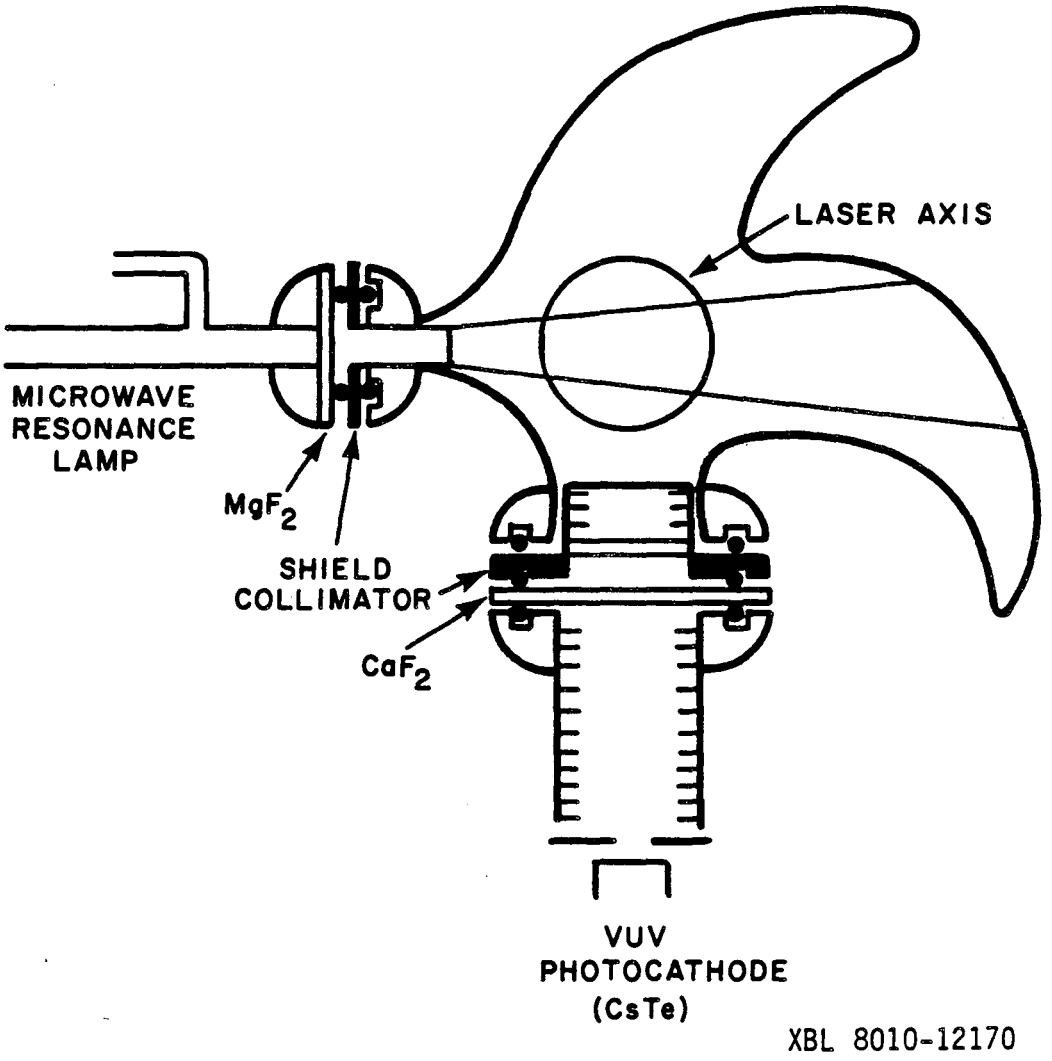

Figure 8. Cl and O atom resonance fluorescence detection system from Nelson.[31]

The microwave driven resonance lamp was designed after Watson[59] and consisted of a No. 9 O-ring joint fitted with a glass inlet close to the lamp window to minimize self reversal. The resonance lamp window (Vycor for HO and MGF_2 for Cl and O lamps) was attached to the lamp by a thin film of Varian Torr-Seal low vapor pressure vacuum epoxy placed around the perimeter of the window to minimize contact between the epoxy and either the lamp gas or VUV emission. The lamp fuel gas pressure was regulated in the pressure range 500-1000 microns, as measured by a thermocouple gauge, by a stainless steel needle valve, and then passed into the lamp. The fuel gas was pumped through, lamp and a liquid nitrogen trap by a mechanical roughing pump with a lamp residence time of approximately 2 seconds.

The microwave source was a current stabilized Burdick Model MW/200 Medical Diathermy which operated at 2.45 GHz. It was coupled to the lamp by a 1 meter waveguide and Evenson cavity. The cavity was air cooled to minimize heat build up and reduce the resulting fluctuations in lamp output.

Hydroxyl radical emission, largely from the (0,0) band of the $A^2\Sigma^+ - X^2\pi_i$ transition near 308 nm, was generated by passing a 3 percent H_2O/Ar mixture of 700 microns total pressure through the resonance lamp. The spectrum of this emission, as recorded with the McPherson 0.3 meter monochromator, is shown in Fig. 9. The spectral intensity and wavelength distribution of the lamp was found to be weakly dependent on pressure between 500 and 1000 microns; however, below 500 microns emission from the lamp is dominated by the (1,1)

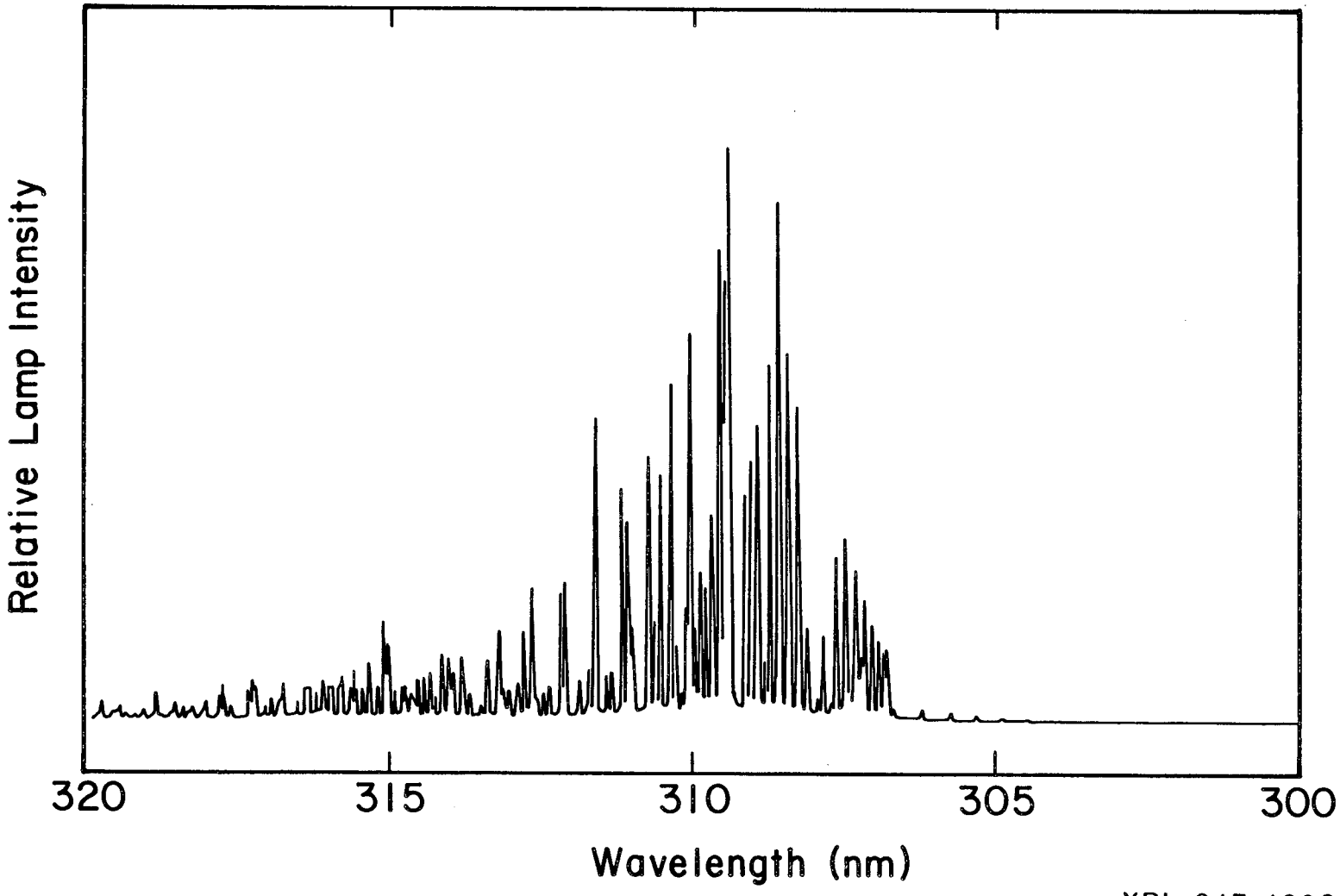

XBL 817-10864

Figure 9. Emission spectrum of HO radical resonance lamp.

band around 315 nm. This emission contributes to the scattered light seen by the photomultiplier while sharply decreasing the detection sensitivity; therefore great care was taken to avoid these conditions. Even under optimum lamp operating conditions, approximately 10 percent of the lamp emission occurs at the (1,0) band at 281 nm. This emission is somewhat advantageous in that it is not seen by the filtered PMT, yet HO radicals in the reaction cell absorbing this emission are quickly quenched by the Ar carrier gas to $v' = 0$ and emit on the (0,0) transition. A Vycor resonance lamp window was chosen in order to exclude O, N, NO and H atom emission resulting from trace O_2, N_2 and H_2 impurities in the Ar carrier gas. The UV and VUV emission from these lines may act as an important steady state photolysis source for precursor molecules, which have high absorption cross sections in this region.

Chlorine atom emission was obtained by passing a stream of 0.1 percent Cl_2 in He[60] through the lamp. The spectrum of the lamp as recorded by Nelson[31] is shown in Fig. 10. The emission is dominated by two members of the ^4P-^2P multiplet at 138.0 nm ($^4P_{3/2} - {}^2P_{3/2}$) and 139.0 nm ($^4P_{5/2} - {}^2P_{3/2}$). Also apparent is a small amount of emission from the O atom triplet at 130 nm, probably a result of trace O_2 impurities in the lamp mixture or O atoms stripped off the lamp walls by the discharge.

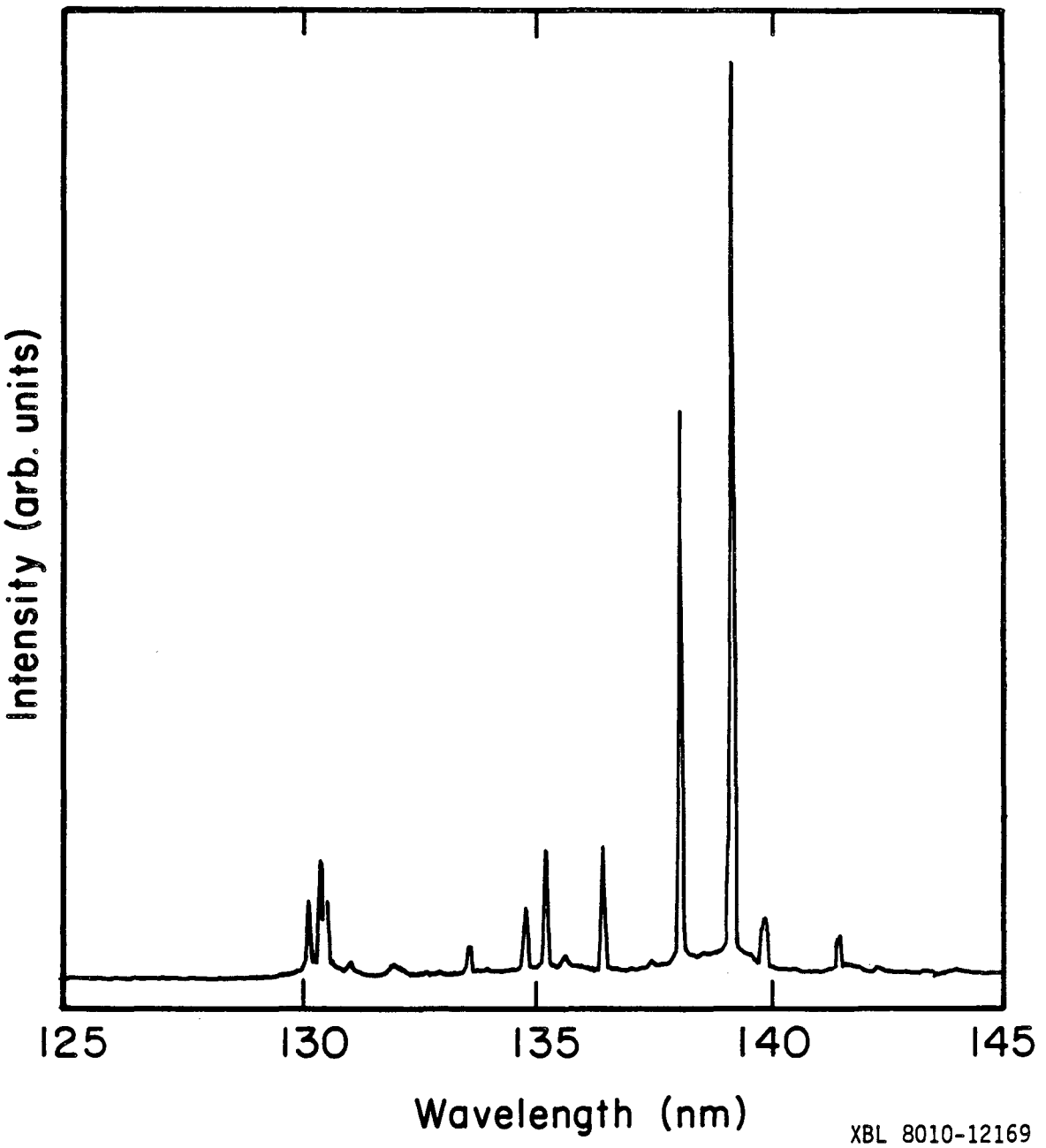

Figure 10. Emission spectrum of Cl atom resonance lamp from Nelson.[31]

The detection system for HO emission is also shown in Fig. 7. The fluorescence excited by the resonance lamp exited the cell through a CaF_2 window and was weakly focussed with three (f/1) Suprasil lenses contained in a baffled optical tube through a 307 nm interference onto the cooled GaAs photocathode of an RCA 31034 photomultiplier. The spectrum of the interference filter is shown in Fig. 11. The photomultiplier tube was operated with a photocathode bias of -1550 V in a magnetically and RF shielded housing, with the dynode string optimized for photon counting. Cold N_2 blow off from a 50 l liquid N_2 dewar was passed through the housing to cool the tube to approximately -20°C while warm, dry N_2 was blown over the housing window to prevent condensation build up. This reduction in the temperature of the photocathode reduced the number of dark counts originating at the cathode from 60,000 to 200 per second. Scattered light from the resonance lamp brought the total tube output in the absence of HO radicals to approximately 10,000 counts s^{-1}.

For Cl atom studies the detection system was modified by removing the silica lenses and interference filter, and shortening the baffled tube. The photomultiplier was changed to a solar blind EMI G26H315 with a CsTe photocathode. The CaF_2 cell window was the only filter element and excluded any Lyman-α (121.6 nm) radiation present. This tube did not require any cooling, as the work function of the photocathode is relatively high, producing 20 dark counts per second. Resonance lamp scatter added another 2000 to 3000 counts s^{-1}.

While the absolute detection sensitivity of the resonance fluorescence system is not required for these experiments, it is

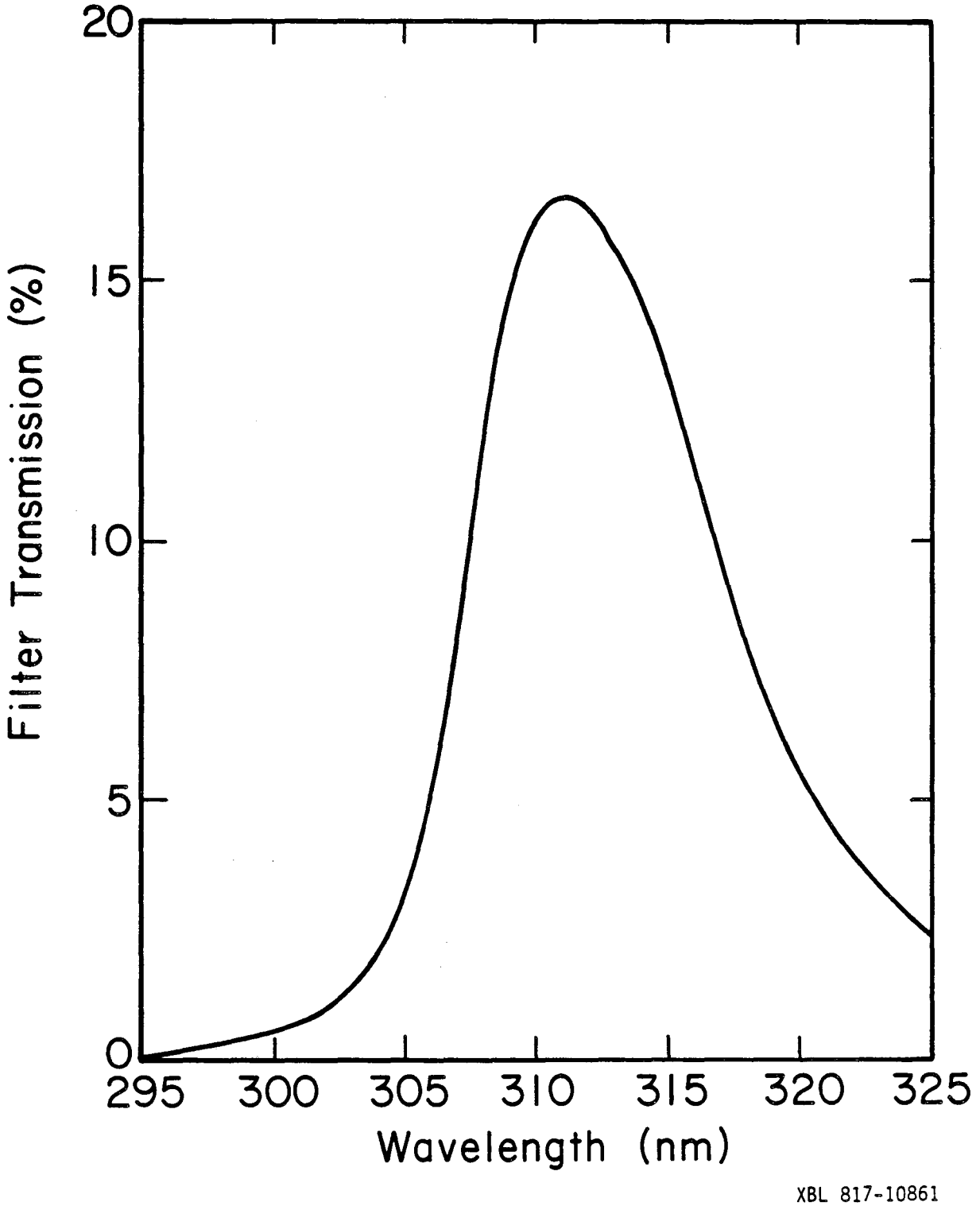

Figure 11. Transmission spectrum of 309 nm interference filter used in HO resonance fluorescence detection system.

necessary to show that the response of the system is linear over the range of concentrations that a species will be observed. This is usually done by photolysing a molecule of known photolytic quantum yield for the species in question and of known absorption cross section at the photolytic wavelength. By measuring the energy of the photolytic pulse, one may then calculate the concentration of radical or atom interest created by the pulse. Correlating the detector response to a variety of initial radical or molecule concentrations covering the range of interest produces a response curve from which sensitivity and linearity may be determined.

For HO radicals the system was calibrated using HNO_3 photolysis at the KrF laser line

$$HNO_3 + h\nu\ (250) \longrightarrow HO + NO_2 \qquad (18)$$

The quantum yield of HO radicals from HNO_3 has been measured as one from 200–315 nm by Johnston, Chang and Whitten,[61] and the absorption cross section for HNO_3 has been determined by Molina and Molica[56] (Table 2). A fixed concentration of HNO_3 in Ar carrier gas was photolysed under experimental pseudo first order conditions over a range photolytic energies. Under these conditions quenching of the $HO(A^2\Sigma^+)$ state is held constant and the signal following the flash in the first order decay is taken as the measure of detector response. The results of this experiment are shown in Table 3 and Fig. 12. The response is seen to be linear from 0.5 $\longrightarrow$ 5 x 10^{11} molecules cm^{-3} with the inverse of the slope giving a detection sensitivity of 3.3 x 10^7 molecules cm^{-3} Hz^{-1}, which is common for these systems.

Table 3. HO radical detection sensitivity.

Laser Fluence[a]	$[HNO_3]$[b]	$[HO]^{c,e}_{t=0}$	Intercept[d]
0.79	5.60	0.85	2337
1.54	5.00	1.49	4291
2.24	5.60	2.42	7214
3.12	5.00	3.01	8541
3.80	6.21	4.72	13661

a photons cm^{-2} $shot^{-1}$ x 10^{-16}

b molecules cm^{-3} x 10^{-14}

c molecules cm^{-3} x 10^{-11}

d Hz $shot^{-1}$

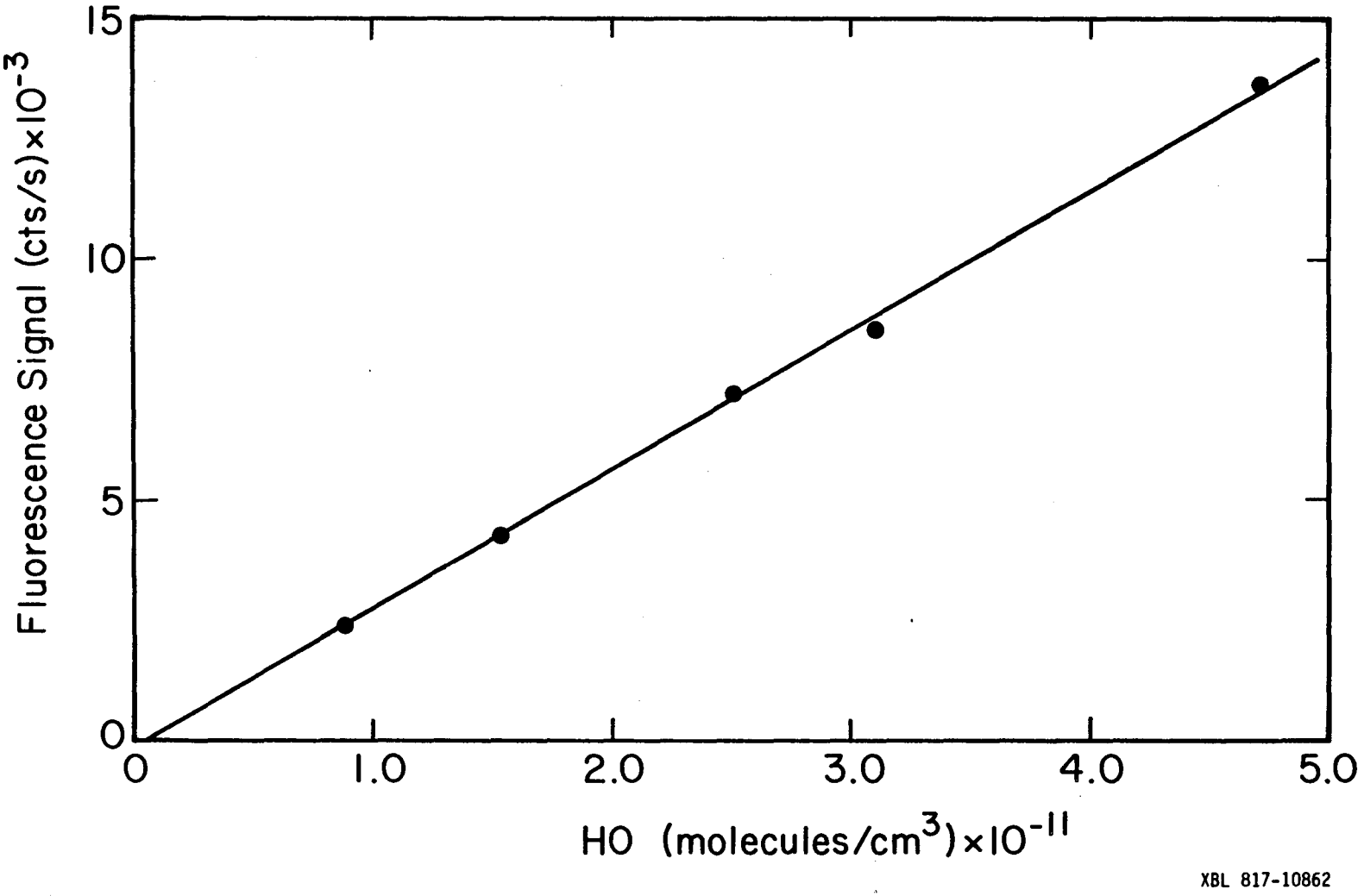

XBL 817-10862

Figure 12. Demonstration of linearity of response and detection sensitivity for HO radical resonance fluorescence system.

The Cl atom detection system was calibrated by Nelson[31] using Cl_2 photolysis with the XeF excimer laser line

$$Cl_2 + h\nu(350) \longrightarrow 2Cl. \qquad (19)$$

Figure 13 shows the calibration as measured by Nelson over the range 2-15 x 10^{10} molecules cm^{-3} with a sensitivity of 4.9 x 10^6 molecules cm^{-3} Hz^{-1}.

The second generation FP/RF cell was identical to the first except the cell arms along the laser axis were lengthened to accomodate fluid flow jackets on either side of the laser/resonance lamp interaction region. The cell was then encased in approximately 2" thick foam insulation. A Neslab Model RTE-4 circulating temperature bath sent either methanol (+20°C to -30°C) or ethylene glycol (+100°C to +20°C) bath fluid through the jackets. Insertion of an Analog Devices Model AD-590 temperature sensor into the interaction region under flowing experimental conditions showed this scheme was inadequate for cooling or heating the cell, and its use was limited to studies at 298K.

The third generation cell shown in Fig. 14 is similar to that described by Wine, Kreutter and Ravishankara.[62] The cell was insulated by a stainless steel vacuum jacket pumped to 10 microns by a trapped glass diffusion pump backed by a rotary roughing pump. It was externally blackened to reduce scattered light from the resonance lamp and then wrapped with aluminum foil to minimize radiative heat exchange with the vacuum jacket. The temperature control jacket on the pyrex cell completely enclosed the interaction region except for entrance

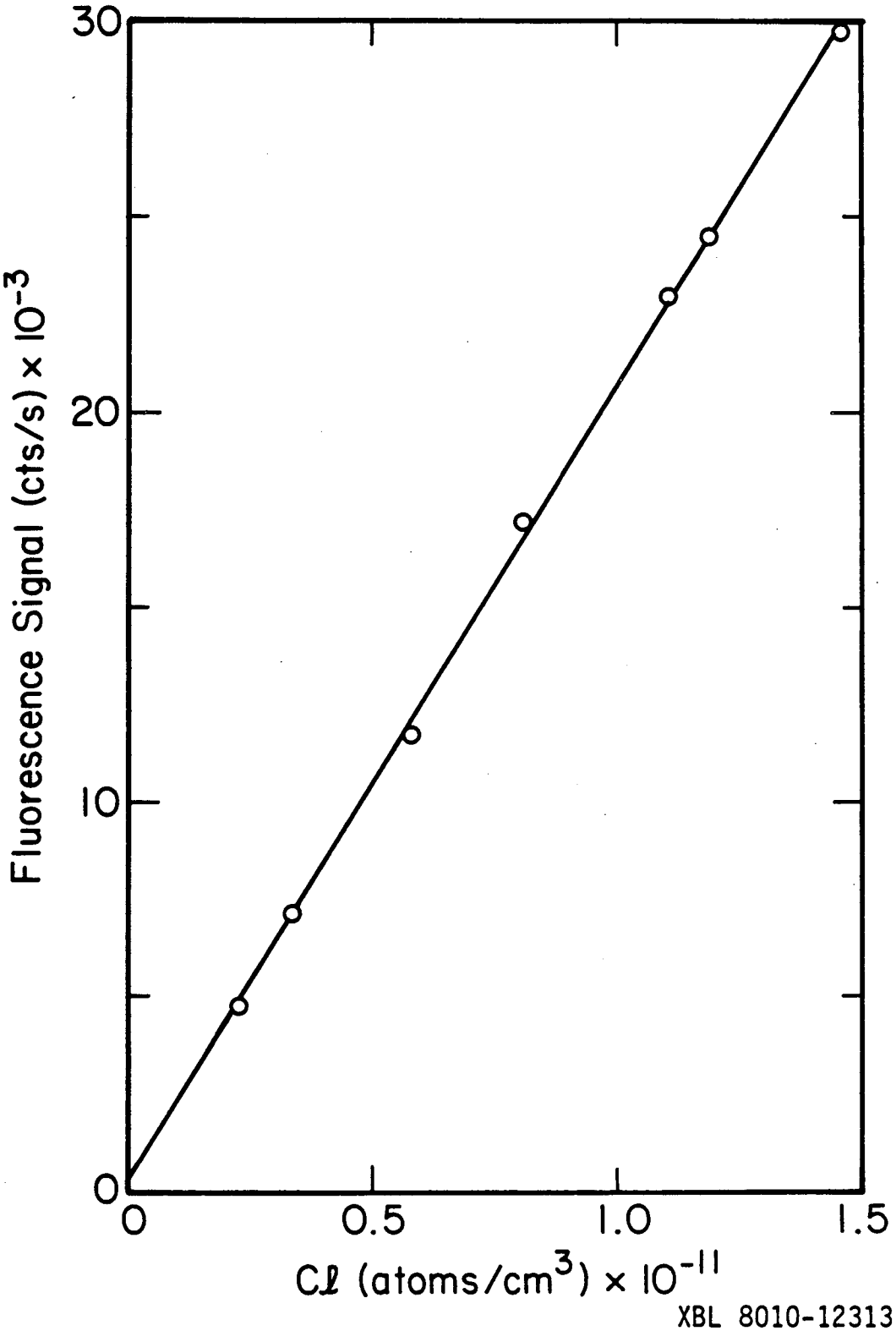

Figure 13. Demonstration of linearity of response and detection sensitivity for Cl atom resonance fluorescence system from Nelson.[31]

Figure 14. Schematic of third generation reaction cell, resonance lamp and detector geometries. PMT, RCA 31034 photomultiplier tube; BRP, 309 nm interference filter; B1 and B2, scattered light baffles; F, Hoya "Peak 320" color filter; W1, CaF_2 window; L1, 1-1/2" dia. x 2" f.l. Suprasil-1 lense; L2, 1" dia. x 1-1/2" f.l. Suprasil-1 lense; W2, Vycor resonance lamp window; RL, resonance lamp; MC, microwave cavity; WH, Woods horn; LA, photolysis laser axis; RC, reaction cell interaction region; RCOJ, reaction cell temperature control outer jacket; VH, vacuum housing; RMI, reaction mixture in; RMO, reaction mixture pump out.

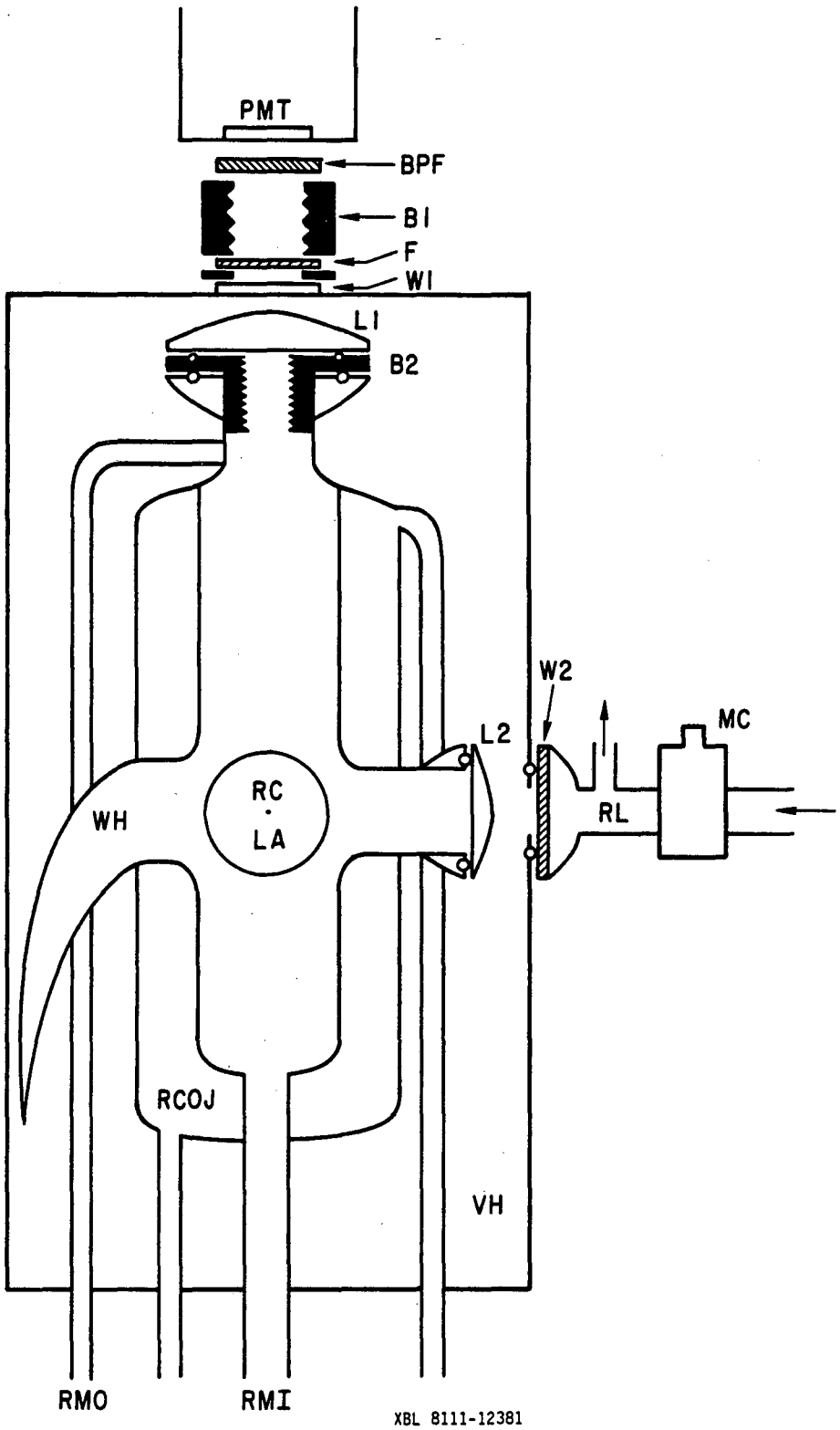
PMT
BPF
B1
F
W1
L1
B2
W2
L2
MC
RC
LA
WH
RL
RCOJ
VH
RMO
RMI
XBL 8111-12381

Figure 14.

and exit windows, and a small woods horn which accepted light from the resonance lamp. The jacket extended down to encase the tube carrying reactants into the cell and acted to equilibrate the gas stream before it entered the interaction region. The cell temperature was again regulated by the Neslab RTE-4 circulating temperature bath from 363K to 250K, with a Neslab Model LT-9 low temperature bath used to cool the cell as low as 218K. An AD-590 temperature sensor, calibrated at the bath temperature, was inserted into the interaction region of the cell under flowing experimental conditions used to measure the actual temperature of the gas stream, which never differed from the bath temperature by more than 3K. The estimated uncertainty in the cell temperature is 1K.

The use of vacuum jacket required that the resonance lamp and photomultiplier be placed further from the interaction region than in previous cells. In order to maintain a reasonable resonance lamp intensity in the cell, an f1.5, 1" diameter, plano convex Suprasil-1 lense was placed 2" from both the interaction region and the window of the resonance lamp, acting as window for the cell. The three lens f1.0 collection system used to gather the fluorescence was replaced by a single, baffled f1.33, 1-1/2" diameter Suprasil-1 lense placed 4" equidistant from both the interaction region and the PMT photocathode. This lense also acted as a cell window. The reduced collection efficiency of the single lens system required less baffling to obtain a signal comparable to the previous system, which in turn resulted in an increase in the amount of scattered laser light detected by the PMT.

To counter this, a Hoya "Peak 320" filter having 60 percent transmission at the resonance line and <0.004 percent transmission at 250nm was inserted before the interference filter used in the otherwise unmodified photomultiplier housing. The reduction in sensitivity that resulted from the use of this filter was compensated by increasing the power to the resonance lamp to 60 watts.

All the cell windows were either Suprasil-1 or CaF_2 and were sealed to either No. 25 or No. 15 O-ring joints by silicone O-rings. The tube running from the monitoring cell to the photolysis cell was made of 1/2" heavy wall (as opposed to 3/8" heavy wall in previous cells) pyrex with minimum distance and curvature in order to avoid pressure drops.

5. Reactant and Carrier Gas Handling

All experiments were performed in a flowing system at a fixed total pressure. The reactant/photolytic precursor concentration was controlled by varying both the immersion temperature and flow rate of carrier gas passing through a saturator containing a small amount of the solid or liquid to be used. The saturator was typically a 10 cm long by 2.5 cm diameter pyrex tube mounted horizontally and equipped with gas exit and entrance ports. Typically, approximately 5 cm^3 of the liquid to be vaporized was placed in the saturator such that the saturating surface area was maximized. Carrier gas was passed through the saturator and vapor from the liquid was entrained in the carrier gas stream before passing into the monitoring and photolysis cell.

Coarse regulation of the vapor concentration was accomplished by placing the saturator into a dewar flask containing a liquid/solid

slush prepared by adding liquid N_2 to the appropriate pure solvent. Table 4 shows the temperatures of various slush baths used for saturation and in the preparation of various reagents. Fine regulation was accomplished by controlling the amount of carrier gas passing through the saturator. After passage through a flow meter, the carrier gas was split into two streams. The flow rate of each stream was controlled by Nupro type "S" stainless steel needle valves. One stream passed through the saturator and was partially saturated, after which it was recombined with the bypass stream and entered either the photolysis or monitoring cell, depending on the experimental mode employed. The flow system was arranged such that the saturator could be completely bypassed and the transmission of the monitoring system in the absence of any precursor (I_0) could be measured.

The usefulness of the external UV monitoring system as a true measure of the precursor/reactant concentration in the photolysis cell is conditional on the verification that: there are no pressure drops due to poor conductance between the monitoring and photolysis cells, there are no thermal heterogeneous or homogeneous reactions that act to change the precursor concentration, or that direct photolysis of the precursor by either the photolysis source or resonance lamp is not appreciable.

The first criterion was satisfied by placing two cross calibrated capacitance manometers at the entrance and exit of the monitoring/photolysis cell system. A minimum amount of tubing with no sharp bends was used between the two cells and a Nupro type "L" throttle valve was placed on the trapped roughing pump at the system exhaust. While

Table 4. Slush baths used in saturation and in the preparation of various reagents

Solvent	T(K)
water	273
carbon tetrachloride	250
O-oxylene	244
acetonitrite	232
m-xylene	225
n-octane	217
trichloroethylene	200
dry ice/isopropanol	196
methanol	175
ethanol	157

operating under experimental conditions, the total input flow rate and the pump throttle valve were adjusted until less than a 1 percent pressure drop was measured. These conditions were at 100 sccm Ar flow rate at 10 torr total pressure. At higher pressures the total flow rate and pump throttle valve were adjusted to maintain the same cell residence time of about 1 second.

The second and third conditions could be satisfied by minimizing the system residence time for the gas and by limiting the output of the resonance lamp to only those lines required for detection. The only true way to verify that these precautions are sufficient is to measure the desired rate constant or quantum yield with the monitoring cell placed before and beyond the photolysis cell, and to show the result is independent of location. The system was set up so as to make this easily possible.

6. Signal Processing and Data Acquisition

The output from the fluorescence collection PMT was sent to a PAR Model 1121 high gain amplifier/discriminator operated in single threshold mode at a level of 0.3 mV. The amplifier/discriminator was interfaced to an SSR Model 1105 photon counter which was modified with an ECL/TTL converter and a high speed line driver. The output signal was recorded by a Nicolet Instruments (Fabritek) Model 1074 Instrument Computer acting as a signal averager in multichannel scaling mode. Typically, 1024 channel segments at channel widths of 2-20 μs were used. The calibration of the width of these channels and the sweep times are detailed in Appendix A.

The signal averager sweep was initiated by the synchronous pulse from a Datapulse Model 102 pulse/delay generator. The laser was

triggered, after a pretrigger period of approximately 225 channels, by the delay pulse from the pulse generator. After averaging 4096 or 8192 laser shots, the data was analyzed by a PDP-8/L minicomputer interfaced to the signal averager and then transferred to paper tape for long term storage.

7. Experimental Procedures and Methods

All experiments done by the resonance fluorescence technique were performed under psuedo-first order conditions in which a family of first order rate constants for the decay of HO or Cl in the presence of a large excess of reactant were measured over a range of reactant concentrations (see Results and Discussion for further details). At the start of each day's experiments all equipment was allowed to warm up for at least 2 hours, or until visible stability had been achieved. The flow system was conditioned with a flow of HNO_3 or H_2O_2 at a concentration greater than contemplated for use later in the day and then the monitor was heated to remove HNO_3 absorbed on the walls.

Each first order rate constant was recorded in the following manner:

1) The entire buffer gas flow was diverted around the saturator and the transmission of the monitor in the absence of reactant/precursor (I_o) was recorded.
2) A portion of the flow was passed through the saturator and adjusted until the desired stable concentration was obtained. This flow was allowed to continue for 10 minutes (approximately 500 cell residence times) during which the gas mixture was allowed to equilibrate with the walls of the cell.

3) The laser was then started and the power meter was monitored until it reached a stable value.
4) The transmission of the monitor with the precursor/reactant flowing (I) and the total pressure (P) were recorded.
5) The energy integration system and the signal averager were started simultaneously.
6) When the desired number of shots were recorded, energy integration was terminated and the final values of I and P were recorded.
7) The buffer gas flow was again diverted around the saturator and the monitor heater was used to heat the monitor to 50°C.
8) The heater was turned off and the muffin fan used to cool the cell to ambient temperature, at which time the final value of I_o was recorded.

Whenever a new sample of HNO_3 was prepared, and periodically during the experiments, the NO_2 content of the HNO_3 was measured using the UV monitor under flowing experimental conditions. The HNO_3 saturator was placed in a warmer than normal slush bath to obtain higher HNO_3 concentrations, which were measured at 200 nm. The wavelength of the monochromator was then quickly changed to 350 nm and the NO_2 concentration measured. In all cases the NO_2 impurity did not exceed the detection limit of 0.05 percent.

The maximum laser repetition rate of 15 Hz was determined by the slowest rate of removal of radicals or atoms from the viewing region. This rate is governed by the sum of diffusion, reaction with buffer gas, and flow. The average first order rate constant for these

processes were 70 s^{-1}. The time between laser shots was chosen such that five radical first order lifetimes (70 ms) had elapsed and the radical concentration was e^{-5} (0.01) times its initial concentration.

When temperature dependent studies were performed the bath fluid was allowed to circulate through the cell for a minimum of 12 hrs prior to use. During this period the cell was filled with one atmosphere of N_2 in order to promote the thermalization of the cell.

C. Flash Photolysis/Laser Absorption Experiments

The flash photolysis/laser absorption experiment is shown in Fig. 15 and detailed below.

1. Photolysis Source

The photolysis source used in these experiments was the same Lumonics TE-860-2M excimer laser described in the previous sections. The only modification to the laser was the replacement of the standard optics with unstable resonator optics to reduce the beam divergence in order to pass the beam down a long absorption cell. This resulted in a reduction of the total pulse energy by 40 percent, however the unfocused energy density of the pulse increased to approximately 150 mJ/cm^2. The beam was slightly smaller than with the standard optics and had a small hole in the center of the beam as a result of the reflecting spot on the unstable resonator output coupler.

2. Energy Measurement

The longer gas residence times in the laser absorption cell required that the laser repetition rate be reduced to 1 Hz and that pulse energy rather than average power be measured. A GenTec Model ED200 pyroelectric joulemeter and a peak reading sample and hold

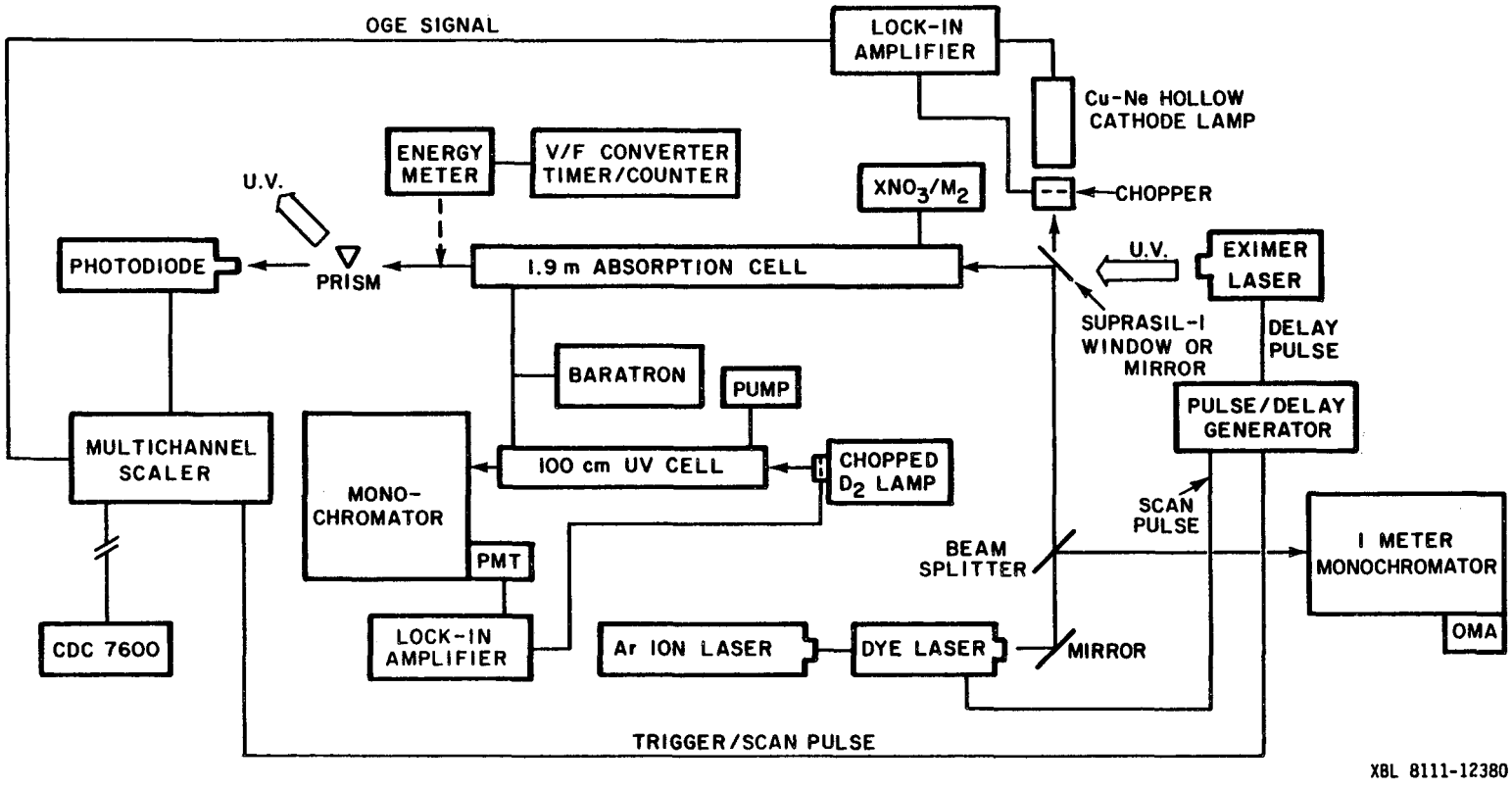

Figure 15. Schematic diagram of FP/LA apparatus.

(PRJ-D) readout with digital display and analog output was used to measure pulse energies. It was interfaced to the energy integration system outlined in Section IIA-2.

Calibration of the joulemeter was done using ClNO gas phase actinometry. Kistiakowsky[63] has shown that the quantum yield for NO production from ClNO photolysis was approximately two. More recent work[55] has shown that the primary process is the formation of Cl atoms followed by the reaction of Cl with ClNO:

$$ClNO + h\nu \longrightarrow Cl(^2P_{3/2,1/2}) + NO(X^2\pi) \qquad (20)$$

$$Cl + ClNO \longrightarrow Cl_2 + NO. \qquad (21)$$

The ClNO photolysis cell had an optical path length of 9.95 cm and volume of 82.25 cm^3. It was externally blackened to prevent photolysis by room light and had a 1.27 cm^2 mask on the cell entrance window to define the photolysis volume (12.64 cm^3). The joulemeter had previously been used with a high energy dye laser and the absoring face had been scorched considerably. A new coating of Nextel 101-C10 flat black enamel (as recommended by the manufacturer), was applied to the face, invalidating previous calibrations. The joulemeter was placed behind the cell with the cell mask insuring that all the energy that was transmitted through the cell fell on the face.

Approximately 120 microns of purified ClNO (see Section IIE for details) was placed in the cell and its absorbance measured at 200 nm with a Cary Model 218C UV-visible spectrometer. The absorption cross

sections used at 200 nm (7.19×10^{-17} cm^2/molecule) and 249 nm (7.5×10^{-19} cm^2/molecule) were those of Ballash and Armstrong.[64] This amount of ClNO was chosen such that the sample was optically thin (<2 percent absorption) at the photolysis wavelength.

The cell was then placed in between the excimer laser and the joulemeter and either 25 or 50 laser shots were fired into the cell with the total energy recorded using the energy integration system. The cell was then removed and the decrease in absorbance measured, from which the change in ClNO concentration could be determined. This procedure was repeated as many as 7 times for each 6 different ClNO photolysis cell fills.

The photolysis of ClNO is first order in ClNO with the rate constant for photolysis give by expression

$$k_{phot} = \frac{1}{2t_{phot}} \ln \frac{[ClNO]_i}{[ClNO]_f} \tag{22}$$

It can be shown that k_{phot} is related to the total photolysis energy by the expression

$$E_{calc}(mJ) \frac{k_{phot} \cdot t_{photo}}{\sigma_{ClNO} \cdot 1.25 \times 10^{15} photons/mJ} \tag{23}$$

$$= 5.33 \times 10^2 \cdot \ln \frac{[ClNO]_i}{[ClNO]_f} \tag{24}$$

The calibration is done by comparing the measured to the total energy calculated from the ClNO absorbances for each photolysis period.

Photolysis energies were corrected for reflection from the cell windows as outlined in Calvert and Pitts.[55] The results of these experiments are shown in Table 5. These results give an average value for (E_{calc}/E_{meas}) of 1.096 ± 0.105, therefore the values obtained with the joulemeter must be multiplied by this factor. The vernier calibration of the PRJ-D readout was adjusted to reflect this result.

3. Dye Laser Probe System

The absorption spectrum of the NO_3 radical is dominated by the intense (0,0) transition at 662 nm. The absorption cross sections and lineshape of the band were measured in this study and are discussed in later sections. This intense transition was chosen for monitoring NO_3 as it was produced in the reaction of HO with HNO_3 and as a product of $ClONO_2$ photolysis.

The laser used as the probe was a Spectra Physics Model 581A single frequency dye laser pumped by a Model 164-05, 5 watt Ar ion laser. The laser was operated using a 50 molar percent mixture of Rhodamine 590 chloride (Pilot R590) and Rhodamine 640 perchlorate (Exciton R640) at concentrations of 1.5×10^{-3} moles/liter in ethylene glycol. The R590 is pumped by the Ar ion laser and collisionally transfers the excitation energy to the lasing R640, which is only weakly absorbing at the pump wavelength. The mixture lased over the 614-672 nm wavelength range. For these experiments, the laser was operated with all the tuning elements except the 3 plate birefringent filter removed. The laser linewidth, as measured using the optogalvanic effect (see Section IID), was approximately 0.5 Å.

Table 5. Joulemeter calibration results.

Absorbance	Total E_{meas}[a]		Total E_{calc}[a]	
$\ln(I_o/I)$ 200 nm	(mJ/cm^2)	$\ln \frac{[ClNO]_i}{[ClNO]_f}$	(mJ/cm^2)	$\frac{E_{calc}}{E_{meas}}$
		Expt. 1		
0[b]	0	0	0	—
1.863[c]	0	0	0	—
1.624	65.1	0.137	73.0	1.121
1.423	63.9	0.132	70.4	1.102
1.246	63.7	0.133	70.9	1.113
1.080	67.8	0.143	76.2	1.124
0.921	69.7	0.159	84.8	1.217
		Expt. 2		
1.253[c]	0			
1.152	54.4	0.084	44.8	0.823
1.050	49.4	0.093	49.6	1.004
0.949	43.0	0.101	53.8	1.251
0.866	40.1	0.092	49.0	1.223
0.801	38.8	0.068	41.6	1.072
0.739	36.9	0.081	43.2	1.170
0.684	35.0	0.077	41.0	1.173
		Expt. 3		
3.802[c]	0	0	0	—
3.008	116.7	0.234	124.9	1.070
2.379	113.8	0.235	125.1	1.099
		Expt. 4		
4.383[c]	0	0	0	—
2.963	210.4	0.426	227.0	1.079
		Expt. 5		
0.776[c]	0	0	0	—
0.571	164.4	0.307	163.5	0.995
		Expt. 6		
1.140[c]	0	0	0	—
0.882	137.2	0.257	136.8	0.997

a E = (recorded energy x 1.171) (12.64 $cm_2/82.25\ cm^2$)
Window reflection factor = 1.171

b Empty cell

c New cell ClNO fill.

The output power of the dye laser was measured using an internal power meter. The power level of the dye laser could be set in three possible ways. Both the dye and Ar ion lasers had photodiodes which monitored their output light level and could feed back to the ion laser power supply to accomplish regulation. In addition, the ion laser could be current stabilized and the current level set to obtain a certain light level. The light level controls were superior to current stabilization for long term stability, but the 10 kHz bandwidth of the light stablization electronics induced a high frequency ripple in the laser output which was intolerable for these experiments. This ripple was not present under current stabilization, and since the DC laser output was stable to within 2 percent over the course of an experiment, this mode was used. Frequency stabilization was better than the laser linewidth during these experiments.

A pellicle was used to split off approximately 8 percent of the beam and directed it through an Interactive Technologies Model CT-103 1 meter monochromator equipped with a 1200 line/mm grating blazed at 5000 Å operated in second order. The output of the monochromator was sent to a PAR Model 1205D vidicon tube from which an optical multichannel analyzer (PAR Model 1205A) displayed the wavelength onto a CRT with a resolution of 0.4 Å. The wavelength scale of the optical multichannel averager was calibrated by overlaying the output from a neon pilot lamp on to the dye laser signal. The neon lines used in this wavelength region, as measured by Paschen[65] were 6721.1, 6678.3, 6598.9, 6532.8 and 6506.5 Å. The dye laser was positioned to the peak of the NO_3 absorption at 6619 Å using this calibration.

4. Reaction Cell and Flow System

The reaction cell consisted of a 191.5 cm optical path length by 3.3 cm i.d., jacketed quartz cell with stainless steel end caps and CaF_2 windows. Flow through the reactor was of the plug type, with the reactant gases entering at one end through a 3/8" Cajon "ultra-torr" fitting and exiting at the opposite end through a 3/4" fitting. After exiting the cell, the gas stream passed down a short section of 3/4" tubing into a UV monitoring system identical to that described in Section IIB-3, and then through a throttled and trapped rotary roughing pump.

Pressures in the cell were measured with an MKS Baratron Model 310BHS-1000 capacitance manometer located between the monitoring and reaction cell. The cell volume was measured by expansions from a calibrated volume to be 1473 cm^3 with the remaining flow system occupying approximately 775 cm^3.

Since an earlier reaction cell/monitoring cell system showed a large pressure drop between the two cells, it was decided to test this newer system with the 3/4" connecting tubing for similar problems. This was done by measuring the absorbance of an NO_2/N_2 mixture flowing through both cells under experimental conditions. The chopped beam from a Liconics Model 401 helium-cadmium laser, operating at 442 nm, was split and passed through both the reaction and monitoring cells. Two similar detectors monitored both beams with their outputs sent to a common lock-in amplifier referenced to the chopper. A simple switch enabled each detector to be read individually. Since a common laser source was used in both cells, the ratio of the absorbances in

each cell was independent of both absorption cross section and spectral resolution. The ratio of number densities in each cell is given by

$$\frac{N^{reac.}}{N^{mon.}} = \frac{\ell^{mon.}}{\ell^{reac.}} \frac{\ln I_o^{reac.}/I^{reac.}}{\ln I_o^{mon.}/I^{mon.}} \qquad (25)$$

which should be one if there are no pressure drops. Table 6 shows the results of several determinations at 10 and 1 Torr total pressure, confirming that the pump throttle valve was the limiting orifice in the flow system. Determination at higher pressures were not conducted, since higher pressures were attained by increasing input flow rates and further throttling the pump.

The photolysis pulse, after passing through a thin Suprasil-1 plate tilted at 45° to the beam axis, was propagated coaxially down the photolysis cell. A circular, 0.5 cm^2, black anodized orifice served to define the beam and excluded the small central hole, insuring a somewhat spatially uniform photolysis pulse. A similar but smaller, 0.178 cm^2, orifice on the cell exit window served to further define the photolysis beam. As a result, the total photolysis volume was larger than the laser probe volume, which was strictly defined by the cell exit orifice. The effect of this scheme was to minimize the effects of diffusion of products and reactants in and out of the probe beam and to insure that the probe sampled only those regions of the cell subject to photolysis.

The dye laser probe beam intersected the photolysis beam at a 90° angle on the face of the Suprasil-1 plate. Approximately 20 percent

Table 6. FP/LA pressure drop calibrations

Experiment	I_o^{reac}	I^{reac}	I_o^{mon}	I^{mon}	N^{reac}/N^{mon}
			P = 10 Torr		
1	555	58	548	175	1.03
2	526	175	535	298	0.98
3	530	171	542	296	0.97
4	520	163	559	307	1.00
5	527	156	564	304	1.02
Average					1.00 ± 0.03
			P = 1 Torr		
6	493	210	556	357	1.00
7	493	220	556	367	1.01
8	505	206	561	357	1.03
Average					1.01 ± 0.02

ℓ^{mon} = 99.3 cm ℓ^{reac} = 191.5 cm

of the beam was reflected off the plate and traveled coaxially to the photolysis beam down the reaction cell. After emerging from the photolysis cell, the two beams were split by a quartz prism, and the probe beam was focused through a 670 nm interference filter on to the face of a fast photodiode detector. Energy measurement was accomplished by inserting the pyroelectric joulemeter in between the cell exit window and the quartz prism. The energy could not be measured during the course of the experiment but instead was measured before and after each experiment, and a simple average was taken.

The handling of reactants and the flow system was very similar to the FP/RF experiments. The higher HNO_3 concentrations used in these experiments required the use of a warmer slush bath for the saturator (244K for the FP/LA vs 232K for FP/RF) and a change in the monitoring wavelength, from 200 nm to 215 nm. Chlorine nitrate was held in a saturator at 195K for the photodissociation experiments.

5. Signal Detection and Data Acquisition

A fast photodiode detector/amplifier of in-house design and construction was used to monitor the photolysis probe beam. The system, shown schematically in Fig. 16, consisted of an EG and G Model SGD-100A silicon photodiode whose output was sent to a National Semiconductor LH0032CD fast operational amplifier. The amplifier was tied to a unity gain National LH0003 current amplifier, which served as a line driver for the 100 ns cable which terminated into a 50 load at the signal averager. The calculated bandwidth of the detector/ amplifier was 10 MHz. This was confirmed by placing a red light emitting diode, powered by a high speed pulse generator, in front of

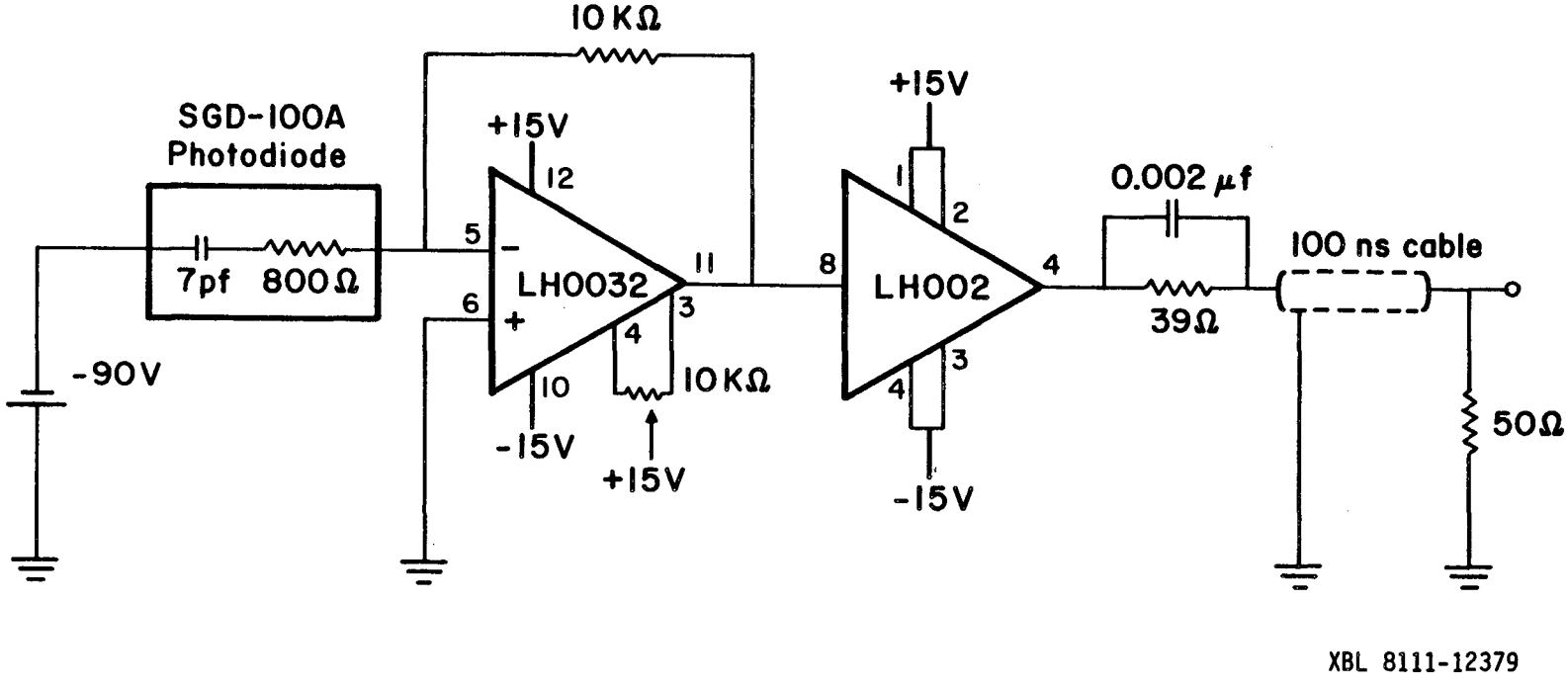

Figure 16. Schamatic diagram of photodiode detector electronics.

the detector face. The detector was able to accurately reproduce 500nS square wave pulses from the pulse gernator, as viewed by an oscilloscope and by the signal averager.

The fast analog signals from the photodiode were recorded using a Biomation Model 805 transient waveform digitizer. The digitized waveforms were transferred to the Fabritek 1074 signal averager/computer system for storage, display and averaging. The timing of the waveform digitizer was verified, and is described in Appendix A. A typical experiment was the sum of either 256 or 512 laser shots. After completion of an experiment, the results were stored on paper tape and later transferred to the Lawrence Berkeley Laboratory computing system for analysis. The photolysis laser and signal averager were triggered in a manner identical to that described in Section IIB-6.

6. Experimental Procedures

As in the FP/RF experiments, the reaction of HO with HNO_3 was studied under pseudo first order conditions. The warm up of the experimental equipment and cell conditioning was conducted as in the FP/RF experiments and the experimental procedure was identical with the following exceptions:

1) The photolysis laser energy was not measured during the experiments but rather an average of 20 shots taken before and after each experiment was recorded.
2) The specific HNO_3 sample used in these experiments was found to have 0.15 percent NO_2, which at higher pressures was a significant perturbation on the HO decay due to reaction (9).

3) The photolysis laser repetition rate was reduced to 1 Hz to avoid significant photolysis of the precursor or accumulation of undesirable photolysis products during the typical 6 second cell residence time.

D. NO_3 Absorption Cross Section Spectrometer

1. Modifications to FP/LA Experiment

This experimental apparatus was virtually identical to the FP/LA experiment with the exceptions noted below:

1) The excimer laser was eliminated and the Suprasil-1 beam splitter was replaced by a 50 percent reflection coated CaF_2 beamsplitter.

2) The fast photodiode detector was replaced by a slower, higher gain, United Detector Technologies PIN-8LC photodiode/amplifier.

3) The dye laser was modified to include a stepping motor (200/revolution) with a 2.5:1 gear ratio to drive the birefringent filter. In some experiments the single frequency tuning elements were used in the dye laser. With these elements it had a line width of less than 200 MHz (0.00029 nm) as measured by a Tropel Model 240 spectrum analyzer and a sweep width of 15 GHz (0.022 nm).

4) The transient waveform digitizer was replaced by an SD-72/4, 4 channel, 9 bit, A/D converter plug in for the Fabritek signal averager. A Wavetek Model III waveform generator was used to synchronously drive both the external address advance of the signal averager and the stepping motor wavelength drive of the dye laser. Typical scan conditions were 2.5 pulses per second covering approximately 0.023 nm per pulse.

5) The single frequency 15 GHz scans were recorded directly on an x-y recorder at scan times of approximately 120 seconds. The "sweep out" of the dye laser etalon controller was used to drive the recorder x-axis. These scans were made only at selected wavelengths, including regions where a neon line was available for wavelength calibration.

6) The UV monitoring system was converted to a visible monitor by replacing the UV grating with a 1200 lines/mm grating blazed at 5000 Å, and using a 4000 Å long pass interference filter as an order sorter for the grating.

7) All experiments were conducted at ambient temperature (295-297K) and atmospheric pressure. The cell temperature was measured by two thermometers strapped to each end of the cell, which always agreed to within 0.4K. The cell pumping system was replaced by a tube which vented the cell exhaust into a nearby fume hood.

2. Wavelength Calibration

The dye laser wavelength was determined by both internal and external methods. The external determination was done using the previously described OMA system. This was used only to position the laser at the starting point for the scans and to observe the laser as it scanned.

Internal calibration of the laser was accomplished using the opto-galvanic effect.[66-68] This was done by simultaneously recording into a second quadrant of the signal averager the impadence change produced in a neon-filled hollow cathode discharge lamp (Perkin Elmer WL36024) when that portion of the beam passing through the CaF_2 beam

splitter into the lamp comes into coincidence with a neon transition. A schematic of the opto-galvanic system is shown in Fig. 17. The wavelengths of these transitions are known within 10^{-3}nm,[65] hence providing excellent calibration. The width of these transitions is about 3 GHz, much narrower than the bandwidth of the laser when operated multimode with the birefringent filter; and these lines were used to estimate the laser bandwidth, which was found to be about 0.05 nm. The laser linewidth and wavelength stepwidth were found to be a non-linear function of position on the dye lasing curve. To account for this, the neon calibration points were fit to a 3 term polynomial, and in this way the wavelength could be determined to within a single channel width of the signal averager over the entire spectral range. The neon lines used for calibration over the entire spectral range of this study (673-614 nm) were 672.15, 667.83, 659.89, 653.29, 650.65, 640.23, 638.30, 633.44, 630.48, 626.65, 621.73, 616.36 and 614.31 nm.

3. Experimental Methods and Data Aquisition

The experiments were performed in a slowly flowing system at one atmosphere pressure such that the residence time in the absorption cell was approximately 1100 seconds. Ozone was picked up in a flow of N_2 through a silica gel trap held at 225K by an m-xylene slush. Its concentration was measured in the reaction cell by absorption at the NO_3 minimum at 650.0 nm, and it was redundantly measured beyond the cell in the external visible monitor at 488.0 nm. A separate stream of 1 percent NO_2 in N_2 was set up; and by switching flows the NO_2 mixture plus the N_2 carrier stream (later to be used for O_3) went

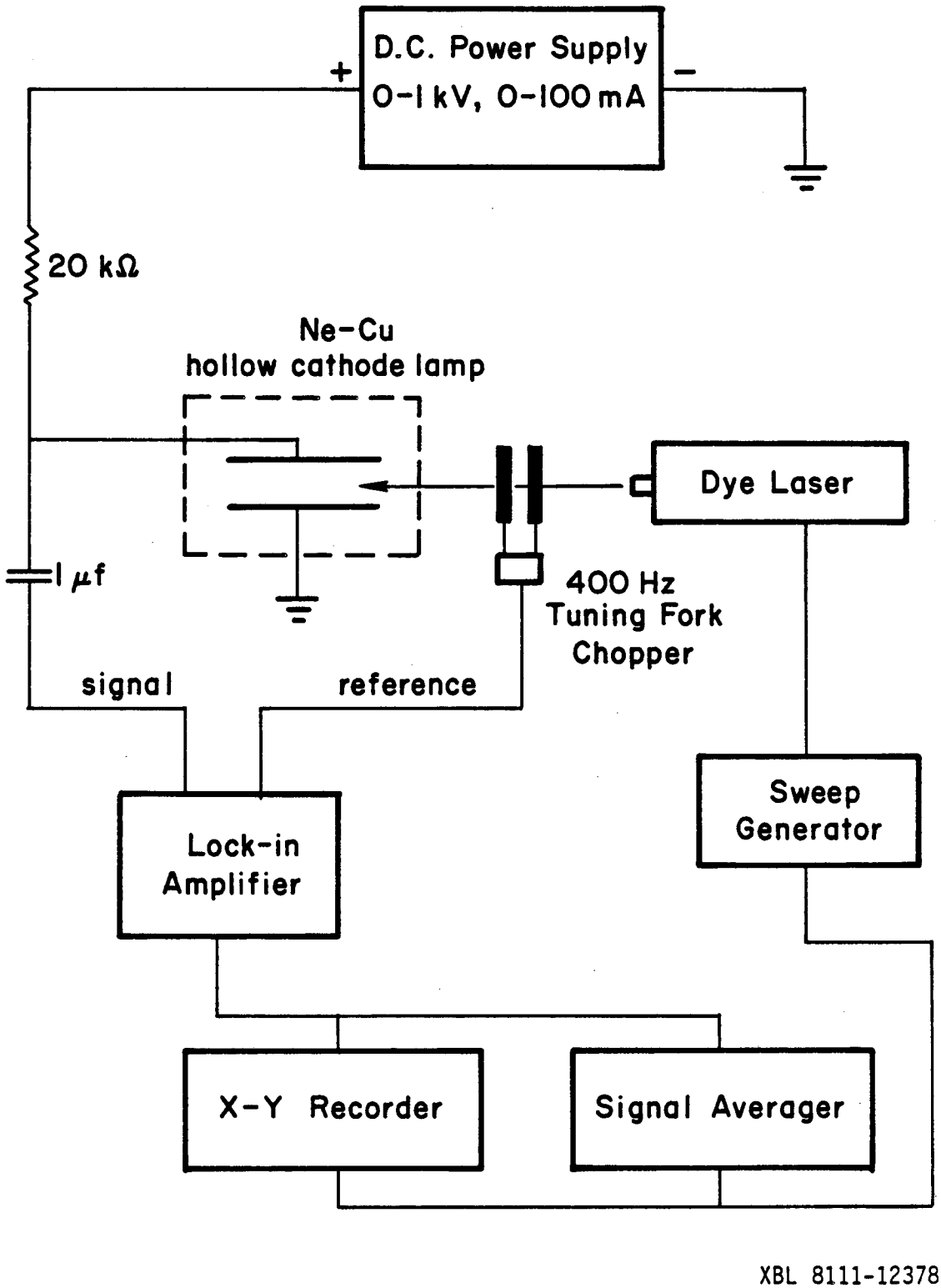

Figure 17. Schematic diagram of opto-galvanic effect laser wavelength calibration system.

through the visible monitor where the NO_2 concentration was measured by light absorption at 488.0 nm (σ = 2.97 x 10^{-19} cm^2 $molecule^{-1}$).[49] The monochromator was set at a bandpass of 0.1 nm to correspond to that used to measure the NO_2 cross section. The flowing streams of O_3 and NO_2, each carried by N_2 at one atmosphere, were mixed in an external manifold with a volume such that the NO_3 concentration was calculated to attain at least 95 percent of its steady state value before entering the reaction cell. The flowing system was monitored at the NO_3 absorption peak at 661.9 nm until the absorption there reached a stable, maximum value. Scans were always started at wavelengths slightly longer than the first neon calibration peak at 672.15 nm and always went to decreasing wavelengths. The ozone cross-sections used at these wavelengths were those of Vigroux:[69] 2.61 x 10^{-21} cm^2 $molecule^{-1}$ at 650.0 nm and 8.78 x 10^{-22} cm^2 $molecule^{-1}$ at 488.0 nm. At each of these wavelengths there was an absorption by NO_3 of about 5 percent, but these small absorptions were corrected for using the average cross sections found by Mitchell et al.[45] and by Graham and Johnston.[44]

E. Reactants and Gases

The carrier gases and excimer laser helium was supplied by Lawrence Berkeley Laboratory and were used without further purification. The several mixtures of NO_2 in N_2, the 0.1 percent Cl_2 in helium, and the 10 percent F_2 in helium mixture used in the excimer laser were supplied by Matheson Company. Typical impurity levels for the gases supplied by LBL, the NO_2 supplied by Matheson and the ClNO used as an actinometer are shown in Table 7. The Kr and Xe used in the excimer

Table 7. Suppliers typical impurity levels for gases used.

	High dry Nitrogen[a]	Pure Helium[a]	Purified Argon[a]	High Purity Helium[b]	High Dry Oxygen[a]	CH_4[a]	NO_2[c]	ClNO[c]
N_2	99.999	1 ppm	5 ppm	14 ppm	500 ppm	e	—	"low"
He	—	99.998	—	99.995	—	—	—	—
Ar	5 ppm	0.1 ppm	99.999	1 ppm	4000 ppm	e	—	—
O_2	1.5 ppm	0.2 ppm	2 ppm	1 ppm	99.5	3	—	"low"
H_2O	1.5 ppm	0.3 ppm	—	12 ppm	1.5 ppm	e	0.06	—
CO_2	—	0.1 ppm	0.5 ppm	1 ppm	10 ppm	e	—	—
Ne	—	—	—	14 ppm	—	e	—	—
THC[d]	—	—	0.5 ppm	1 ppm	3	99.99	—	—
H_2	—	—	1 ppm	1 ppm	—	—	—	—
NO	—	—	—	—	—	—	<5 ppm	—
ClNO	—	—	—	—	—	—	Nil	99.2
NO_2	—	—	—	—	—	—	99.9	0.5

a LBL issue.

b Matheson Co., used in halogen/helium mixtures.

c Matheson Co., supplier.

d Total hydrocarbons as CH_4.

e Total < 100 ppm.

laser were Airco grade 4.5 (99.995 percent) which met or exceeded the purity requirements stated by the laser manufacturer.

The preparation and purification of each reactant used is described in the following sections.

1. Nitric Acid

Nitric acid was prepared by the method described by Johnston, Chang and Whitten.[61] A slurry of potassium or sodium nitrate in 96 percent H_2SO_4, prepared in a 250 ml round bottom flask, chilled, and degassed, was held at ~300K. Anhydrous nitric acid was distilled from the reaction vessel into a storage flask immersed in an O-xylene slush at 244K, with the first and last portions of distillate being discarded. The slurry was kept below 313K to minimize decomposition of HNO_3, and the receiving flask was maintained above 233K to avoid bringing water or H_2SO_4 over with the HNO_3.

The NO_2 impurity present in the HNO_3 was found to be as high as 0.2 percent. The lowest impurity levels were found when an excess of H_2SO_4 was used. No difference in the quality of the product was observed when $NaNO_3$ was substituted for KNO_3; however, it was noted that the finer $NaNO_3$ granules seemed to give a higher yield of HNO_3. When not in use the HNO_3, a clear liquid and a white solid, was stored at 196K for as long as 30 days without any change in impurity levels.

2. Hydrogen Peroxide

Hydrogen perioxide was purchased as a 90 or 98 percent solution from FMC Corporation. The peroxide contained a trace amount of a non-volatile inorganic sodium salt used as a stabilizer. Molina[70]

has shown that the amount of stabilizer introduced into the gas phase under the saturation method employed here is negligible.

3. Chlorine

The Cl_2 used as a precursor for photolytic production of Cl atoms in the reaction with HNO_3 was obtained from Matheson as "high purity" (99.5 percent). It was purified by several freeze-thaw distillations and stored in a darkened bulb until use.

4. Nitrosyl Chloride

The ClNO used as a gas phase actinometer was also obtained from Matheson as "97 percent min." It was also purified by several freeze-thaw distillations from 196 to 77K and stored in a darkened bulb.

5. Ozone

Ozone was prepared in the following manner. A stream of O_2 was purified by passing it through a silica tube with copper turnings at 900K and through a column of 5 percent palladium or alumina at 620K to convert hydrocarbon impurities to CO_2 and H_2O, which were removed by absorption on columns of ascarite and P_2O_5-coated glass beads. The purified O_2 was passed through an Ozone Research and Equipment Company silent discharge ozonator, where about 7 percent of the O_2 was converted to O_3. After leaving the ozonator, the O_3/O_2 mixture was passed through a silica gel trap at 196K where the O_3 was preferentially adsorbed and stored for later use.

6. Di-nitrogen Pentoxide

Di-nitrogen pentoxide was prepared by reacting NO_2 saturated high purity O_2 with a large excess of O_3 in O_2 emerging from the ozonator, as described by Schott and Davidson.[41] The $N_2O_5/O_3/O_2$

stream was passed through a trap held at 196K where the N_2O_5 was deposited as thin, needle-like white crystals, with the rest of the mixture emerging from the trap. The N_2O_5 was used immediately after preparation to avoid complications arising from the thermal decomposition.

7. Chlorine Monoxide

Chlorine monoxide (used in the preparation of $ClONO_2$) was prepared by the method of Cady.[71] Anhydrous Cl_2 was further dried by bubbling through 18M sulfuric acid and then passed through a 1 meter long, 2.5 cm O.D. pyrex tube packed with a porous bed of yellow mercury (II) oxide mixed with crushed glass. The reaction

$$2Cl_2 + (n+1)\ HgO \longrightarrow Cl_2O + HgCl_2\ nH_2O \qquad (26)$$

converts some of the Cl_2 to Cl_2O. The stream then passed through a trap held at 196K and outfitted with a P_2O_5 drying tube. Chlorine monoxide, containing about 20 percent Cl_2, condensed in the cold trap and was stored at 196K for further use.

8. Chlorine Nitrate

Chlorine nitrate was prepared via the reaction of Cl_2O with N_2O_5 by the method of Schmeisser.[72]

$$Cl_2O + N_2O_5 \longrightarrow 2ClONO_2 \qquad (27)$$

Cl_2O was condensed into a trap containing excess, freshly prepared, N_2O_5. The trap was equipped with a P_2O_5 drying tube and placed

in a trichloroethylene slush at 200K. The slush was allowed to warm to 273K during which reaction (27) occurred. The $ClONO_2$ was distilled from the trap held at 175K (methanol slush) into a trap at 157K (ethanol slush), leaving behind any residual NO_2, N_2O_5 or HNO_3 (an impurity in the N_2O_5). The $ClONO_2$ was then pumped-on at 157K to remove any CL_2 and Cl_2O impurities. Both impurities were removed below their detection limit by UV absorption. Absorption cross-sections measured on the final product agreed well with Molina and Molina.[57] The $ClNO_3$ was stored at 196K until further use.

III. RESULTS

A. Hydroxyl Radical Kinetics

1. Interpretation of data.

All the experiments presented in this section (as well as the $Cl+HNO_3$ experiments) were performed under pseudo-first order conditions in which the ratio of precursor/reactant to radical concentrations were always greater than 100 and often as high as 10^4. In these experiments no second or third order processes affecting the radical concentrations were found to be important. The hyroxyl radical concentration as a function of the time after the generating photolytic flash in given by

$$[HO]_t = [HO]_{t=0} \, e^{-k't} \tag{28}$$

where the first order rate constant k' is given by the expression

$$k' = k\,[\text{Reactant}] + k_d \quad . \tag{29}$$

The quantity k is a second order rate constant for the reaction of HO radicals with the reactant and any impurity proportional to the reactant concentration (e.g., NO_2 in HNO_3 reactant). The rate constant k_d is the sum of first or psuedo-first order rate constants describing the removal of HO radicals by diffusion out of the viewing region, reaction with the carrier gas or its impurities, or any other removal process not proportional to the reactant concentration. The quantity k' in (28) is best determined by linearizing the expression to give

$$\ln([HO]_t) = \ln([HO]_{t=0}) - k't \qquad (30)$$

and using a least squares analysis to obtain k' and $\ln([HO]_{t=0})$.

In the resonance fluorescence experiments, the number of fluorescence counts recorded in each channel of the signal averager is proportional to the HO radical concentration. A pretrigger period was recorded in which the number of fluorescence counts not resulting from HO radicals produced in the flash could be determined for later subtraction from the entire HO radical decay. Following the essentially instantaneous production of HO radicals in the flash, the HO concentration decays exponentially with the proportional fluorescence signal returning to the pretrigger baseline during the recording period on all but the slowest of decays. Since any proportionality constants cancel, linearization of the of the fluorescence signal is equivalent to expression (30) with the $\ln(\text{Signal}_{t=0})$ related to the HO radical concentration by the system calibration. A typical experimental run is shown in Fig. 18. The linearization of the fluorescence signal and the least squares fit to that data is shown in Fig. 19. The least squares fit was always started 50 channels after the laser fires to avoid possible problems of non-linear response of the PMT following exposure to any scattered laser light. The weighting of the fluorescence signal in the least squares fit was adjusted to reflect the linearization of the signal as outlined in Bevington.[74] The first order rate constants obtained from the least squares fit were plotted as a function of precursor concentration, from which the second order rate constant (k) and the quantity k_d in (30) may be obtained from the slope and intercept of the straight line fit to the data.

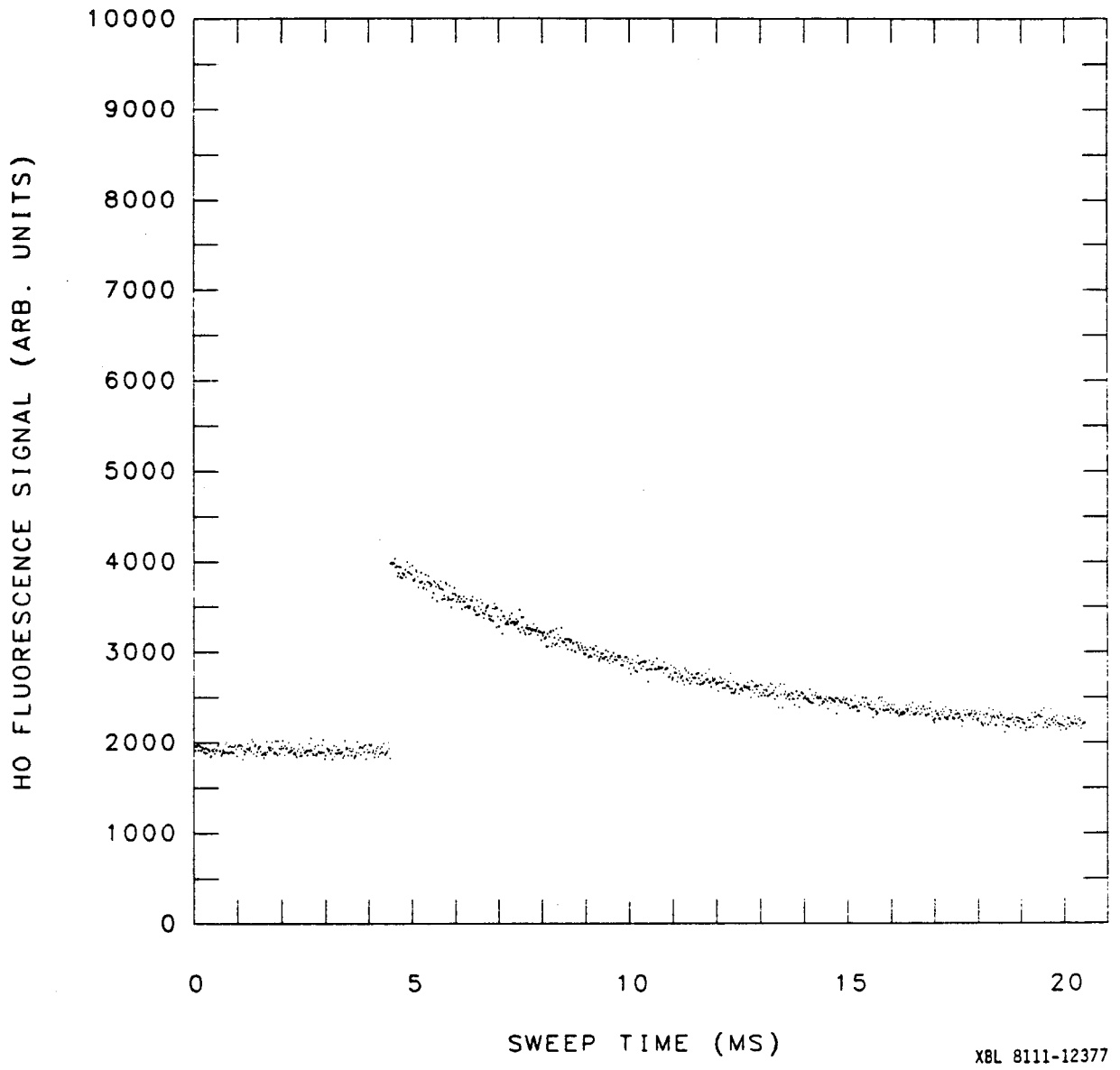

Figure 18. Typical fluorescence signal for 8192 shots as recorded using signal averager.

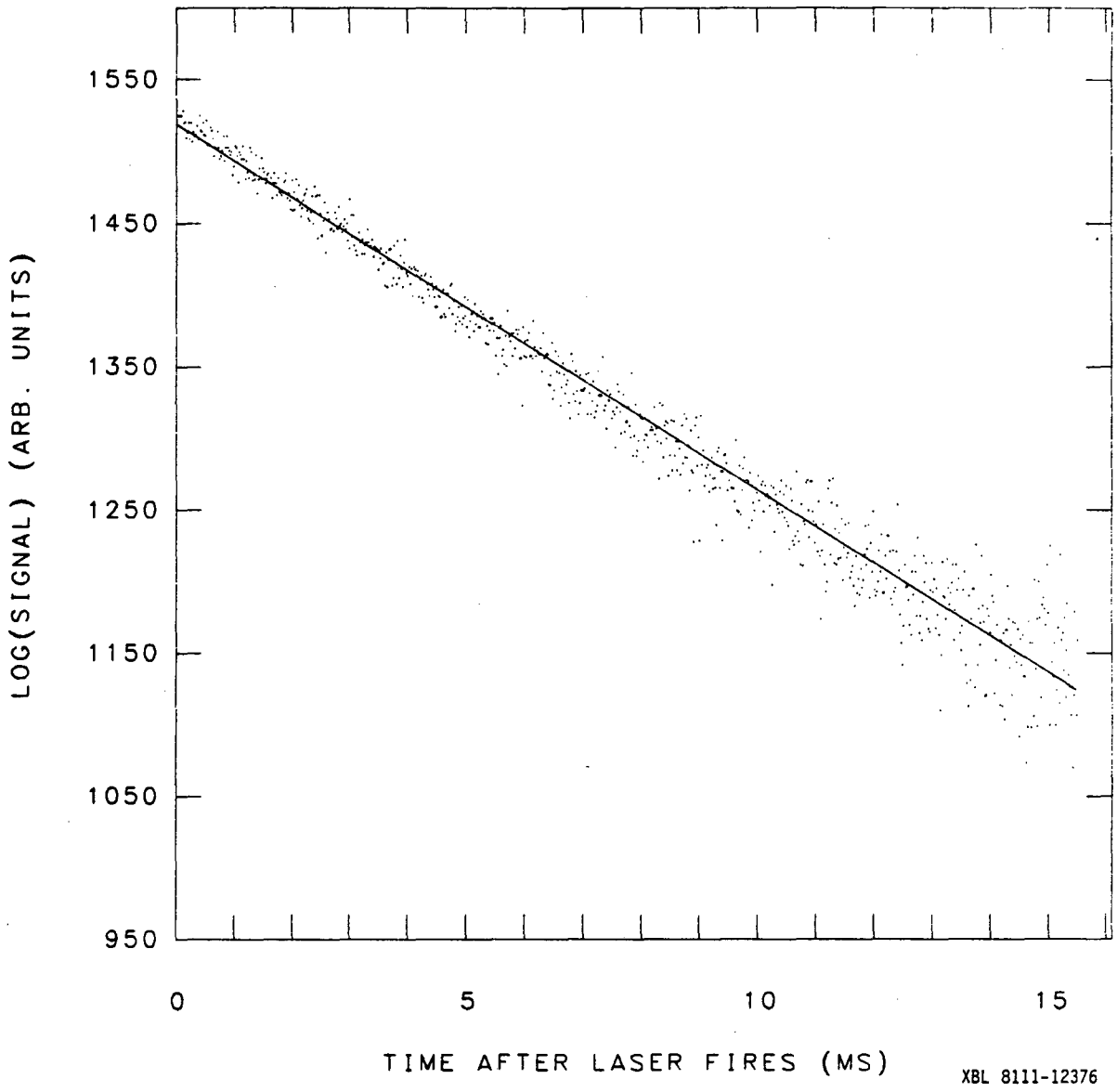

Figure 19. Linearization of decay in Fig. 18, dots, and linear least squares fit to data, solid line. Least squares fit starts 1 ms after laser fires.

The concentration of NO_2 in the HNO_3 samples used in the FP/RF experiments was always found to be less than the detection limit of 0.05 percent. Corrections to k' due to the contribution of reaction (9) are negligible under these conditions (see Appendix B) and were not applied. No corrections to k' in the reaction of HO with H_2O_2 were necessary.

The time evolution of the NO_3 product from the reaction of HO with HNO_3 is governed by the reactions

$$HO + HNO_3 \longrightarrow NO_3 + H_2O \qquad (2)$$

$$HO + NO_2 \xrightarrow{M} HNO_3 \qquad (9)$$

$$NO_3 \longrightarrow \text{(diffusion, reaction, etc.)} \qquad (31)$$

where k_{31} is a rate constant describing various removal rates for NO_3 over the sweep time of the experiment. If one defines the following parameters as

$$\alpha_1 = k_{31}$$

$$\alpha_2 = k_2[HNO_3] + k_9[NO_2][M]$$

$$\alpha_3 = k_9[NO_2][M]$$

then the differential equations for the time behavior of HO and NO_3 are given by

$$\frac{d[HO]}{dt} = -\alpha_2[HO] \qquad (32)$$

$$\frac{d[NO_3]}{dt} = (\alpha_2-\alpha_3)[HO] - \alpha_1[NO_3] \quad . \tag{33}$$

These differential equations can be solved[75] to give the expression

$$[HO]_t = [HO]_{t=o}\, e^{-\alpha_1 t} \tag{34}$$

which is identical to the result in the resonance fluorescence experiments and the expression

$$[NO_3]_t = [HO]_{t=o} \left(\frac{\alpha_2-\alpha_3}{\alpha_2-\alpha_1}\right) \left(e^{-\alpha_1 t} - e^{-\alpha_2 t}\right) \quad . \tag{35}$$

The quantity of $\alpha_2-\alpha_3$ is the psuedo-first order rate constant for reaction (2).

The data in these experiments were recorded in transmission mode. After a pretrigger period of 200 channels, the photolysis laser is fired and a rapid decrease in the transmitted laser intensity ensues as the NO_3 product from reaction (2) builds up. After peaking, the NO_3 slowly is removed by processes described by k_{31} and the intensity slowly returns to baseline (though usually not on the time scale of the rise). Taking the average value of the transmission during the pretrigger period as I_o, and knowing the absorption cross section at the monitoring wavelength (see Section IIID), Beer's law was used to calculate the $[NO_3]$ at any time during the sweep

$$[NO_3]_t = \ln\left(I_o/I_t\right) \Big/ \sigma_{NO_3} \quad . \tag{36}$$

The time domain spectrum of NO_3 was then fit to a double exponential expression of the form

$$[NO_3]_t = C \left(\frac{\alpha_2-\alpha_3}{\alpha_2-\alpha_1}\right) \left(e^{-\alpha_1 t} - e^{-\alpha_2 t}\right) \tag{37}$$

using the non-linear least squares fitting routine VARPRO[76] supplied as a library routine in the Lawrence Berkeley Laboratory computing system. The routine returns the values of α_1, α_2 and C. The quantity α_3 is calculated from the known pressure, NO_2 concentration, and rate constant for reaction (9). Figure 20 shows a typical experiment as recorded and scaled to 100 percent transmission while Fig. 21 shows the same data converted to $[NO_3]$ and the double exponential fit to the data.

The product yield of NO_3 from reaction (2), ϕ_{prod}, is defined as

$$\phi_{prod} = \frac{NO_3 \text{ produced}}{HO \text{ reacted with } HNO_3} = \frac{C}{[HO]_{t=o}} \tag{38}$$

where the ratio of fitting parameters in the fit $(\alpha_2-\alpha_3/\alpha_2-\alpha_1)$, modify the fitting parameter C to reflect the partitioning of $[HO]_{t=o}$ between reactions (2) and (9). The quantity $[HO]_{t=o}$ is calculated from the measured photolysis energy, HNO_3 precursor concentration, and the known HNO_3 absorption cross section at the photolysis wavelength

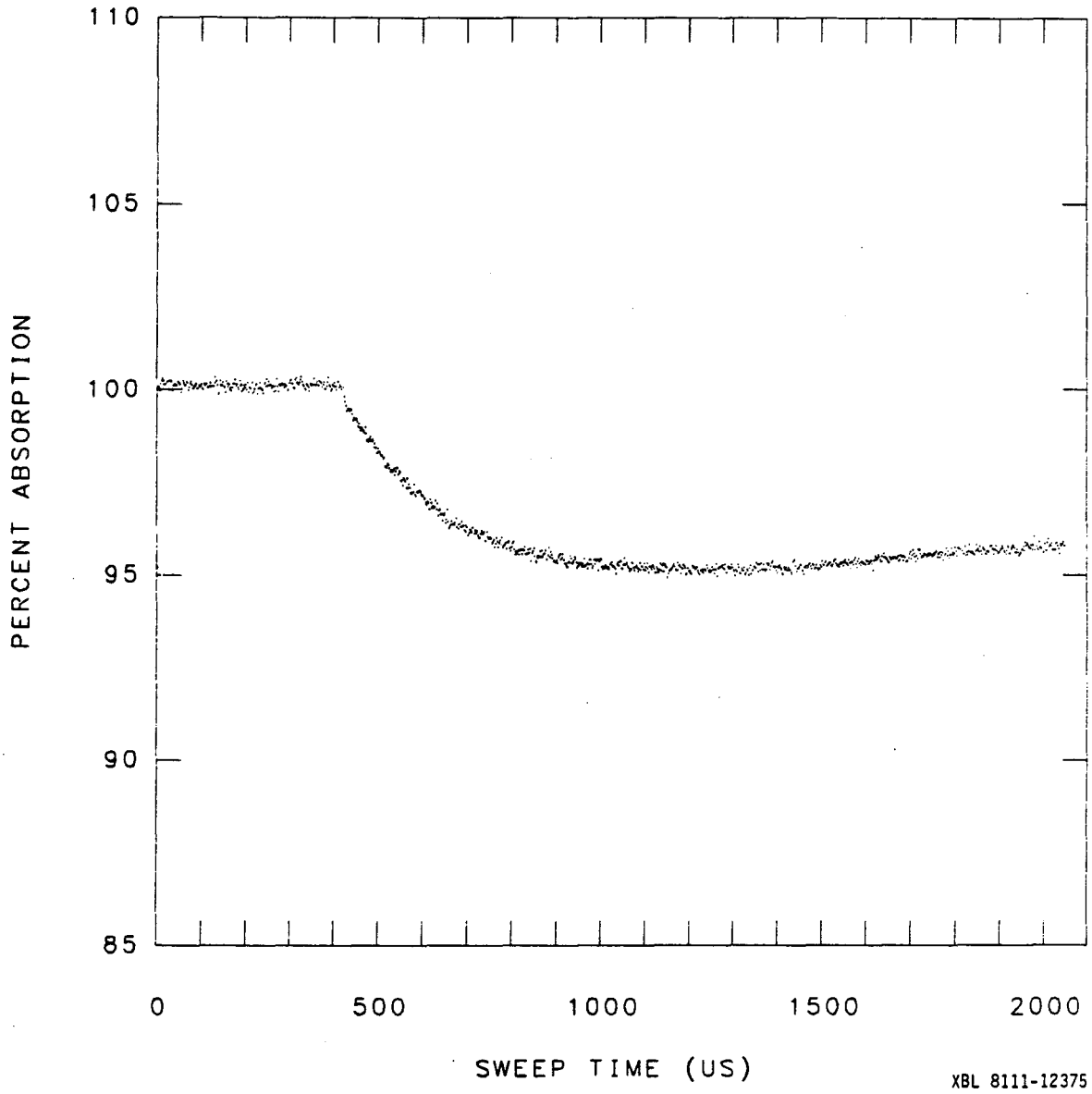

Figure 20. Typical HNO_3 FP/LA data as recorded and scaled to 100% transmission.

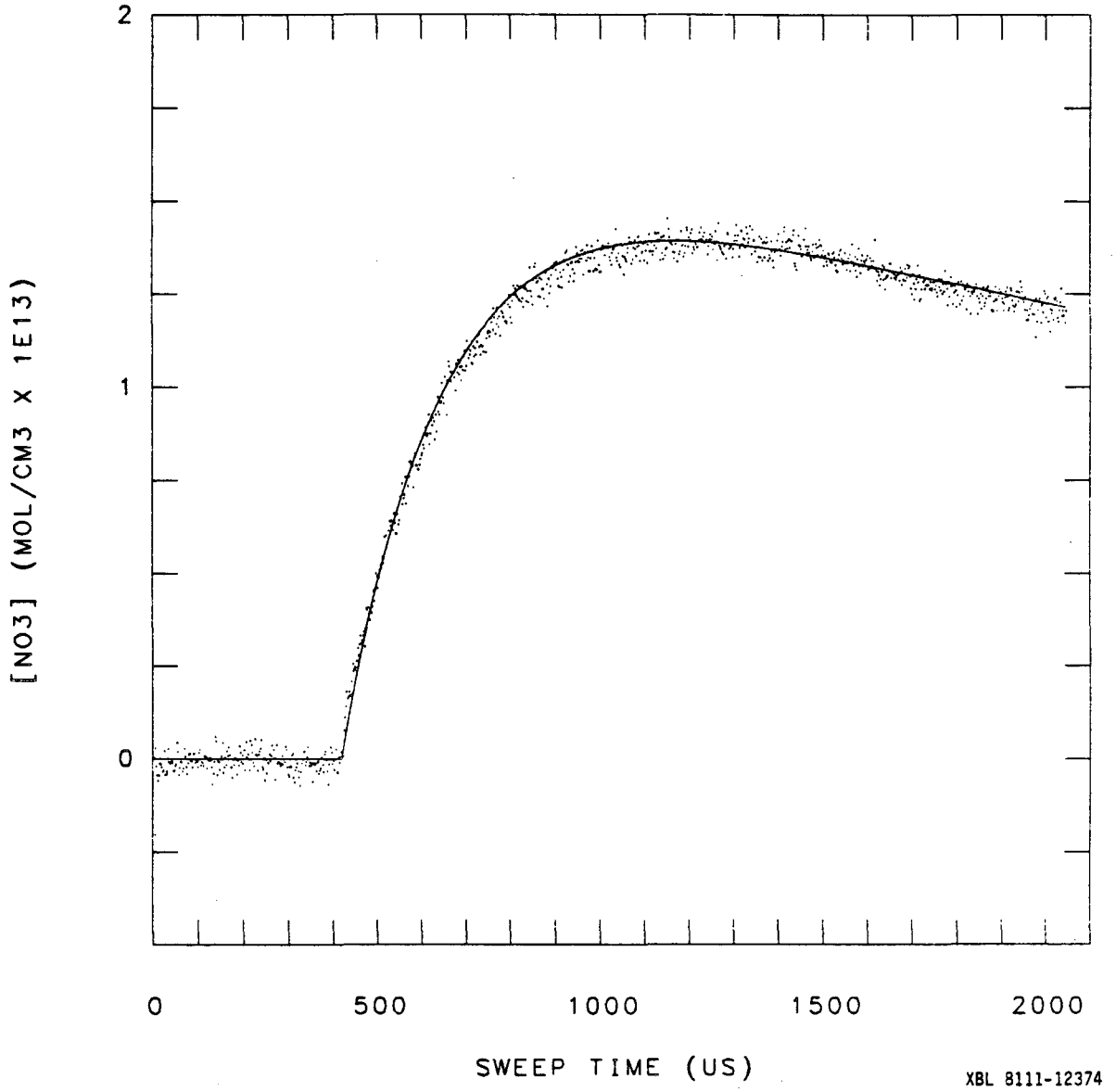

Figure 21. Data from Fig. 20 converted to NO_3 concentration, dots, and double exponential fit to data, solid line.

$$[HO]_{t=o} = E\sigma[HNO_3]\phi_{phot} \quad . \tag{39}$$

Here E is the energy in photons/cm^{-2} $shot^{-1}$ (corrected for window attenuation and reflection), σ is the absorption cross section for HNO_3 in cm^2 $molecule^{-1}$, the $[HNO_3]$ is given in molecules cm^{-3} and ϕ_{phot} is the HO photolytic quantum yield from HNO_3 (1 molecule $photon^{-1}$). The second order rate constant for reaction (2) is given by

$$k_2 = \frac{(\alpha_2-\alpha_3)}{[HNO_3]} \quad . \tag{40}$$

Note that while k_2 would not be influenced by diffusion of HO out of the reaction zone or reaction of HO with the carrier gas or its impurities, the product yield of NO_3 would. This would be reflected in a pressure or M gas dependence for the quantity.

2. FP/RF Study of the Reaction of HO with HNO_3

This reaction was studied over a 145K temperature range from 218K to 363K at HNO_3 concentrations from $2\text{-}40\times10^{14}$ molecules cm^{-3}. Total cell pressure ranged from 10 to 50 Torr with Ar acting as the carrier gas in all cases. Ar was chosen as the carrier gas because of its poor ability to quench the $HO(A^2\Sigma^+)$ state.

$$HO(A^2\Sigma^+) + M \longrightarrow HO(X^2\pi) + M \tag{41}$$

The Schofield[77] review of radiative lifetimes and quenching rate constants for the $HO(A^2\Sigma^+)$ state gives an average radiative lifetime

of 0.76μs for the (0,0) transition and typical electronic quenching rate constants of 2.2×10^{-11} and 1.0×10^{-11} cm^3 $molecules^{-1}$ s^{-1} for N_2 and O_2, and upper limits of 1×10^{-14} and 4×10^{-14} cm^3 $molecule^{-1}s^{-1}$ for He and Ar. The HO fluorescence quantum efficiencies for these gases are 1.00:0.99:0.16:0.04 for $He:Ar:N_2:O_2$ at 10 Torr total carrier gas pressure. Argon was chosen over He because of its better efficiency at quenching $v'=1$ to $v'=0$ in the $HO(A^2\Sigma^+)$ state ($k_q(Ar) = 3 \times 10^{-12}$ cm^3 $molecule^{-1}s^{-1}$ and $k_q(He) = 1 \times 10^{-12}$ $cm^3 molecules^{-1}s^{-1}$) which may be populated by emission from the resonance lamp. The photolysis laser output energy was always adjusted to maintain a HO radical concentration of less than 4×10^{11} molecules cm^{-3} immediately following the laser pulse. Most experiments were performed with the UV monitoring cell placed before the photolysis cell; however, experiments were performed with monitoring cell beyond the photolysis cell and at longer cell residence times. Rate constants for the reaction were measured at 10 and 25 Torr total pressure for the temperatures 218, 250, 273, 298, 323 and 363K. Nitric acid concentrations, measured in the monitor at ~295K, were corrected for changes in gas density between the photolysis and monitoring cell via the expression

$$[HNO_3]_{phot} = (T_{mon}/T_{phot})\ [HNO_3]_{mon} \quad . \qquad (42)$$

The data recorded in these experiments is detailed in Tables 8-16 with the first order plots of the data shown in Figs. 22-27. At 298K these data give a results for k_2 of $(1.31 \pm 0.24) \times 10^{-13}$ cm^3

Table 8. Kinetic results for the reaction of HO with HNO_3 at 218K.

HNO_3 (molecules cm^{-3} x 10^{-14})	measured k' (s^{-1})
P = 10 Torr[a]	
2.13	128.1 ± 0.5
2.32	134.6 ± 0.7
5.04	205.2 ± 0.5
7.92	291.3 ± 1.3
11.0	403.9 ± 2.8
13.7	490.9 ± 2.9
13.8	472.7 ± 3.2
P = 25 Torr[b]	
2.10	148.1 ± 0.7
5.00	239.5 ± 1.2
7.97	324.5 ± 1.2
10.7	412.4 ± 3.2
13.7	495.3 ± 3.4

[a] k_2 (30.8±4.18)x10^{-14} cm^3 $molecule^{-1}s^{-1}$ Intercept = 58.2 s^{-1}
[b] k_2 (30.0±3.56)x10^{-14} cm^3 $molecule^{-1}s^{-1}$ Intercept = 87.1 s^{-1}

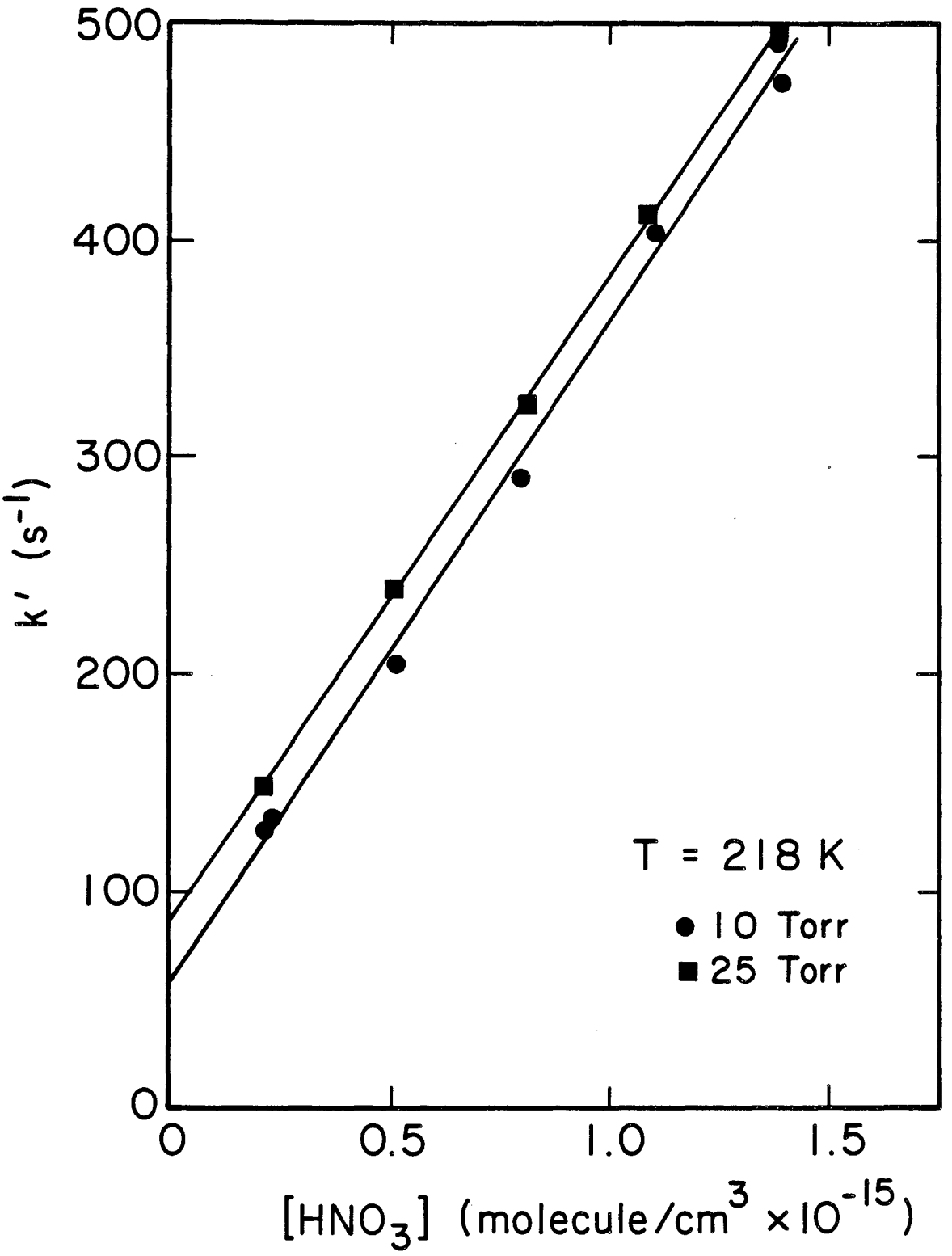

Figure 22. First order plot for reaction of HO with HNO_3 at 218K and 10 and 25 Torr.

Table 9. Kinetic results for the reaction of HO with HNO_3 at 250K.

HNO_3 (molecules $cm^{-3} \times 10^{-14}$)	measured k' (s^{-1})
P = 10 Torr[a]	
3.33	136.0 ± 0.5
7.17	206.0 ± 0.5
11.1	295.7 ± 1.0
15.1	358.3 ± 1.3
18.9	437.2 ± 1.6
P = 25 Torr[b]	
1.89	103.6 ± 0.7
4.86	165.3 ± 0.4
9.57	261.4 ± 0.7
15.4	365.4 ± 1.9
19.1	452.9 ± 2.8

[a] k_2 (19.3±2.92)x10^{-14} cm^3 $molecule^{-1}s^{-1}$ Intercept = 71.9 s^{-1}
[b] k_2 (19.9±2.78)x10^{-14} cm^3 $molecule^{-1}s^{-1}$ Intercept = 67.1 s^{-1}

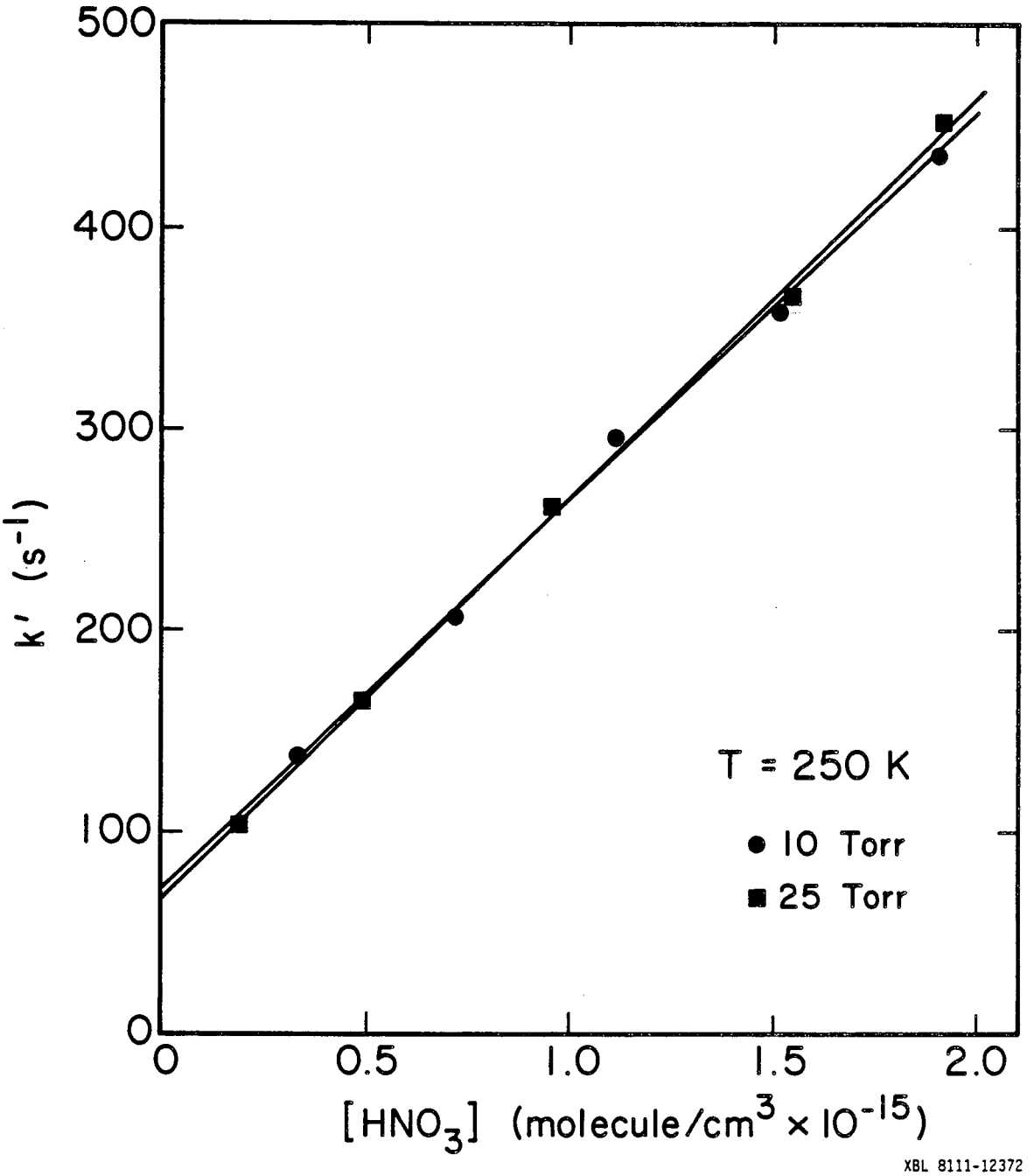

Figure 23. First order plot for reaction of HO with HNO_3 at 250K and 10 and 25 Torr.

Table 10. Kinetic results for the reaction of HO with HNO_3 at 273K.

HNO_3 (molecules cm^{-3} x 10^{-14})	measured k' (s^{-1})
P = 10 Torr[a]	
3.00	127.0 ± 0.5
5.90	167.4 ± 0.5
9.05	225.8 ± 1.1
12.7	275.3 ± 1.5
21.1	393.5 ± 1.9
P = 25 Torr[b]	
1.84	99.2 ± 09.5
5.09	148.3 ± 0.4
8.23	195.4 ± 0.6
10.9	240.6 ± 1.0
20.1	379.5 ± 1.4

[a] k_2 (14.8±2.22)x10^{-14} cm^3 $molecule^{-1}s^{-1}$ Intercept = 84.9 s^{-1}
[b] k_2 (15.4±1.82)x10^{-14} cm^3 $molecule^{-1}s^{-1}$ Intercept = 70.5 s^{-1}

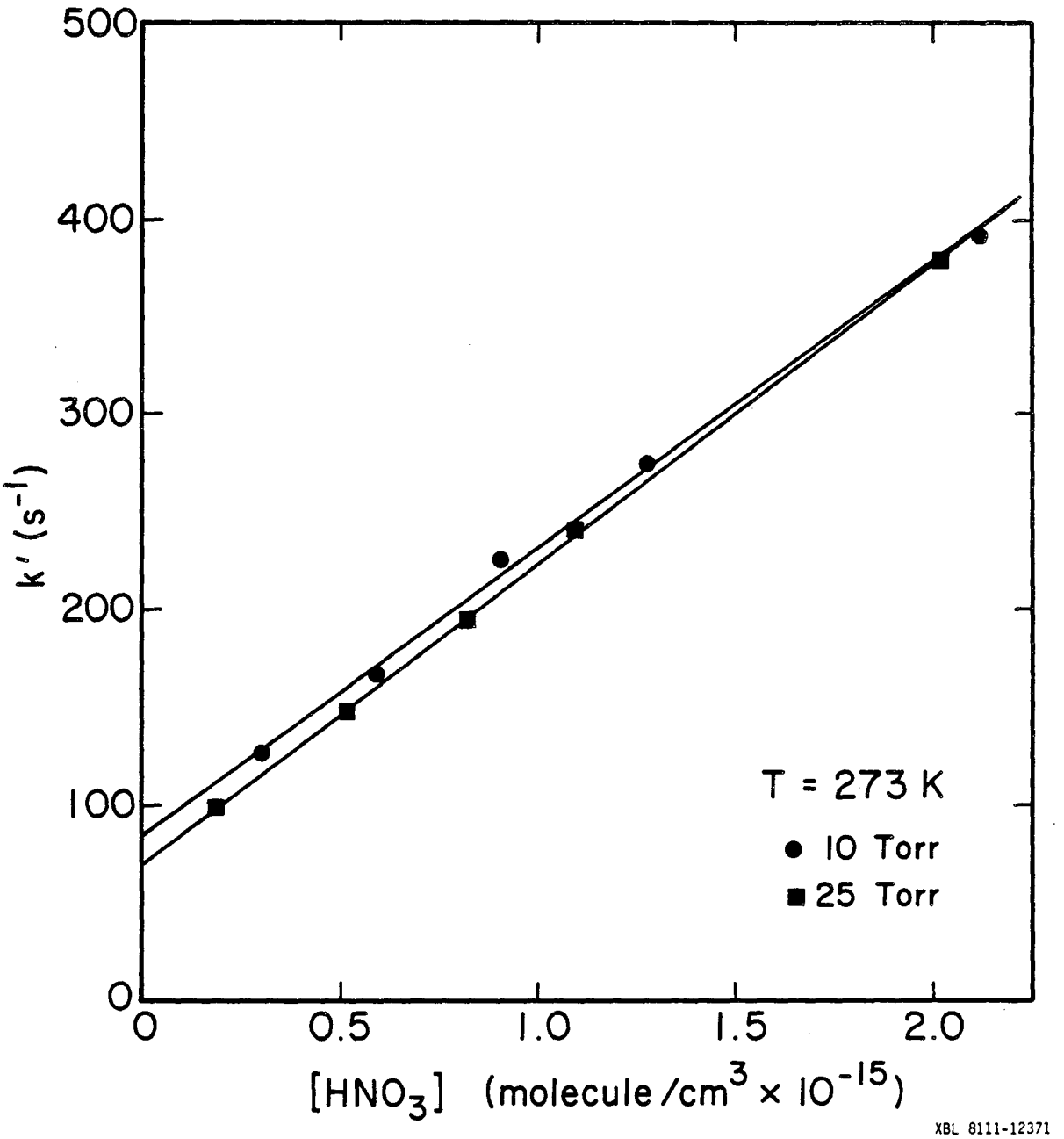

Figure 24. First order plot for the reaction of HO with HNO_3 at 273K and 10 and 25 Torr.

Table 11. Kinetic results for reaction of HO with HNO_3 in second generation cell at 10 Torr and 298K.

HNO_3 (molecules cm^{-3} x 10^{-14}	measured k' (s^{-1})
1.83	91.3
1.22	100.3
2.44	96.4
2.61	102.7
2.71	109.4
4.20	122.1
4.53	131.2
4.61	127.8
4.98	134.9
6.52	154.4
7.59	164.3
7.63	157.3
9.40	201.4
9.83	183.9
11.8	229.0
12.8	236.8
15.5	270.7
20.1	331.7
25.4	399.2
33.8	521.6
41.7	639.4

$k_2 = (13.5 \pm 1.71) \times 10^{-14}$ cm^3 $molecule^{-1}s^{-1}$ Intercept = 65.0

Table 12. Kinetic results for the reaction of HO with HNO_3 in second generation cell at 298K.

HNO_3 (molecules cm^{-3} x 10^{-14})	measured k' (s^{-1})
P = 25 Torr[a]	
2.16	70.5
5.12	106.3
8.00	142.6
10.0	174.4
11.6	193.4
18.5	284.8
24.0	357.4
30.2	448.9
P = 50 Torr[b]	
2.15	55.2
3.82	78.5
3.94	81.3
6.39	114.8
9.42	156.2
10.6	166.2

[a] $k_2 = (13.5 \pm 1.72) \times 10^{-14}$ cm^3 $molecule^{-1}s^{-1}$ Intercept = 37.8 s^{-1}

[b] $k_2 = (13.3 \pm 1.71) \times 10^{-14}$ cm^3 $molecule^{-1}s^{-1}$ Intercept = 28.0 s^{-1}

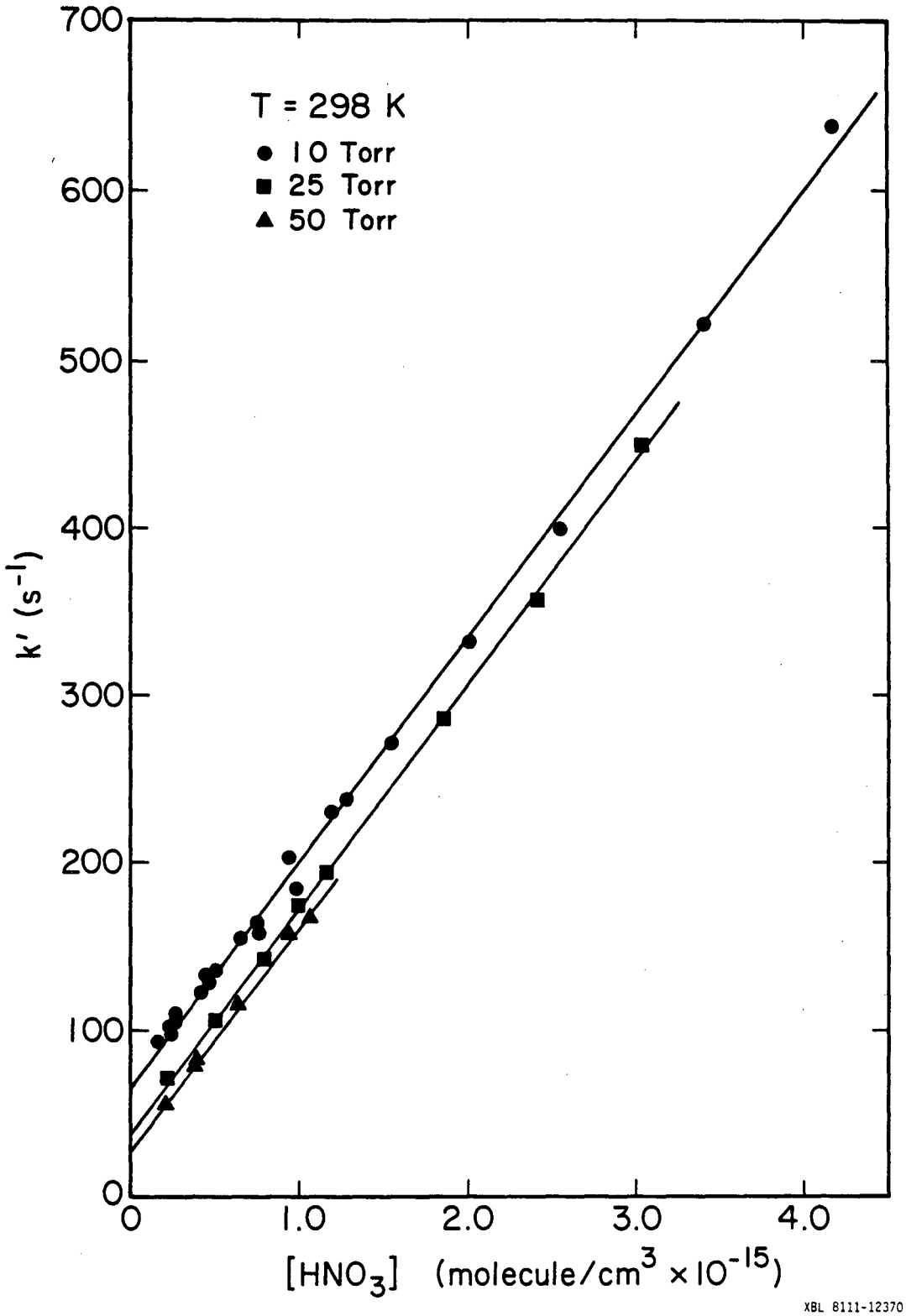

Figure 25. First order plot for reaction of HO with HNO_3 at 298K and 10, 25 and 50 Torr.

Table 13. Kinetic results for reaction of HO with HNO_3 under various test conditions at 10 Torr and 298K in second generation cell.

HNO_3 (molecules cm^{-3} x 10^{-14})	measured k' (s^{-1})
Monitor beyond photolysis cell[a]	
2.53	106.4
93.8	212.9
16.2	292.4
17.6	313.6
30.1	469.5
42.1	670.8
Monitor before photolysis cell[b]	
5.18	124.2
10.9	209.3
21.4	351.8
43.9	652.3
Double photolysis cell residence time[c]	
9.15	171.4
24.0	360.8
33.0	498.4

[a] k_2 (14.0±2.75)x10^{-14} cm^3 $molecule^{-1}s^{-1}$ Intercept = 68.5 s^{-1}
[b] k_2 (13.6±1.97)x10^{-14} cm^3 $molecule^{-1}s^{-1}$ Intercept = 58.3 s^{-1}
[c] k_2 (13.6±3.62)x10^{-14} cm^3 $molecule^{-1}s^{-1}$ Intercept = 43.3 s^{-1}

Table 14. Kinetic results for the reaction of HO with HNO_3 at 298K with third generation cell.

HNO_3 (molecules cm^{-3} x 10^{-14})	measured k' (s^{-1})
P = 10 Torr[a]	
3.00	128.3 ± 0.5
6.23	168.2 ± 0.4
9.12	203.7 ± 0.6
12.8	257.8 ± 1.1
22.5	374.6 ± 1.7
22.6	380.7 ± 1.7
P = 25 Torr[b]	
1.95	102.1 ± 0.4
5.00	139.4 ± 0.5
8.03	178.0 ± 0.5
11.3	219.9 ± 0.6
15.2	262.7 ± 1.0
20.4	326.9 ± 1.2

[a] k_2 (12.8±1.71)x10^{-14} cm^3 $molecule^{-1}s^{-1}$ Intercept = 89.4 s^{-1}
[b] k_2 (12.1±1.45)x10^{-14} cm^3 $molecule^{-1}s^{-1}$ Intercept = 78.7 s^{-1}

Table 15. Kinetic results for the reaction of HO with HNO_3 at 323K.

HNO_3 (molecules $cm^{-3} \times 10^{-14}$)	measured k' (s^{-1})
P = 10 Torr[a]	
1.79	123.9 ± 0.5
5.35	161.4 ± 0.4
9.01	193.1 ± 0.4
12.3	233.5 ± 0.8
16.8	293.9 ± 1.2
P = 25 Torr[b]	
2.01	103.5 ± 0.4
4.93	133.4 ± 0.4
8.27	168.4 ± 0.4
11.3	198.2 ± 0.4
15.3	239.4 ± 0.7
20.8	299.0 ± 1.0

[a] k_2 $(11.2 \pm 1.99) \times 10^{-14}$ cm^3 $molecule^{-1}s^{-1}$ Intercept = 100.0 s^{-1}
[b] k_2 $(10.4 \pm 1.25) \times 10^{-14}$ cm^3 $molecule^{-1}s^{-1}$ Intercept = 82.2 s^{-1}

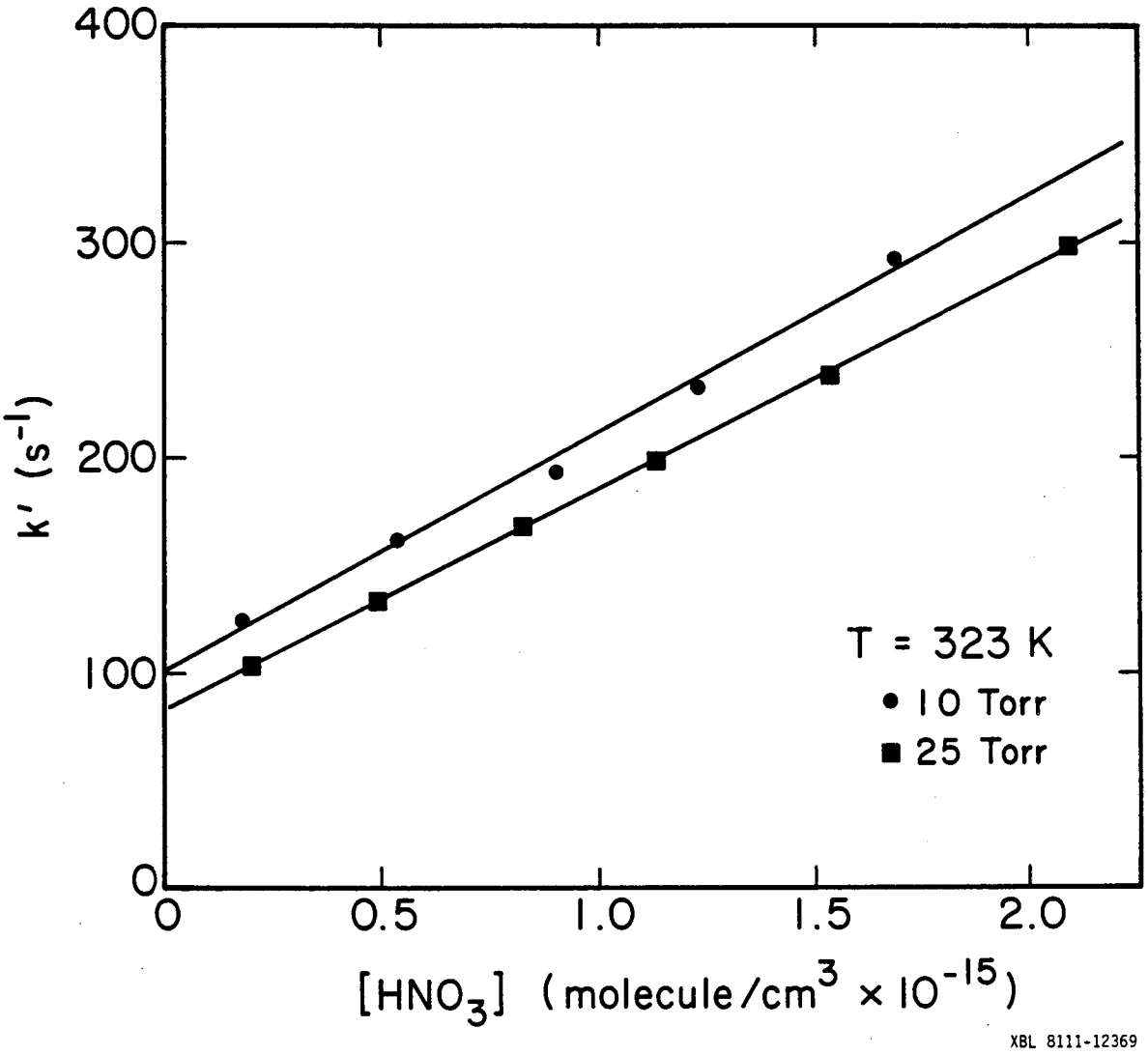

Figure 26. First order plot for reaction of HO with HNO_3 at 323K and 10 and 25 Torr.

Table 16. Kinetic results for the reaction of HO with HNO_3 at 363K

HNO_3 (molecules cm^{-3} x 10^{-14})	measured k' (s^{-1})
P = 10 Torr[a]	
2.04	137.7 ± 0.5
2.92	134.9 ± 0.6
4.94	160.0 ± 0.5
6.10	168.0 ± 0.4
8.05	185.5 ± 0.7
13.1	249.4 ± 1.0
13.2	242.0 ± 0.8
19.4	309.2 ± 1.3
19.5	313.6 ± 1.3
P = 25 Torr[b]	
1.96	105.2 ± 0.4
4.84	127.4 ± 0.3
8.01	158.3 ± 0.4
14.6	221.2 ± 0.5
19.9	268.0 ± 0.6

[a] k_2 (10.4±1.55)x10^{-14} cm^3 $molecule^{-1}s^{-1}$ Intercept = 107.8 s^{-1}
[b] k_2 (9.21±1.23)x10^{-14} cm^3 $molecule^{-1}s^{-1}$ Intercept = 85.2 s^{-1}

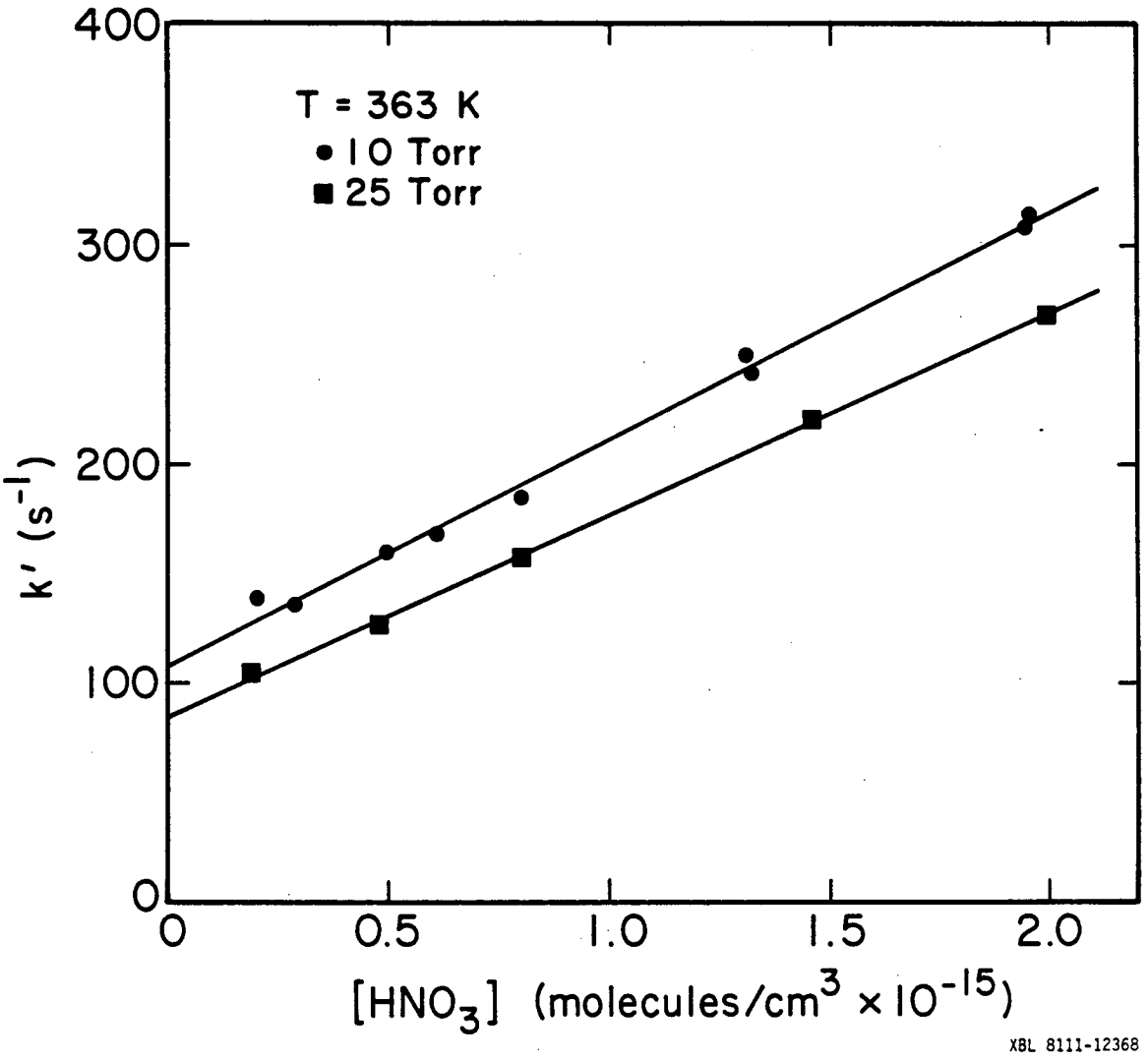

Figure 27. First order plot for the reaction of HO with HNO_3 at 363K and 10 and 25 Torr.

molecule^{-1}s^{-1}, independent of pressure, cell residence time or monitor location. This data, and all other data recorded at various temperatures, is summarized in Table 17 and Figs. 28 and 29. All error limits reported are 95 percent confidence limits based on best estimates of both statistical and systematic uncertainties. The error limits of the averaged values were set to include all the error limits of the contributing data. The results appear independent of pressure, within the error limits of the individual points. There does appear to be some decrease in reaction rate with increasing temperature. The intercepts for each of the first order plots scale according to what one expects for diffusion as a function of pressure. These intercepts appear to come closer in value with decreasing temperature and finally cross between 250 and 218K. An Arrhenius type plot for the intercepts at each pressure (Fig. 30) gives surprisingly straight lines with the exception of the point for 25 Torr at 218K.

The observed temperature dependence of the reaction was analyzed by fitting the averaged values for the rate constant at each temperature to the classical Arrhenius expression

$$\ln k(T) = \ln A - (E/R)/T \qquad (43)$$

and to an alternate expression

$$\ln k(T) = \ln A + n \ln \left(\frac{300}{T}\right) \quad . \qquad (43)$$

Table 17. Summary of FP/RF results for reaction of HO with HNO_3

Pressure Torr at 298K	Linear Flow Rate[d] cm s^{-1}	Number of First Order Rate Constants	$(k \pm 2\sigma) \times 10^{14}$ cm^3 $molecule^{-1}s^{-1}$	Average k[a]
		363K		
10	18	9	10.4 ± 1.6	
25	18	5	9.21 ± 1.2	9.64 ± 2.4
		323K		
10	18	5	11.2±2.0	
25	18	6	10.4±1.3	10.6±2.6
		298K		
10	25[b]	21	13.5 ± 1.7	
10	25[b,c]	6	14.0 ± 2.7	
10	25[b]	4	13.6 ± 2.0	
10	12.5[b]	4	13.6 ± 3.6	
10	18	6	12.8 ± 1.7	
25	25[b]	8	13.5 ± 1.7	
25	18	6	12.1 ± 1.5	
50	25[b]	6	13.3 ± 1.7	13.1 ± 2.4
		273K		
10	18	5	14.8 ± 2.2	
25	18	5	15.4 ± 1.8	15.2 ± 2.6
		250K		
10	18	5	19.3 ± 2.9	
25	18	5	19.9 ± 2.8	19.6 ± 3.2
		218K		
10	18	7	30.8 ± 4.2	
25	18	5	30.0 ± 3.6	30.4 ± 4.6

a Error limits are set to include 2σ error limits of all points.
b Performed in second generation cell
c Monitor placed beyond photolysis cell
d Linear flow rate through interaction region

If either expression is a valid description, a plot of ln[k(T)] vs 1/T (42) or ln(300/T) should result in a straight line. In the case of the Arrhenius model, the slope of the line should yield an "activation temperature" (E/R) while the intercept gives the natural logarithm of the "pre-exponential factor." The alternate expression is meant to test for a situation where a T^n dependence in a partition function governing the rate is strongly evidenced. In this case, the slope of the line gives the value of the exponent n, and the intercept again gives the natural logarithm of a pre-exponential factor. These plots are shown in Figs. 28 and 29. Both appear to be linear within the error limits of the individual points with the models resulting in the rate expressions

$$k_2 = (1.52\pm0.43)\times10^{-14}\exp(644\pm79/T)\,cm^3molecule^{-1}s^{-1} \qquad (45)$$

for the Arrhenius model and

$$k_2=(1.33\pm0.05)\times10^{-13}\left(\frac{300}{T}\right)^{(2.29\pm0.26)}\,cm^3molecule^{-1}s^{-1} \qquad (46)$$

for the alternate expression. The variance for the fit to (45) is approximately 2.5 times less than that for (46). The significance of these results will be discussed in Section IVA.

3. FP/RF Study of the Reaction of HO with H_2O_2

This rate constant for this reaction was determined at 298K and 10 Torr total Ar pressure. Hydrogen peroxide concentrations ranged from $3\text{-}23\times10^{14}$ molecules cm^{-3}. Initial HO radical concentrations at 2×10^{11} and 2×10^{12} molecules cm^{-3} were explored. The absorption cross section at the 200 nm monitoring wavelength is small enough so

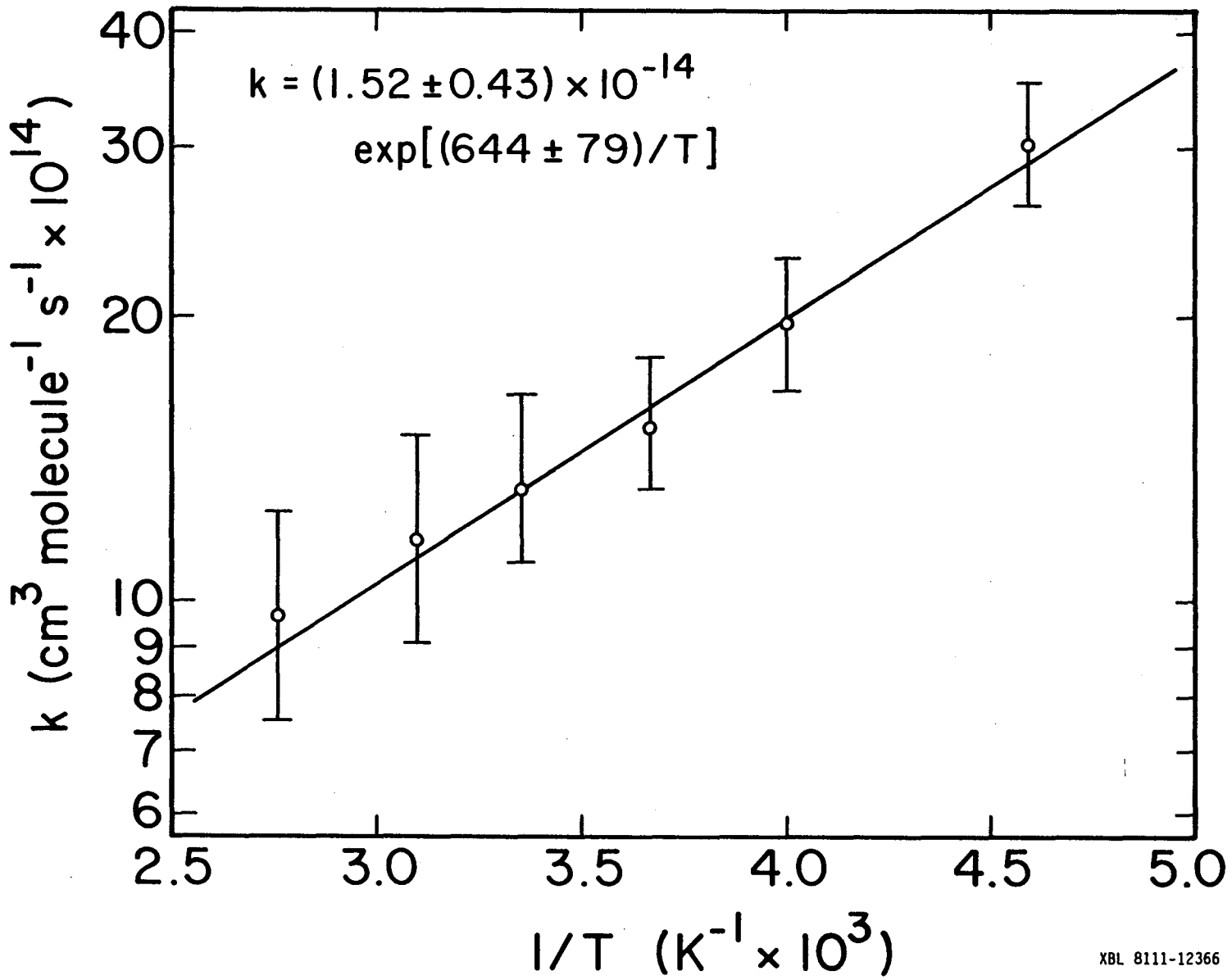

Figure 28. Arrhenius plot for reaction of HO with HNO_3 from 218-363K.

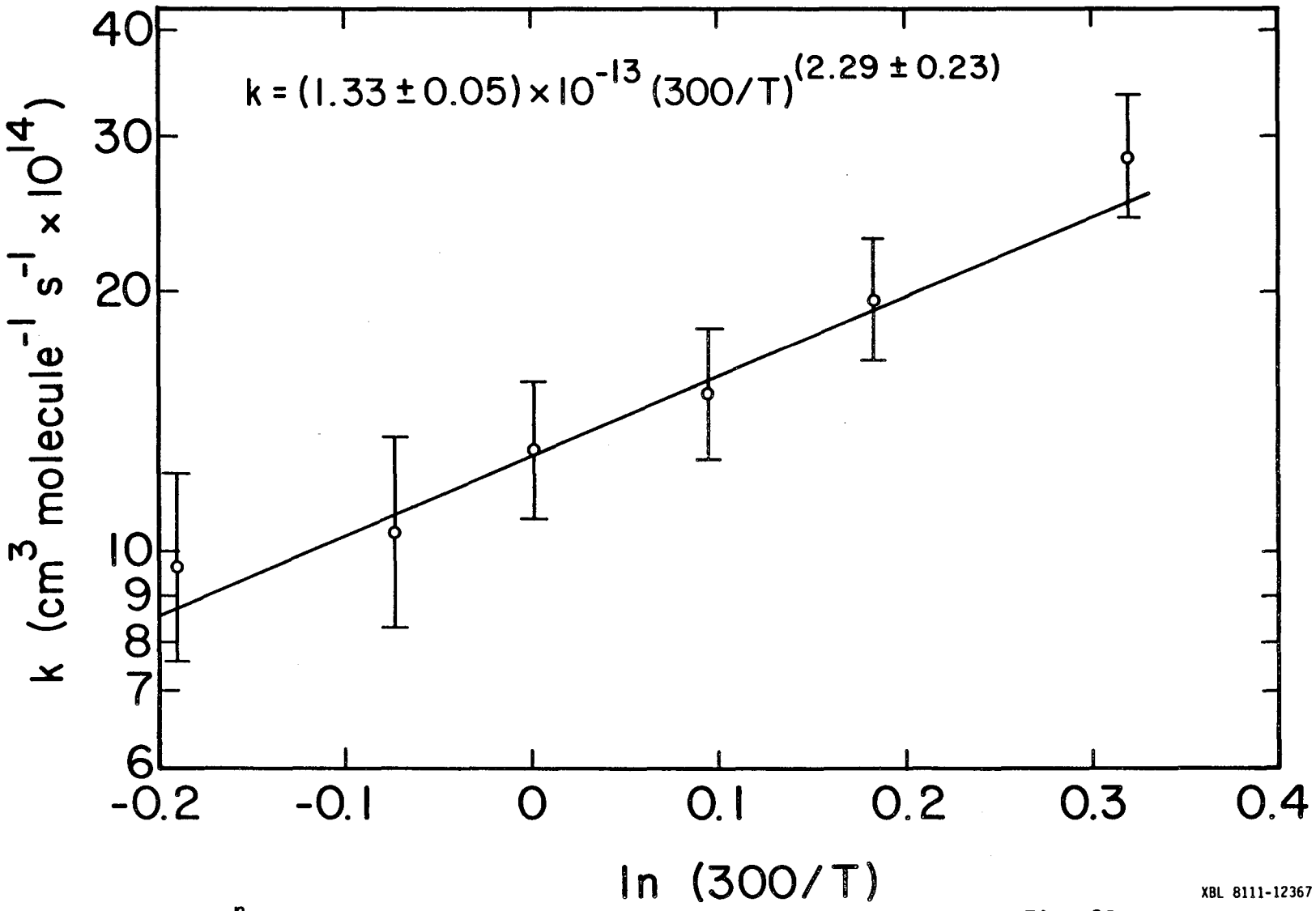

Figure 29. T^n type plot for reaction of HO with HNO_3 over same range as Fig. 28.

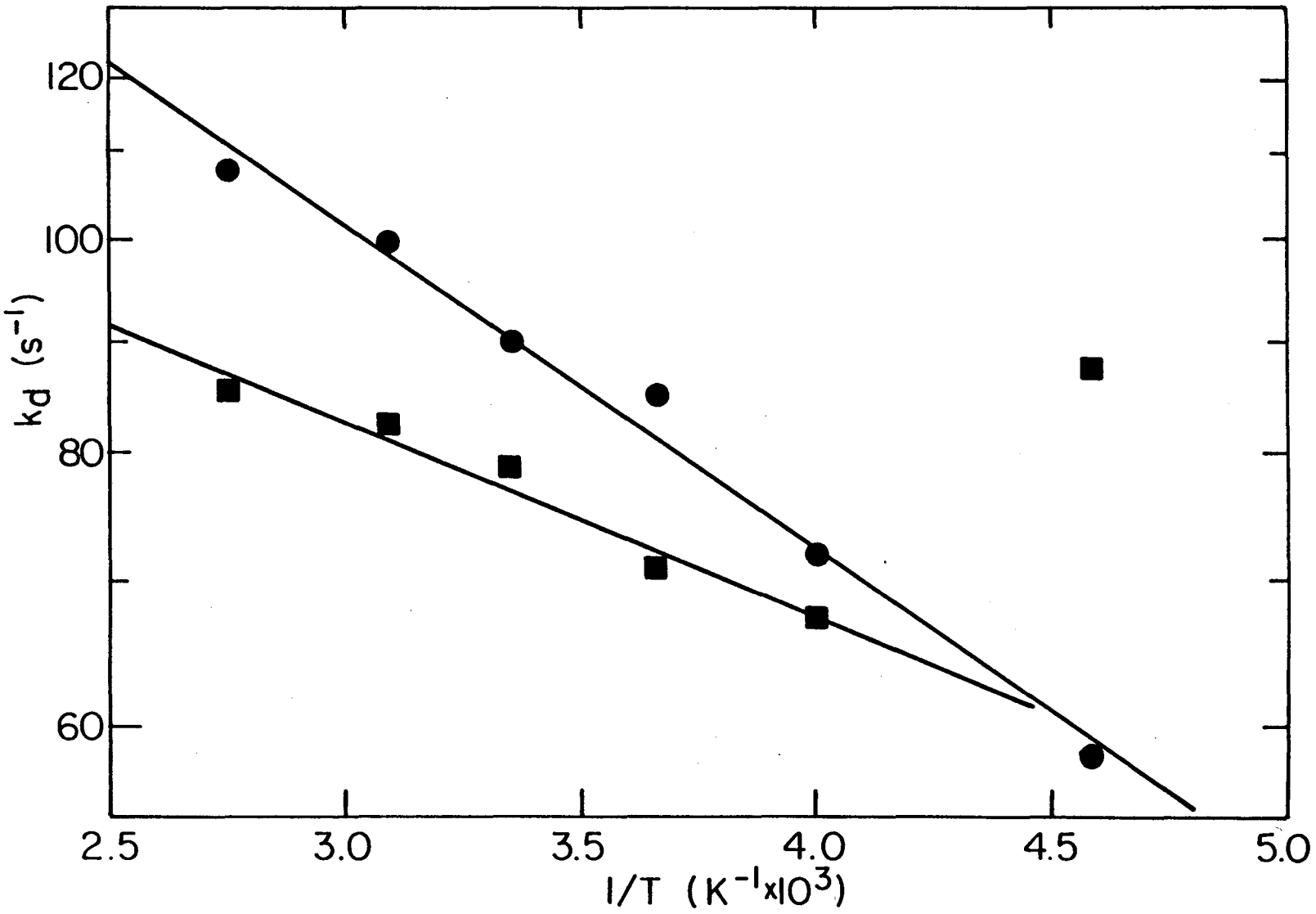

XBL8110-6920

Figure 30. Arrhenius plot for k_d determined in third generation resonance fluorescence cell. ●, 10 Torr; ■ 25 Torr.

Table 18. Kinetic results for the reaction of HO with H_2O_2 at 10 Torr and 298K

HNO_3 (molecules cm^{-3} x 10^{-14})	measured k' (s^{-1})
P = 10 Torr[a]	
2.98	587
2.78	603
3.05	682
3.83	789[a]
5.05	947[a]
5.02	996
6.70	1260
7.52	1361[a]
7.34	1435[a]
10.2	1891
11.6	2248[a]
14.7	2768[a]
14.8	2817
15.6	2925[a]
16.0	3032
17.9	3233
21.8	3990
23.0	4259[a]

a $k_4 = (1.81 \pm 0.24) \times 10^{-12}$ cm^3 $molecule^{-1}$ s^{-1}
Intercept = 79.1 s^{-1}
Initial [HO] = 2 x 10^{12} molecules cm^{-1}, all others at 2x10^{11} molecules cm^{-3}

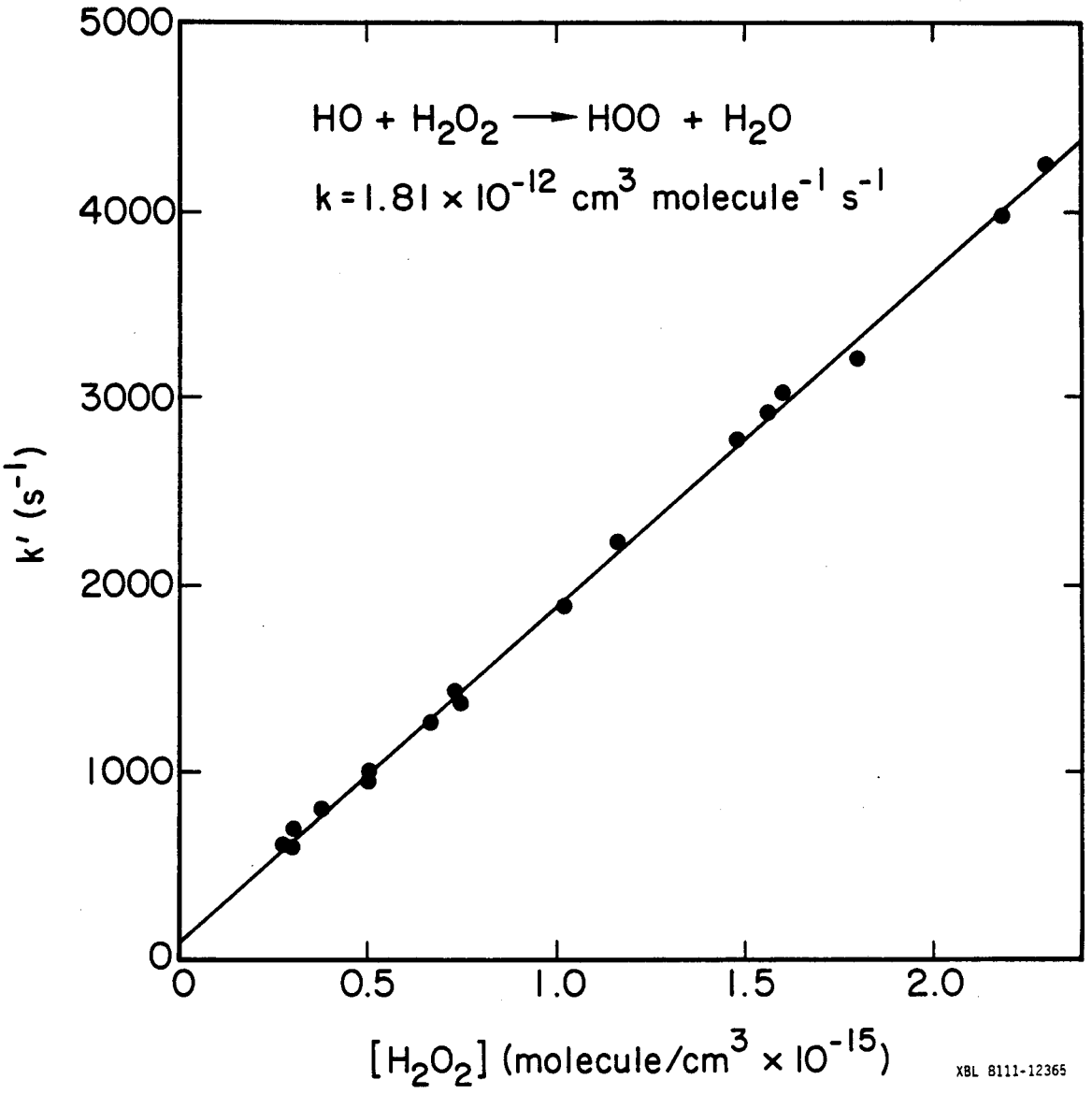

Figure 31. First order plot for reaction of HO with H_2O_2 at 298K and 10 Torr.

that even at the highest H_2O_2 concentrations explored the monitoring beam was only attenuated by 10 percent. Therefore, the major uncertainty in the rate constant results from the uncertainty in the H_2O_2 concentration.

The data for this study is given in Table 18 and a first order plot is shown in Fig. 31. the result is seen to be independent of initial HO concentration and a rate constant of $(1.81\pm0.24)\times10^{-12}$ cm^3 $molecule^{-1}s^{-1}$ has been determined for the reaction.

4. FP/LA Study of the Reaction of HO with HNO_3

The NO_3 rise time and yield following HNO_3 photolysis was studied at HNO_3 concentrations of 6×10^{15} and 2×10^{16} molecules cm^{-3}. Pressures of 10, 30, 50 and 745 Torr Ar and N_2 were employed at laser fluences of approximately 2, 5 and 18 x 10^{16} photons cm^{-2}. Experiments at 6×10^{15} molecules cm^{-3} were conducted only at the higher two fluences due to lack of signal at 2×10^{16} photons cm^{-2}. All experiments were conducted at ambient (~295K) temperatures. An NO_3 absorption cross section of 1.9 x 10^{-17} cm^2 $molecule^{-1}$ at the 662 nm monitoring wavelength, as determined in the next section, was employed in the data analysis. The HNO_3 sample used in these experiments was found to contain 0.15 percent NO_2. The observed rate constants and quantum yields were corrected via expression (35) using rate constants determined in Appendix B.

The results of these experiments are given in Tables 19-22. Immediately apparent from these results are that the apparent rate constants and product yields are somewhat pressure, M gas, HNO_3

Table 19. HNO_3 FP/LA results at high fluences and $[HNO_3]$ 6×10^{15} molecules cm^{-3}

$[HNO_3] \times 10^{-15}$ molecules cm^{-3}	$k_2 \times 10^{13}$ $cm^3 molecules^{-1} s^{-1}$	$E \times 10^{-16}$ photons cm^{-2}	ϕ_{prod}	Carrier Gas	Pressure Torr
6.05	4.12	18.8	0.41	Ar	10
5.72	2.92	17.3	0.60	Ar	30
5.97	2.34	16.1	0.73	Ar	50
5.84	3.58	16.5	0.42	N_2	10
5.81	2.67	17.6	0.66	N_2	30
5.81	2.31	17.1	0.74	N_2	50
6.08	2.49	4.37	0.58	Ar	10
5.87	2.62	4.64	0.62	Ar	10
6.08	2.59	3.38	0.79	Ar	30
5.91	2.23	4.49	0.81	Ar	50
5.93	3.32	4.76	0.47	N_2	10
5.98	2.18	4.31	0.79	N_2	30
5.90	1.89	4.40	1.00	N_2	50

Table 20. HNO_3 FP/LA results at high fluences and $[HNO_3]$ 2×10^{16} molecules cm^{-3}

$[HNO_3] \times 10^{-15}$ molecules cm^{-3}	$k_2 \times 10^{13}$ $cm^3 molecules^{-1} s^{-1}$	$E \times 10^{-16}$ photons cm^{-2}	ϕ_{prod}	Carrier Gas	Pressure Torr
1.94	2.45	17.0	0.62	Ar	10
1.99	2.37	18.3	0.71	Ar	30
2.01	2.41	18.8	0.72	Ar	50
	<2.41±0.04>				
1.97	2.44	19.1	0.65	N_2	10
1.99	2.36	18.8	0.74	N_2	30
2.00	2.32	19.1	0.78	N_2	50
	<2.37±0.06>				
2.03	2.08	5.39	0.78	Ar	10
2.00	1.93	5.26	0.92	Ar	30
2.04	1.92	5.29	0.97	Ar	50
	<1.98±0.09>				
1.98	2.32	5.40	0.76	N_2	10
2.00	1.88	5.25	1.01	N_2	30
2.02	1.91	5.35	1.04	N_2	50
	<2.04±0.25>				

Table 21. HNO_3 FP/LA results at low fluence, $[HNO_3]$ 2 x 10^{16} molecules cm^{-3} and Ar carrier gas

$[HNO_3] \times 10^{-15}$ molecules cm^{-3}	$k_2 \times 10^{13}$ $cm^3 molecules^{-1} s^{-1}$	$E \times 10^{-16}$ photons cm^{-2}	ϕ_{prod}	Pressure Torr
1.99	1.14	1.45	0.90	10
1.96	1.44	1.46	0.88	10
1.99	1.29	1.40	0.98	10
	<2.41±0.04>	<1.82±0.33>	<1.06±0.13>	
1.96	1.50	1.50	0.97	50
2.00	1.65	1.78	1.15	50
1.99	1.59	1.74	1.13	50
	<1.58±0.08>	<1.67±0.15>	<1.05±0.16>	
2.14	1.73	1.42	0.91	745
1.97	2.07	2.04	1.13	746
1.98	1.98	2.11	1.06	745
1.98	1.82	1.92	1.06	745
1.98	1.82	1.92	1.06	745
1.94	1.85	1.83	1.09	745
1.98	1.84	2.15	1.09	744
2.00	1.84	2.09	1.11	744
	<1.88±0.11>	<1.94±0.25>	<1.06±0.07>	

Table 22. HNO_3 FP/LA results at low fluences, $[HNO_3]$ 2 x 10^{16} molecules cm^{-3} and N_2 carrier gas

$[HNO_3] \times 10^{-16}$ molecules cm^{-3}	$k_2 \times 10^{13}$ $cm^3 molecule^{-1} s^{-1}$	$E \times 10^{-16}$ photons cm^{-2}	ϕ_{prod}	Pressure Torr
1.96	1.35	1.52	0.91	10
2.05	1.71	1.69	0.97	10
2.02	1.56	1.69	0.91	10
	<1.54±0.18>	<1.62±0.10>	<0.90±0.02>	
1.98	1.65	1.50	0.88	30
2.03	1.64	1.60	0.98	30
2.02	1.57	1.65	1.02	30
	<1.62±0.04>	<1.58±0.08>	<0.96±0.07>	
1.96	1.51	1.50	0.98	50
2.04	1.28	1.61	1.14	50
2.03	1.46	1.52	1.05	50
	<1.42±0.12>	<1.54±0.06>	<1.06±0.08>	
2.03	1.70	2.07	1.33	745
2.03	1.76	2.09	1.17	745
2.05	1.72	2.01	1.22	744
208	1.70	2.04	1.21	744
2.11	1.61	1.98	1.25	744
	<1.70±0.05>	<2.04±0.04>	<1.24±0.06>	

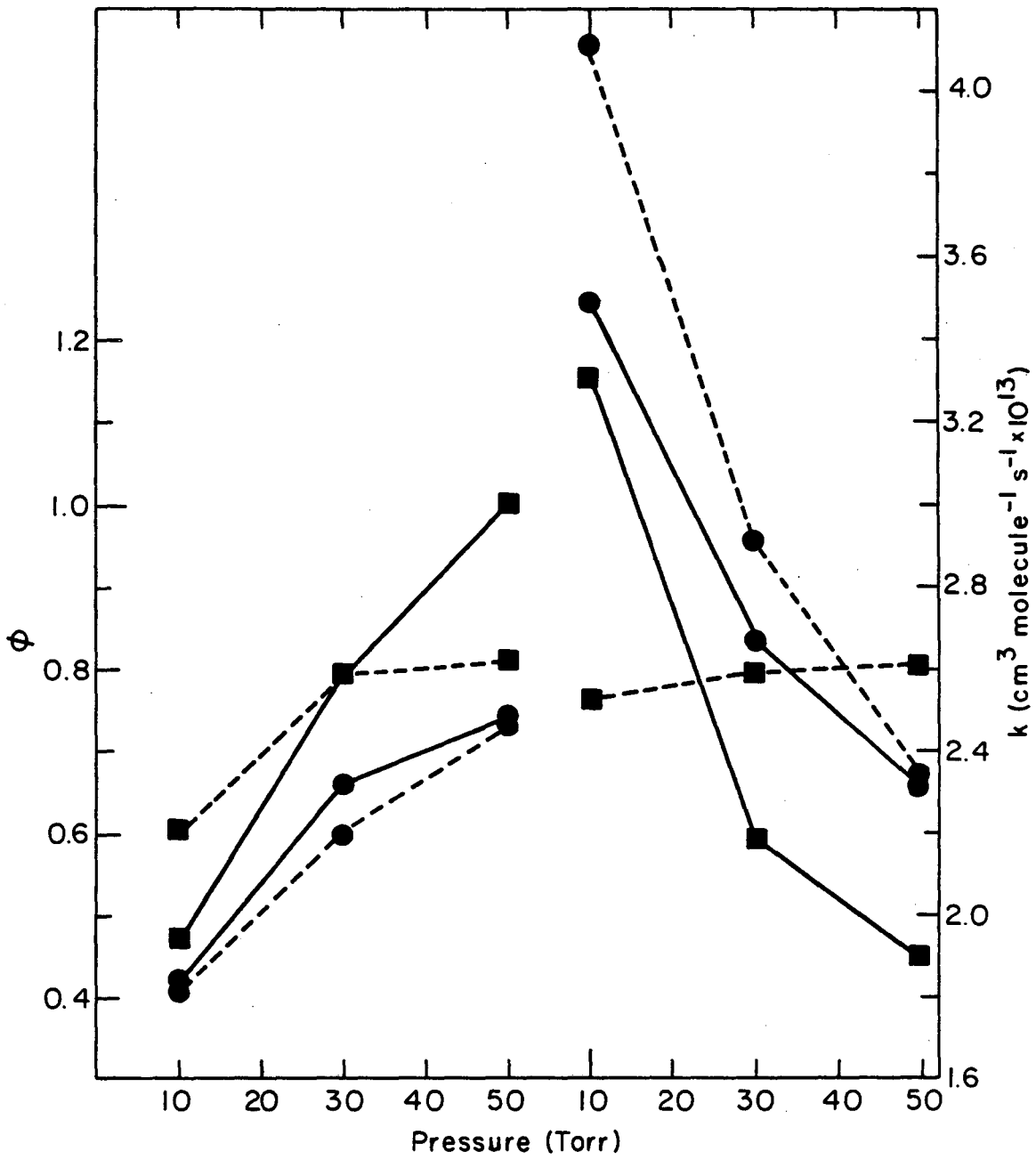

Figure 32. FP/LA results for $[HNO_3] \approx 6 \times 10^{15}$ molecules cm^{-3} as a function of pressure. Dashed line, M = Ar; solid line, M = N_2; ●, high fluence; ■, moderate fluence.

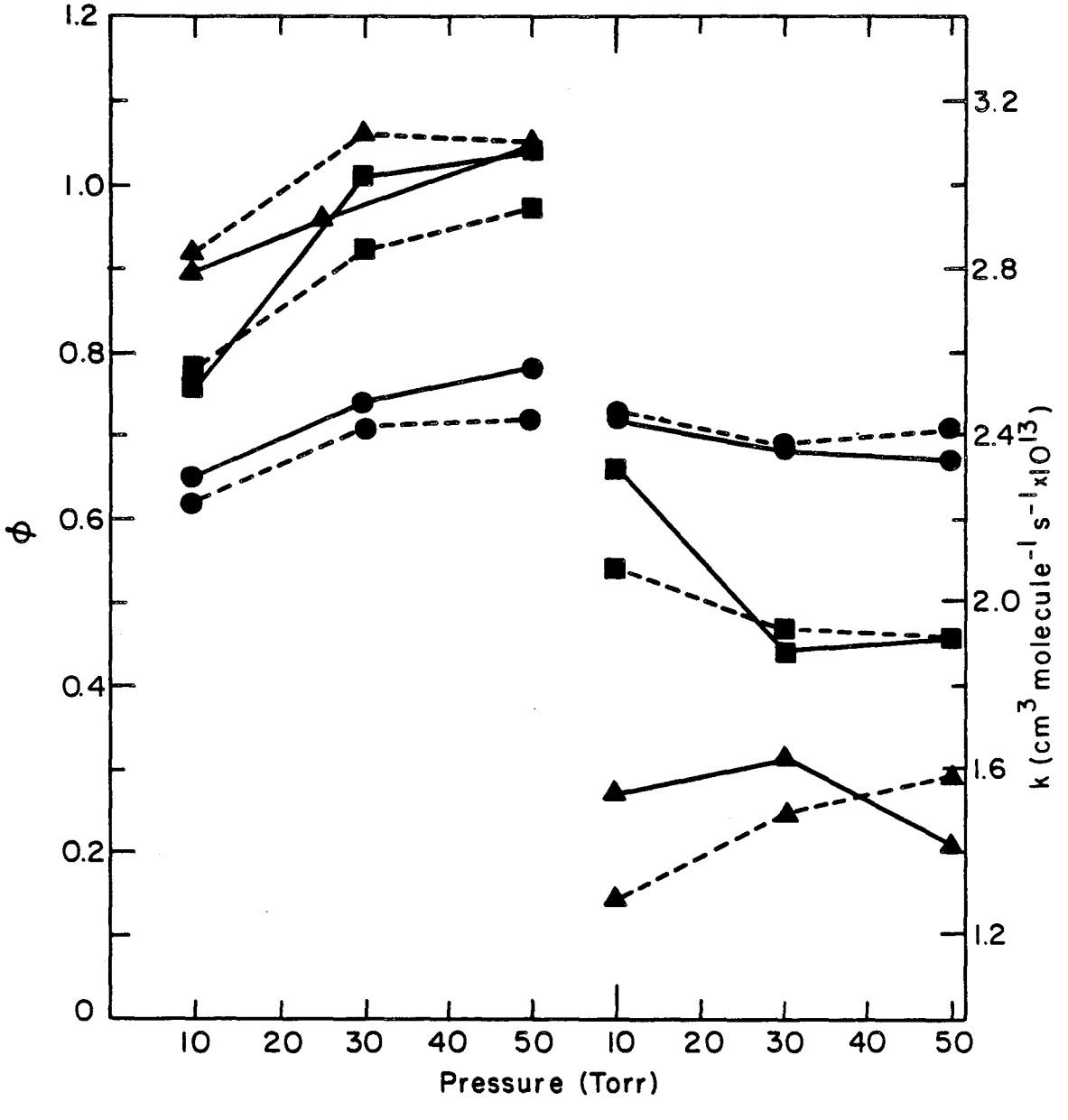

Figure 33. FP/LA data for $[HNO_3] \approx 2 \times 10^{16}$ molecules cm^{-3} as a function of pressure. Dashed line, M = Ar; solid line, M = N_2; ●, high fluence; ■, moderate fluence; ▲, low fluence. Points are averaged values where over-determined.

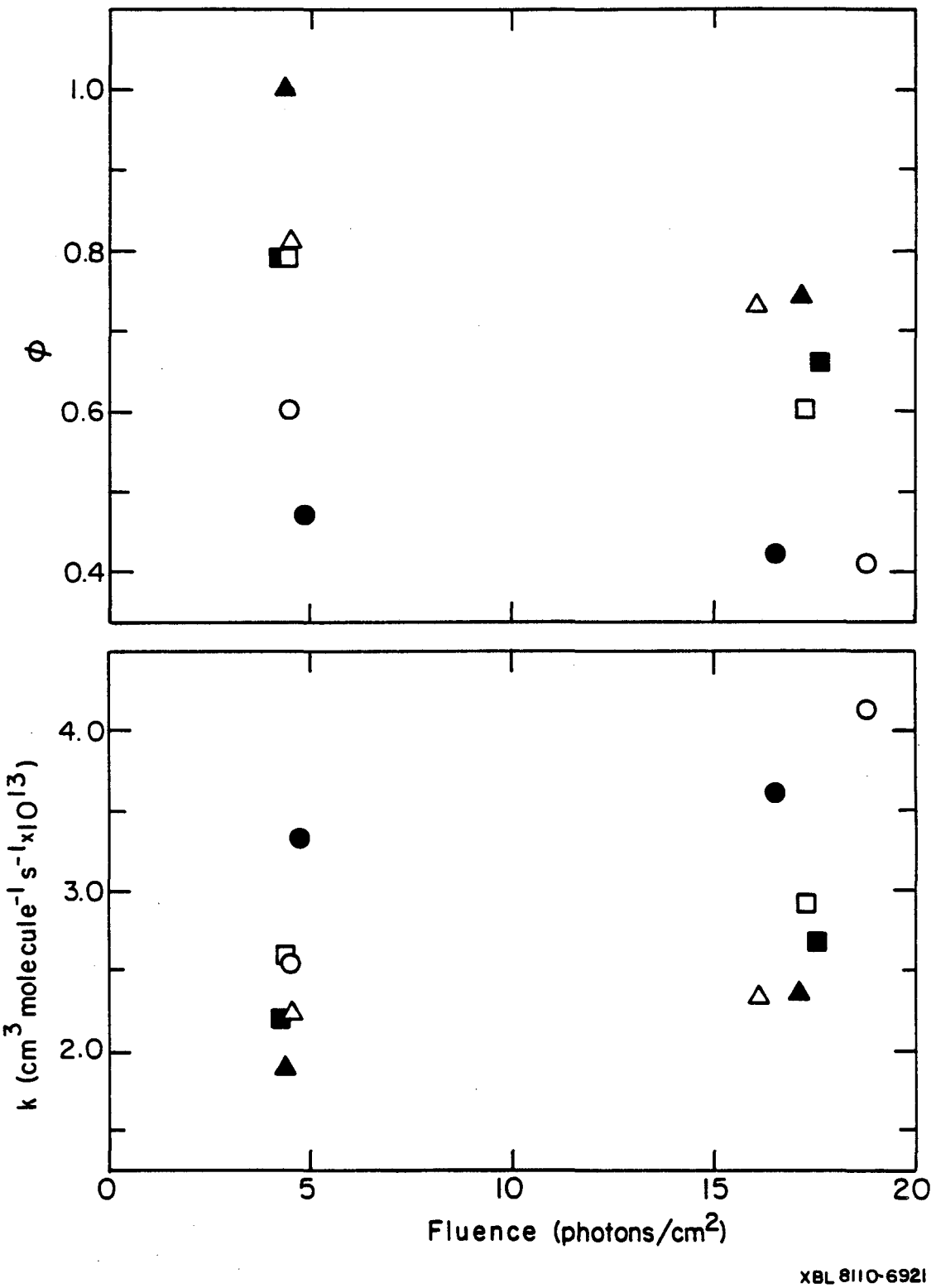

Figure 34. FP/LA data for $[HNO_3] \approx 6 \times 10^{15}$ molecules cm^{-3} as a function of fluence. ○, Ar at 10 Torr; □, Ar at 30 Torr; △, Ar at 50 Torr; , N_2 at 10 Torr; ■, N_2 at 30 Torr; ▲ N_2 at 50 Torr.

Figure 35. FP/LA results for $[HNO_3] \approx 2 \times 10^{16}$ molecules cm^{-3} as a function of fluence. ○, Ar at 10 Torr; □, Ar at 30 Torr; △, Ar at 50 Torr; ⊕, Ar at 745 Torr; ●, N_2 at 10 Torr; ■, N_2 at 30 Torr; ▲, N_2 at 50 Torr; +, N_2 at 745 Torr. Points are averaged values where overdetermined.

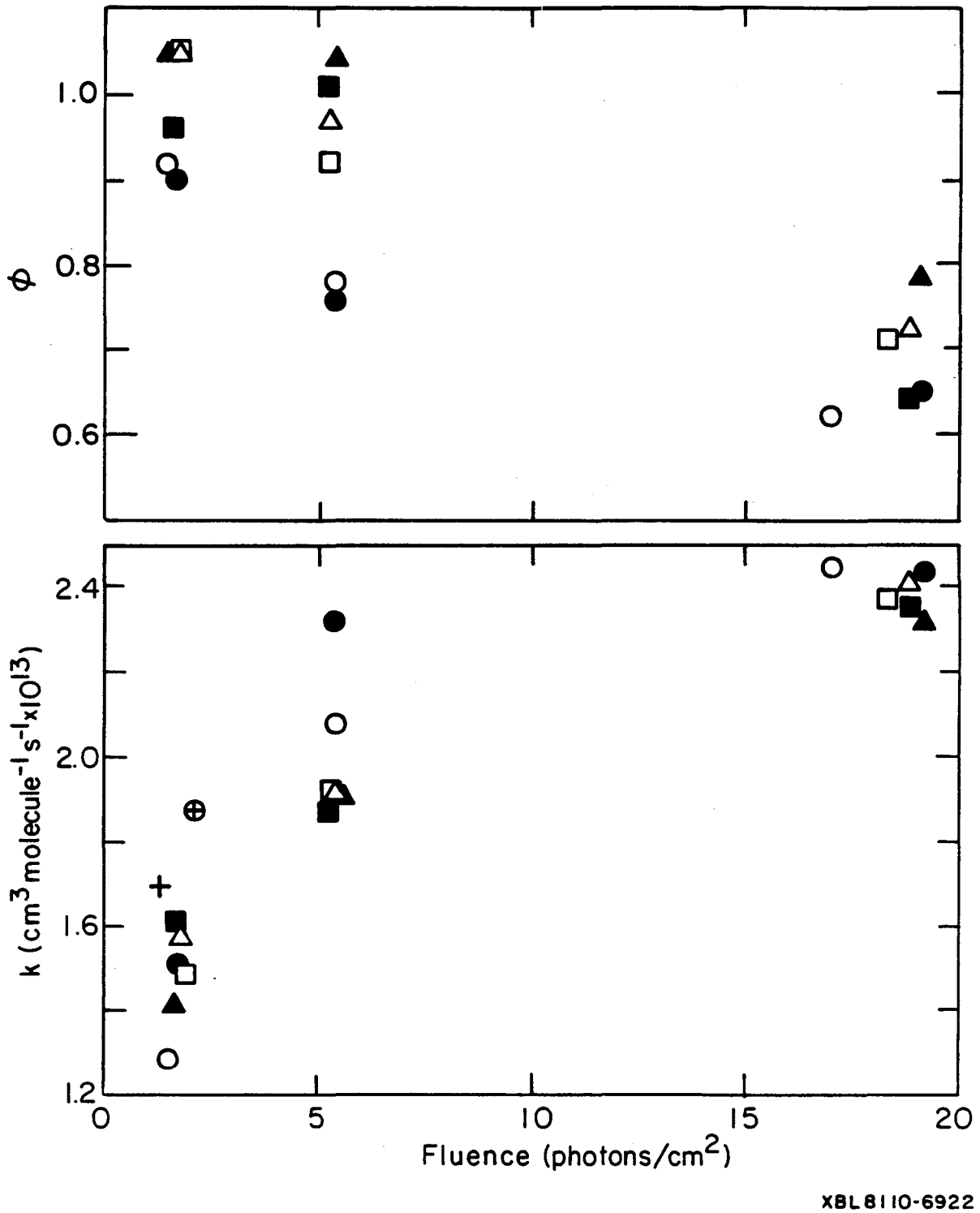
1.0
0.8
0.6
φ
2.4
2.0
1.6
1.2
k (cm3 molecule-1 s-1 x 10^13)
0
5
10
15
20
Fluence (photons/cm2)
XBL8110-6922

Figure 35

Figure 36. Correlation diagram of k vs $\emptyset$ for HNO_3 FP/LA results. ○, high fluence and □ moderate fluence at $[HNO_3] \approx 6 \times 10^{15}$ molecules cm^{-3}; ●, high fluence, ■, moderate fluence and ▲, low fluence at $[HNO_3] \approx 2 \times 10^{16}$ molecules cm^{-3}. All pressures are shown and points are averaged values where overdetermined.

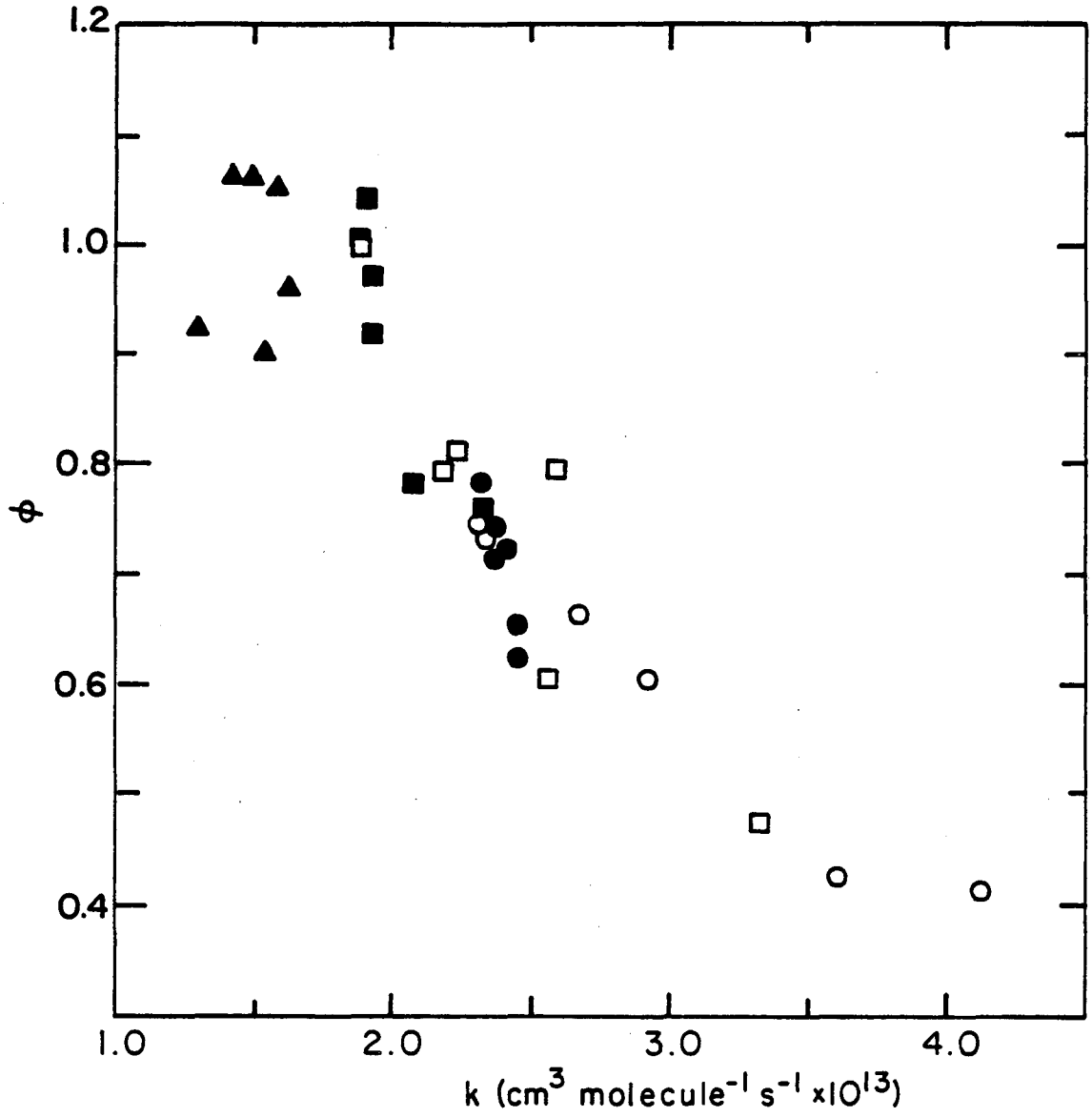

XBL8110-6924

Figure 36

concentration and fluence dependent. Figures 32-36 depict these dependencies as well as an apparent self correlation between the rate constant and product yields. The significance of these results will be disucssed in Section IVA, however, it does appear from these results that the NO_3 product yield is approximately one, with the value of k_2 approaching that value obtained in the FP/RF experiments as the conditions used in both experiments converge.

B. The Reaction of Cl with HNO_3

1. FP/RF Study.

The FP/RF study was done by photolysing Cl_2/HNO_3 mixtures Ar with the 350 nm XeF laser line. Nitric acid is transparent to this wavelength while Cl_2 is strongly dissociated. The HNO_3/Ar mixture was prepared identically as in the HO experiments but, before entering the monitoring cell, an additional mixture of Cl_2 in Ar was added and the HNO_3 concentration measured. The Cl_2 concentration was approximately $3x10^{14}$ molecules cm^{-3} with the photolysis pulse producing ~10^{11} Cl atoms cm^{-3}. This small amount of Cl_2 was the source of considerable noise due to the emission from a molecular chlorine rydberg series excited by the Cl atom lamp, as noted by Clyne and Cruse.[60] This emission extends from 135 to 180 nm; all wavelengths at which the unfiltered PMT is sensitive. As a result of this large noise signal, the Cl atom decay could only be followed for one lifetime.

The rate constant was studied at 295K and 10 Torr of Ar buffer gas. The HNO_3 concentration ranged from 2-$20x10^{15}$ molecules cm^{-3} due to the low rate of reaction with Cl atoms. The rate constant measured

Table 23. Kinetic results for reaction of Cl with HNO_3

HNO_3 (molecules cm^{-3} x 10^{-15})	measured k' (s^{-1})
2.06	95
2.58	92
5.60	96
7.40	108
10.0	116
10.7	126
10.7	137
14.5	153
14.5	160
18.2	187
18.2	203
20.8	202

$k_{10} = (6.48 \pm 1.65) \times 10^{-15}$ cm^3 $molecule^{-1}$ s^{-1}
Intercept = 67 s^{-1}

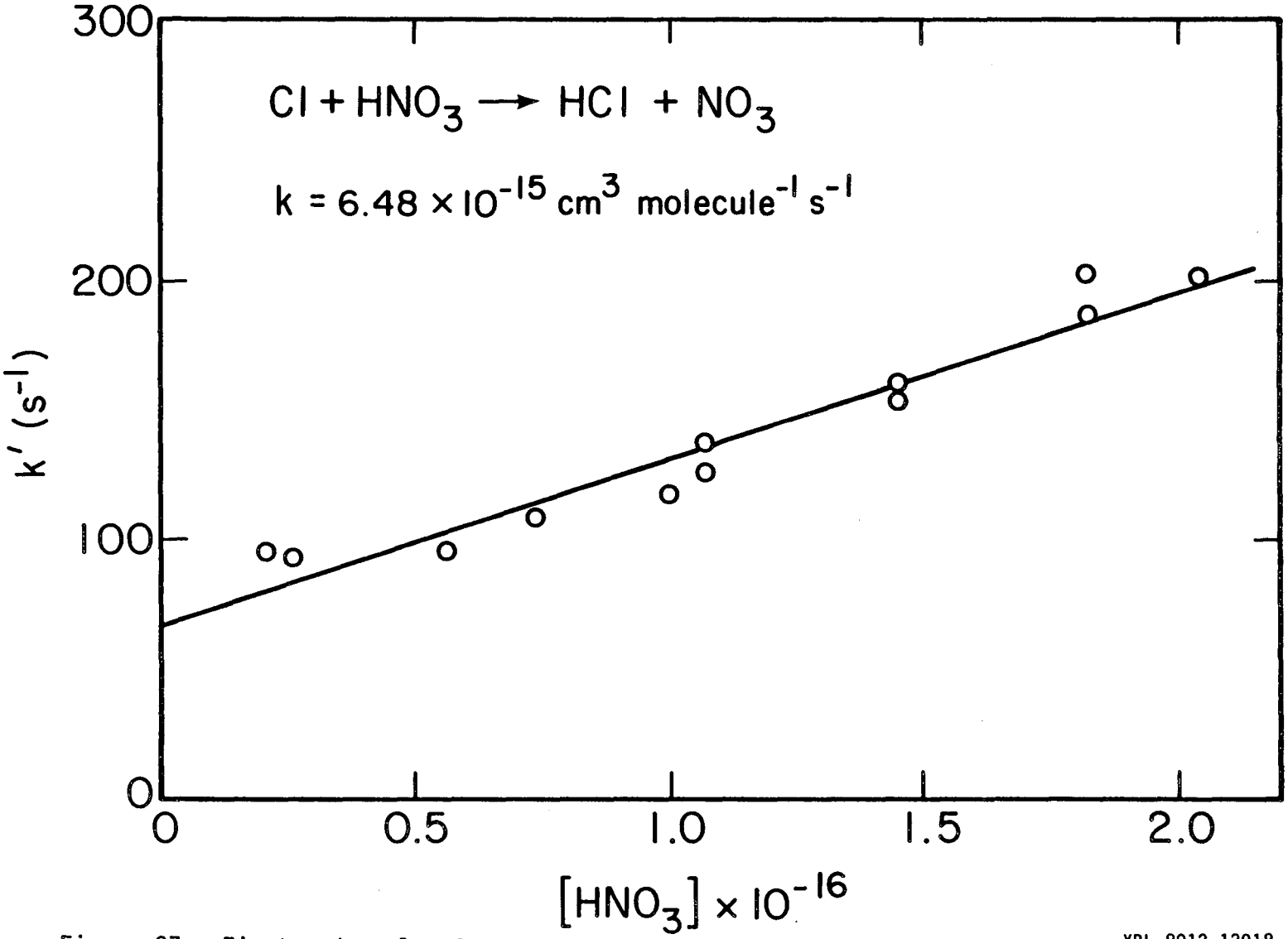

Figure 37. First order plot for reaction of Cl atoms with HNO_3 at 10 Torr and 298K. XBL 8012-12918

in these experiments was $(6.48 \pm 1.65) \times 10^{-15}$ cm^3 $molecule^{-1}s^{-1}$. The data for the experiments is given in Table 23 and the first order plot is shown in Fig. 37.

2. FP/LA Study.

It was hoped that the study of this reaction would compliment the HO radical study in both systems, since both were thought to be simple H atom abstractions with NO_3 as product. The method of mixed flows was again employed to obtain the Cl_2/HNO_3 mixtures; however, a tank of 100 ppm Cl_2 in N_2 was used as a Cl atom source. Photolysis energies and Cl_2 precursor concentrations were adjusted to give approximately the same signal levels as in the HO radical experiments.

These experiments could detect no NO_3 as a product of the reaction. The experiments were then conducted over a wide range of Cl_2 and HNO_3 concentrations under both flowing and static cell conditions. From these experiments an upper limit of 0.05 could be placed on the NO_3 product yield. The significance of these results will be examined in the next chapter.

C. The NO_3 Photodissociation Quantum Yield from $ClONO_2$

The 249.5 nm photolysis of $ClONO_2$ was studied at concentrations from ~$3-8 \times 10^{14}$ molecules cm^{-3}. Laser fluences from $2-18 \times 10^{16}$ photons cm^{-2} at total pressures of 20 and 100 Torr were employed. In some experiments CH_4 was added as a scavenger for any Cl atoms produced in the photolysis such that the secondary reaction

$$Cl + ClONO_2 \longrightarrow \text{products} \qquad (47)$$

which may produce NO_3, is not important. Using the rate constant for (47) measured by Kurylo and Manning[34] and the rate constant for the reaction of Cl with CH_4 recommended by DeMore et al.,[6] under experimental conditions most favorable to the partitioning of Cl to $ClONO_2$ vs. CH_4, reaction (47) would only capture 0.24 percent of the Cl atoms produced with a Cl lifetime of 18μs.

The time domain behavior of NO_3 in a typical $ClONO_2$ photolysis experiment is shown in Fig. 38. This particular experiment was conducted using 6.19×10^{14} molecules cm^{-3} of $ClONO_2$, a laser fluence of 17.2×10^{16} photons cm^{-2} and a carrier gas mix of 17 Torr CH_4 and 3 Torr Ar. Argon was always present in these experiments since it was used to flow through the $ClONO_2$ saturator; CH_4 was never allowed to enter the saturator. The time resolution of the experiments was 2μs per point. The figure shows a prompt rise in the NO_3 concentration coincident with the laser pulse followed by a slow secondary rise (peaking at ~200μs following the flash) of apprxoimately 15 percent of the initial increase. This rise occurs independent of the presence of CH_4, however its magnitude decreases with the amount of CH_4 present. The significance of this secondary rise will be discussed later. The amount of NO_3 initially formed by the photolysis was determined by inspection from the prompt rise using Beer's law.

The results of these experiments are shown in Tables 24 and 25, and displayed as a function of a laser fluence in Fig. 39. These results appear to be independent of fluence, $ClONO_2$ concentration, pressure or carrier gas composition. The average value of the NO_3 quantum yield is 0.55 ± 0.10 ($\pm 2\sigma$).

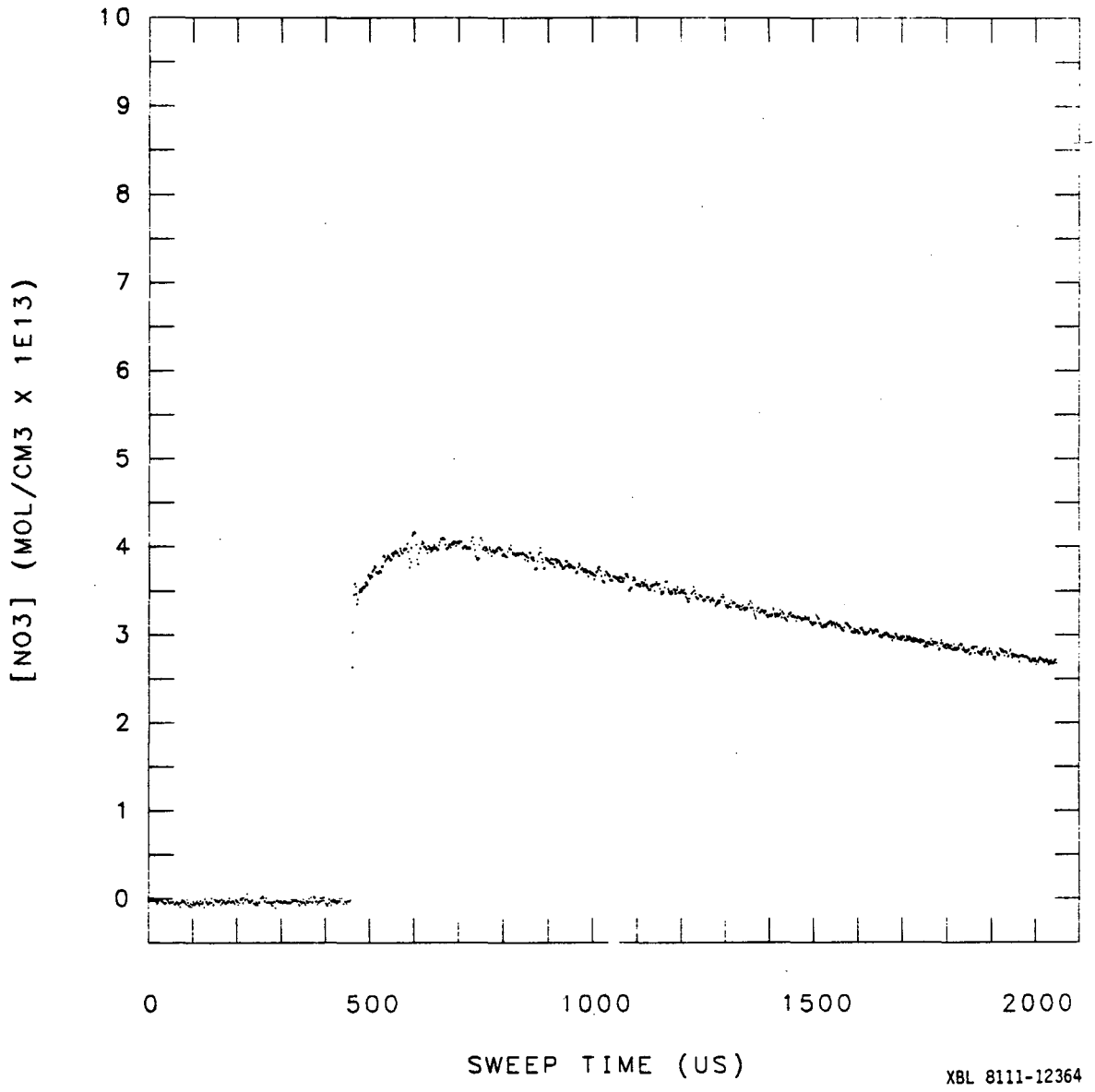

Figure 38. Typical data for NO_3 quantum yields from $ClONO_2$ photolysis at 298K.

Table 24. NO_3 quantum yields from $ClONO_2$ photolysis in Ar buffer gas.

$[ClNO_3]_{ss} \times 10^{-14}$	$E \times 10^{-16}$	$[ClNO_3]_{phot} \times 10^{-13}$	$[NO_3]_{t=o} 10^{-13}$	ϕ_{NO_3}	Pressure
molecule cm^{-3}	photons cm^{-2}	molecules cm^{-3}	molecules s^{-3} cm		Torr
4.88	4.93	1.92	1.11	0.58	20
8.03	15.9	8.14	4.50	0.55	20
6.96	2.97	1.32	0.725	0.55	20
6.90	10.3	4.54	2.88	0.63	20
6.64	2.92	1.24	0.703	0.57	100
6.29	17.6	7.06	4.18	0.59	100
6.15	15.1	5.92	3.79	0.64	100
				<0.59±0.08)	

Table 25. NO_3 quantum yields from $ClONO_2$ photolysis in CH_4/Ar carrier gas mixtures.

$[ClNO_3]x10^{-14}$	$Ex10^{-16}$	$[ClNO_3]_{phot}x10^{-13}$	$[NO_3]_{t=0}x10^{-13}$	ϕ_{NO_3}	Pressure
molecule cm^{-3}	photons cm^{-2}	molecules cm^{-3}	molecules cm^{-3}		CH_4/Ar=P(Torr)
6.01	4.49	1.71	0.932	0.55	17/3=20
7.21	2.24	1.03	0.582	0.57	17/3=20
7.06	1.23	0.555	0.291	0.52	17/3=20
6.01	5.32	2.04	1.17	0.57	17/3=20
6.19	17.2	6.80	3.50	0.51	17/3=20
6.84	8.34	3.64	1.99	0.55	17/3=20
6.99	18.4	8.24	4.16	0.50	60/40=100
7.06	8.25	3.72	2.16	0.58	60/40=100
7.23	4.30	1.99	0.978	0.49	60/40=100
6.80	2.42	1.05	0.623	0.59	60/40=100
3.08	12.8	2.51	1.41	0.56	95/5=100
3.02	4.10	0.763	0.339	0.44	95/5=100
3.05	13.4	2.56	1.24	0.48	905/5=100
3.09	6.73	1.33	0.731	0.55	95/5=100
				<0.53±0.08>	

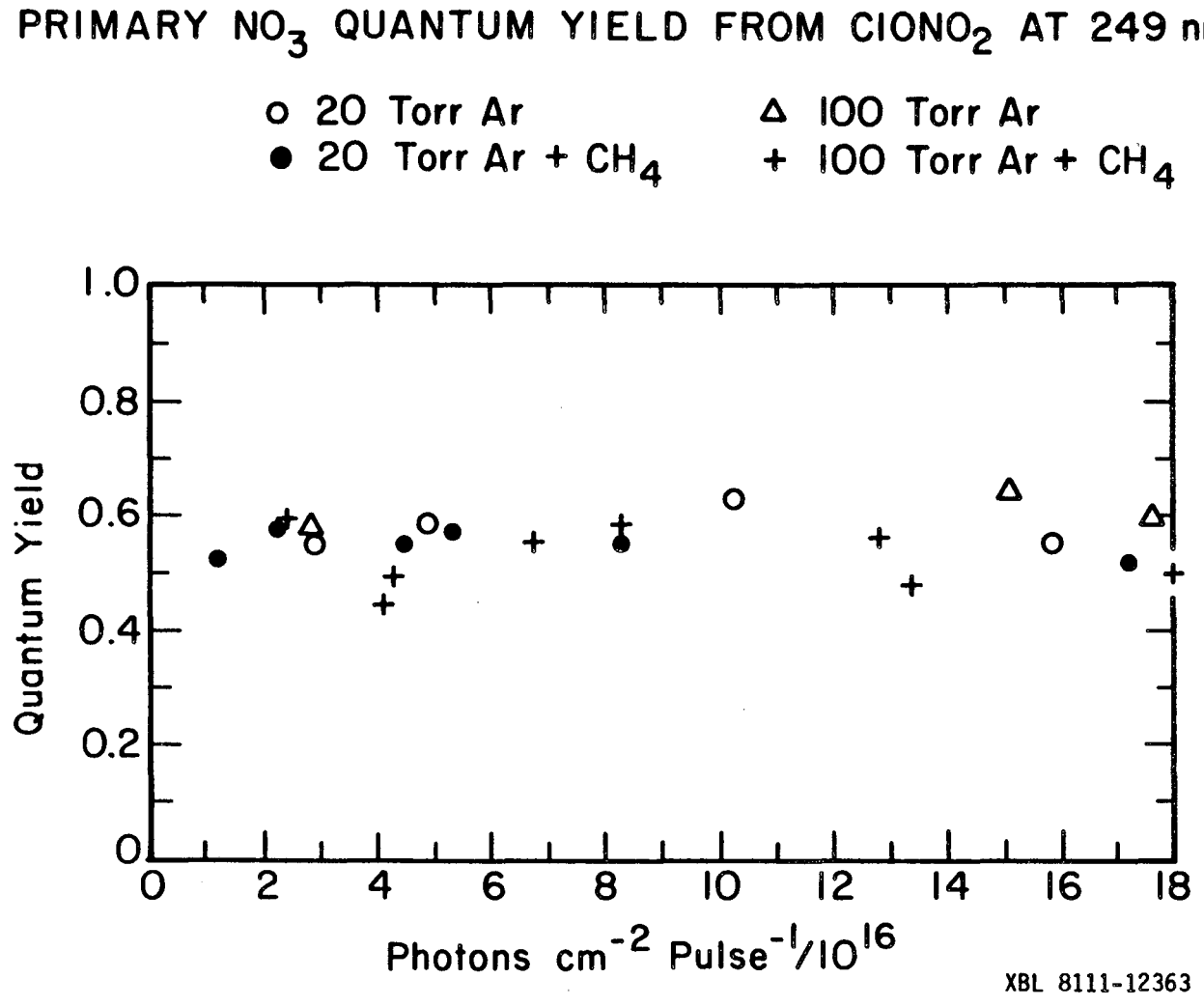

Figure 39. Summary of data from all $ClONO_2$ photolysis experiments under varying conditions of fluence and carrier gas mixture.

D. Absorption Cross Section and Lineshape for the NO_3 (0,0) Band

The NO_3 cross section were measured using the multimode laser of 0.05 nm linewidth and scanning from 672 to 648 nm. Twelve spectra at three different NO_2 input concentrations and six different ozone steady-state concentrations were recorded over this range. The chemistry of this systemis characterized by the reactions

$$N_2O_5 \xrightarrow{M} NO_2 + NO_3 \qquad (12)$$

$$NO_2 + NO_3 \xrightarrow{M} N_2O_5 \qquad (13)$$

$$NO_2 + O_3 \longrightarrow NO_3 + O_2 \qquad (14)$$

$$2NO_3 \longrightarrow 2N + O_2 \qquad (15)$$

$$N_2O_5 + H_2O \text{ (walls)} \longrightarrow 2HNO_3 \qquad (16)$$

To a good first approximation the steady-state concentration of NO_3 is given by

$$NO_3 = (K\, k_{14}/2k_{15})^{1/3}\, [O_3][N_2O_5] \qquad (15)$$

where K is the equilibirum constant k_{12}/k_{13}. Di-nitrogen pentoxide is able to extract water bonded to silica, and we have never been able to produce N_2O_5 completely free from HNO_3. In these experiments the apparatus was conditioned by lengthy exposure to N_2O_5 before the spectra were taken, HNO_3 was not measured during these runs, but from previous experience it is estimated that between 10 and 20 percent

of the N_2O_5 was converted to HNO_3. Because of the one-third power dependence of NO_3 on the concentration of N_2O_5, these considerations indicate that the concentrations of NO_3 calculated here are 3 to 7 percent too high, because of the partial conversion of N_2O_5 to HNO_3. The rate constants and equilibrium constants used are those of Graham and Johnston[44]

$$K = (8.4 \pm 1.8) \times 10^{26}\ e^{-11178/T}\ \text{molecules cm}^{-3} \qquad (49)$$

$$k_{14} = (1.34 \pm 0.11) \times 10^{-13-2466/T}\ \text{cm}^3\ \text{molecule}^{-1}\text{s}^{-1} \qquad (50)$$

$$k_{15} = (8.5 \pm 2.8) \times 10^{-13}\ e^{-2451/T}\ \text{cm}^3\ \text{molecule}^{-1}\text{s}^{-1} \qquad (51)$$

Although (15) is a good first approximation to the NO_3 concentration, there are additional corrections due to the finite rate of reaction (12) and to flow-in and flow-out of the cell. These corrections were carried out using the CHEMK[78] computer program. Secondary reactions initiated by the reaction, $NO_2 + NO_3 \longrightarrow NO + O_2 + NO_2$, were found to have negligible effect in this system. From the measured O_3 concentration, a stored ozone spectrum was scaled and subtracted from the observed absorptions to give optical densities due to NO_3. The cross sections were evaluated from

$$\sigma = \ln(I_0/I)/[NO_3]\ L \qquad (52)$$

where the concentration of NO_3 (molecules cm^{-3}) was found as described above and L was the optical pathlength, 191.5 cm. The

absorption spectra were evaluated between 672 and 648 nm for each of 12 experimental conditions, which are summarized in Table 26. The peak absorption was found to occur at 661.9 nm, and the peak cross sections are listed in Table 26. The average of the cross sections at the peak is 1.61 ± 0.34 (2σ) $\times 10^{-17}$ cm^2 molecule^{-1}.

The point-by-point average of the 12 spectra is plotted as a function of wave number (14910 to 15290 cm^{-1}) as curve A of Fig. 40. Experimental points are entered for every 2 cm^{-1}. The experimental curve appears to show some structure, for example near the peak. To see if this apparent structure is reproducible, four runs and their average are presented in Fig. 41 over a narrow range around the peak as identified by the horizontal bar in the upper center of Fig. 40. Over the 1.25 nm range between 661.45 and 662.70 nm, the four spectra and their average are entered from observations made at every 0.023 nm. The magnitude of experimental error is visible from the magnified spectra in Fig. 41 and it seems that the apparent structure near the peak of curve A in Fig. 40 is experimental noise.

By operating the dye laser in single frequency mode 0.00029 nm wide and with 0.022 nm sweep width, a sharp test was made concerning fine structure in the NO_3 spectrum. Curve A in Fig. 42 shows the opto-galvanic effect as the laser swept through a transition in the neon-filled hollow cathode lamp. Curve B shows the absorption spectrum through an $O_3/N_2O_5/NO_3$ mixture over the same wavelength range as curve A, which is located on Fig. 40 by the arrow at 15154 cm^{-1}. The flat curve shows no sign of rotational or other fine structure in the spectrum. Curve C shows a similar flat curve through the NO_3

Table 26. Experimental conditions and maximum cross sections.

$[NO_2]_o$ molecule $cm^{-3}/10^{16}$	$[O_3]_{ss}$ molecue $cm^{-3}/10^{17}$	$[NO_3]_{calc}$ molecule $cm^{-3}/10^{14}$	T K	σ_{max} molecule $cm^2/10^{-17}$
7.65	10.0	3.95	297.3	1.66
7.65	10.0	3.95	297.3	1.64
7.65	4.74	2.79	295.8	1.83
7.65	4.95	2.85	295.8	1.79
4.75	6.33	2.76	295.5	1.58
4.75	7.48	2.98	295.5	1.53
4.75	5.48	2.62	295.7	1.77
4.75	5.47	2.65	295.9	1.81
2.02	21.7	3.69	296.5	1.31
2.02	20.4	3.61	296.5	1.38
2.02	10.4	2.93	295.8	1.46
2.02	10.1	2.89	295.8	1.52

Figure 40. Absorption spectra of the (0,0) band of NO_3.

A. The average of 12 determinations in this study.

B. The average over each nm as reported by Graham and Johnston.[44] C. The reported points, ●, connected by smooth curve as reported by Mitchell et al.[45] Δ The height and location of the peak of Ref. 49. |—| The wavenumber range of Fig. 41. The arrows are wvenumber range of Fig. 41.

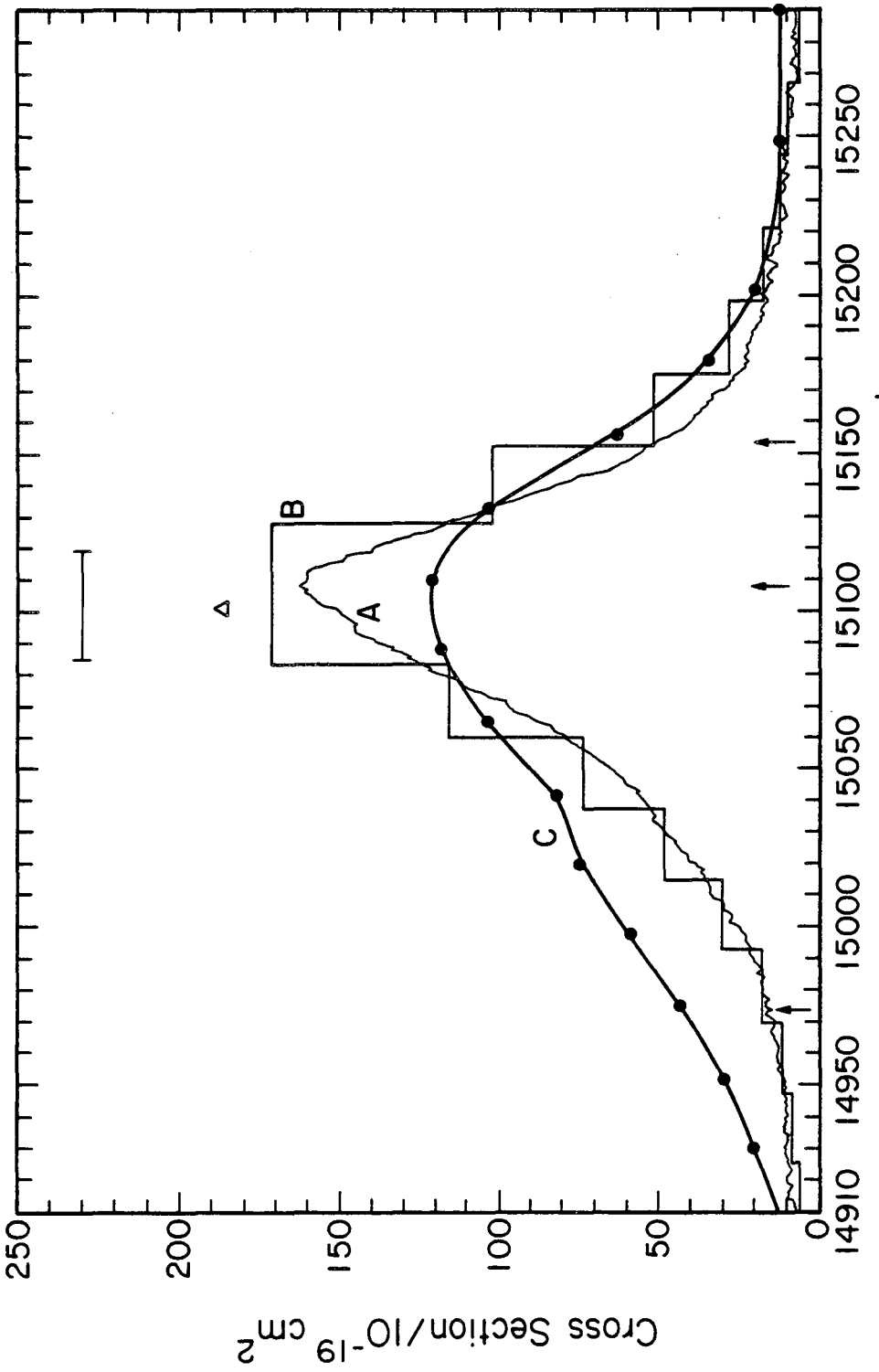

XBL 817-10867

Figure 40

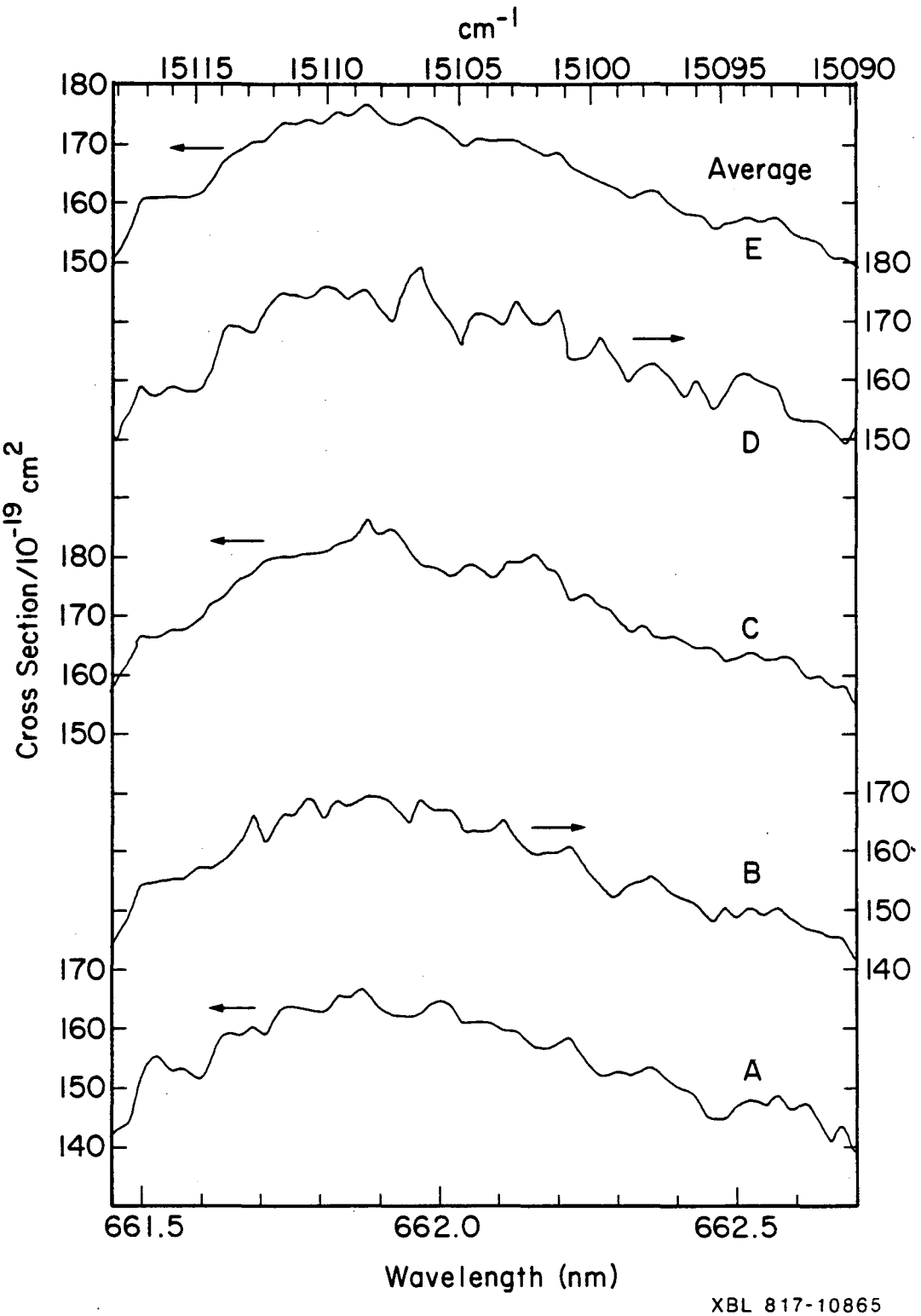

Figure 41. Expanded spectra near the peak of the NO_3 (0,0) band, compare |—| in Fig. 40. A-D are 4 experimental runs and E is average of all four.

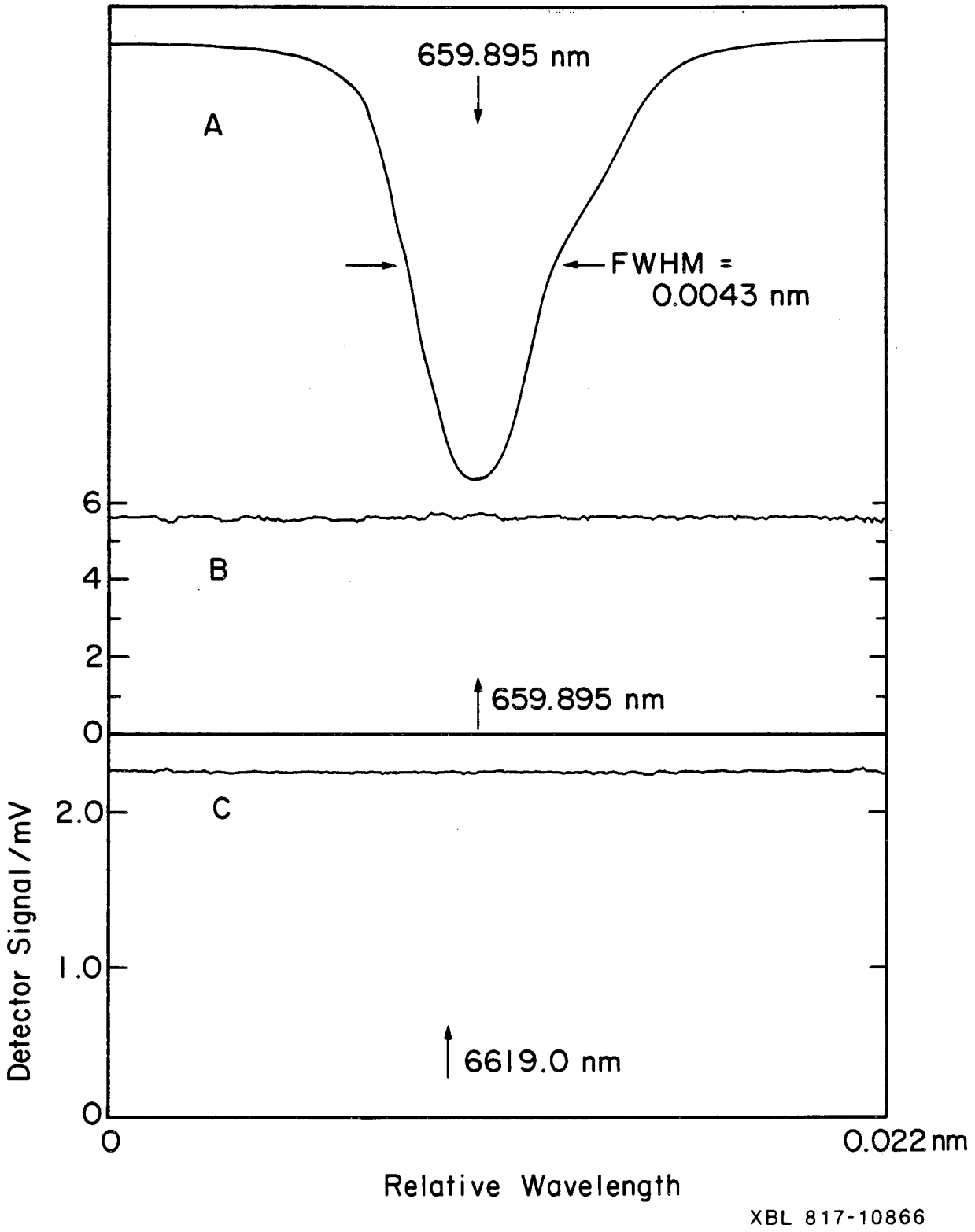

Figure 42. Very high resolution spectral scans with single-frequency dye laser. A. Opto-galvanic spectrum of neon line at 659.895 nm. B. Simultaneous NO_3 spectral scan through same wavelength region. C. NO_3 spectral scan near the (0,0) band maximum at 661.9 nm.

peak, as located by the arrow at 15108 cm^{-1} in Fig. 40; and another sweep at 14974 cm^{-1} showed no structure in the spectrum.

The scanning multimode laser with 0.05 nm resolution was used to cover the range from 14900-16300 cm^{-1}, and some points obtained by Graham and Johnston between 14600 and 14900 are included in Fig. 43. This spectrum includes the strong peak of Fig. 40 assigned as the (0,0) transition by Ramsay[42] and the strong peak at 623.22 nm, which Ramsay identified as the (0,1) transition of the symmetric stretching vibration.

IV. Discussion and Conclusions

A. The Reaction of HO with HNO_3

The rate constant measured for this reaction using flash photolysis/resonance fluorescence was $(1.52 \pm 0.43) \times 10^{-14} \exp(644 \pm 79/T)$ cm^3 $molecule^{-1}s^{-1}$. This result, in comparison with recent work, is shown in Table 27. Due to the relatively large uncertainty in the NO_3 flash photolysis/laser absorption experiments and their peculiar energy and pressure dependences, it is not really possible to place a single number on the rate constant measured from these experiments.

The strong dependence of the rate constant on the absorption cross section at the monitoring wavelength makes it necessary to insure a proper value is used. This study used UV absorption at 200 nm to measure HNO_3. A summary of measured absorption cross sections at that wavelength is given in Table 28. The results fall into two regimes: static determinations using pressure to determine HNO_3 concentrations, and flowing systems where the HNO_3 was trapped and titrated. Flowing systems are preferred for HNO_3 cross section determinations due to the affinity of HNO_3 for cell walls. In flowing systems an equilibrium is established between the walls and the gas phase and, after an initial passivation period, the concentration is independent of the walls. In static systems wall absorptions equivalent to anywhere from $1-10 \times 10^{15}$ molecules cm^{-3} have been noted. This reduction in the gas phase concentration in static systems results in a lower measured cross section based on pressure measurements, as evidenced in Table 28. The two measurements done in flowing systems agree within 1 percent. The cross section of Molina and Molina[56] was chosen on the basis of lower uncertainty in the result.

Table 27. Summary of kinetic results for the reaction of HO with HNO_3

Temperature Range(K)	k_{298}	A	$k(t)^{a,b}$ E/R(K)	Method	Reference
298	1.7×10^{-13}	-----	-----	Flash photolysis/kinetic spectroscopy	13
208	1.3×10^{-13}	-----	-----	Flash photolysis/resonance absorption	14
230-490	9.0×10^{-14}	9.0×10^{-14}	0	Flash photolysis/resonance absorption	15
228-472	8.0×10^{-14}	8.0×10^{-14}	0	Flash photolysis/resonance absorption	16
270-470	8.9×10^{-14}	8.9×10^{-14}	0	Discharge flow/resonance fluorescence	17
224-366	$1.3^{a} \times 10^{-15}$	1.52×10^{-14}	-649	Flash photolysis/resonance fluorescence	21
298	8.2×10^{-14}	-----	-----	Flash photolysis/resonance fluorescence	22
218-363	1.32×10^{-13}	1.52×10^{-14}	-644	Flash photolysis/resonance fluorescence	this work

a cm^3 $molecule^{-1}s^{-1}$

b $k(T) = A \exp(-E/RT)$

Table 28. Measured HNO_3 absorption cross sections near 200 nm

λ (nm)	σ $cm^2 \times 10^{18}$	Method	Reference
198.9	6.19	Static/Pressure Measurement	85
199	6.3	Static/Pressure Measurement	49
200	5.5	Static/Pressure Measurement	49
200	6.61	Flowing/Titration	56
200	6.5	Flowing/Titration	31
200	6.0	Static/Pressure Measurement	31

Accurate Arrhenius parameters require that the temperature of the gas be known very well. Placement of temperature sensors on the cell walls is not adequate since the gas may not thermalize during its residence time or the resonance lamp may heat the gas sample. In this experiment, the temperature sensor was placed in the flowing gas stream at the reaction center with the resonance lamp operating and the cell at experimental pressures. The sensor was calibrated by immersion in the temperature bath fluid with the fluid temperature measured by 3 different calibrated thermometers. Calibration linearity was found to be ±1K over a 100K temperature difference from the calibration point, however the sensor was never used further than 5K from a calibration point. Overall accuracy is estimated to be ±1K.

The intercepts obtained from the first order plots are shown in Fig. 30 plotted in Arrhenius form for experiments performed in the third generation cell. At all temperatures except 218K intercepts scale with pressure as one would expect for a diffusion controlled process (i.e., $k_d \propto 1/P$). However, the temperature dependence of k_d fits the Arrhenius form fairly well, suggesting that reaction with some component of the carrier gas is important as opposed to diffusion, which would scale as $T^{1/2}$. The Arrhenius parameters for these fits are: A = 284 s^{-1}, E/R = 341k^{-1} at 10 Torr and A = 206 s^{-1}, E/R = 153k^{-1} at 25 Torr. A T^n dependence plot gives n = -1.22 at 10 Torr and n = -0.69 at 25 Torr with about the same variance as the Arrhenius fit. Since flow rates through the reaction zone remained constant for each pressure, any contribution to k_d due to flow would be the same. The fact that the slope of the lines at each pressure are different may indicate a third

order process is occurring. However, without knowing the exact level of each of the impurities in the argon carrier gas, little can be said about the exact processes governing this rate. It is not clear what happened at 218K, although it is possible that the composition of the carrier gas may have changed as the tank pressure decreased. Since the rate constants measured at either pressure were very close, no further effort was made to investigate this effect.

The rate constant measured for the reaction of HO with HNO_3 was found to be linar over a 23 fold range of HNO_3 concentration and a 5 fold range of pressure. First order decays were followed for 1.5-3 HO lifetimes. Both the Arrhenius plot (Fig. 28) and the T^n dependence plot (Fig. 29) are linear within the 2σ error bars over a 145K temperature range, however the relative variances of the fits would favor the Arrhenius form. The appearance of the plot would suggest some curvature with flattening out at higher temperatures, but this can not be confirmed due to the size of the error limits.

The inverse temperature dependence reported by Wine et al.[21] and observed here, the close agreement with those results raises serious questions about mechanism of this reaction. Typical hydrogen abstraction reactions by hydroxyl radicals, including the reaction of HO with H_2O_2 studied here, show small positive or no temperature dependences. Another unusual feature of the reaction is the low A factor, which is apprxoimately 170 times less than the analogous reactions of HO with H_2O_2, CH_4, and HCl. The departure of these factors from those observed for simple stripping reations would suggest that the reaction is not a direct hydrogen atom abstraction but rather porceeds through some low temperature stabilized reaction complex or van der Walls molecule:

$$HO + HNO_3 \underset{<-----}{\overset{M(?)}{----->}} (HO\ HNO_3) \longrightarrow H_2O + NO_3 \quad . \qquad (53)$$

Often these types of reactions have M dependent complex formation steps, especially where the complex partners have few internal degrees of freedom and the translational energy of the collision must be taken up by a third body. Neither study has observed a pressure dependence at any temperature; however, at a recent talk by Margitan[25] he presented preliminary results showing as much as a 40 percent pressure dependence over a 100 torr range at low temperatures. The effect appears to occur only below 298K with a temperature dependence comparable to that observed here and by Wine et al.[21] It may be that the internal modes of HNO_3 are sufficient to take up the collision energy and any pressure effect may manifest itself only over a wide pressure range.

Complex formation in the reaction of HO with HNO_3 may have its analogy in the reaction of Cl with HNO_3, where the expected products of H atom abstraction are not observed. One possibility for investigating complex formation in the reaction of HO with HNO_3 may be a flow tube study using O^{18} labeled HNO_3 and diode laser detection of either H_2O^{18} or H_2O^{16} labeled product, with HO radicals made by reaction of H with NO_2.

There is excellent agreement between these results and those of Wine et al.,[21] and their disagreement with previous studies is very difficult to explain. The previous studies, including one performed in this laboratory only a year ago, were all very carefully done or preliminary studies which may be reinterpreted to explain differences

from the previously accepted values. The early results of Husain and Norrish[13] were done in a static system with relatively few data points taken. Though no specific amount of NO_2 impurity was quoted, it would appear that it may be as high as 1 percent based on the amount of HNO_3 photolysed and the photolysis of the NO_3 product. At the experimental pressure of 500 Torr N_2, a 0.25 percent NO_2 impurity would require a correction reducing their result for k_2 to 1.3×10^{-13} cm^3 $molecule^{-1}s^{-1}$ and a 1 percent impurity could give a rate constant of approximately 8×10^{-14} cm^3 $molecule^{-1}s^{-1}$. The observation of the NO_3 product in the experiment is somewhat curious in that the reported NO_3 risetime of 15μs (nominal) is 10 times less than the corresponding HO decay of 140μs for a 5 Torr HNO_3 sample. Either this points to a serious problem with the experiment or perhaps a typographical error in which the NO_3 rise time should be 150μs. Since the amount of NO_2 impurity was not carefully controlled, no serious reinterpretation can be attempted.

The three results reported from the laboratories of Ian Smith were all flash photolysis/resonance absorption experiments conducted under varying amounts of NO_2 impurity. The study of Morely and Smith[14] consisted of a few points determined as part of a study of the reaction of HO with NO_2. They measured $k_2 = 1.3 \pm 0.5 \times 10^{-13}$ cm^3 $molecule^{-1}s^{-1}$, uncorrected for the contribution due to reaction (9). In a later note by Zellner and Smith[15] reporting some preliminary results, NO_2 impurity levels of approximately 1.4 percent were measured and these results as well as the results of Morely and

Smith[14] were corrected to yield a measured k_2 ranging from 1.1-0.7 x 10^{-13} cm^3 $molecule^{-1}s^{-1}$ at temperatures between 405 and 240K. The final report of the results of Smith and Zellner[16] utilized samples of HNO_3 containing low enough impurities of NO_2 such that no corrections due to reaction (9) were necessary, even at the lowest temperature studied. The rate constant (k_2 = 8x10^{-14} cm^3 $molecule^{-1}s^{-1}$) was found to be independent of temperature from 240-406K.

One possible problem with the results of Smith and Zellner[15,16] was the fact that the experiments were conducted in static systems where the concentration of HNO_3 was measured by expansions of mixtures of HNO_3 in a diluent gas stored in a glass bulb. The great affinity of HNO_3 for pyrex walls may result in a significant fraction of the HNO_3 placed in the storage bulb going to the walls and reducing the effective HNO_3 concentration. Furthermore, expansion of these mixtures into the long-path, high surface to volume ratio resonance absorption cells may further reduce the effective HNO_3 concentration due to wall absorption. Both of these effects would lead to a lower measured rate constant; however, the degree of wall conditioning, the surface-to-volume ratio of both the storage and photolysis cells and the amount of HNO_3 decomposition are all apparatus specific and difficult to evaluate, hence it is not possible to try and determine the magnitude of any possible corrections to the measured results.

The flow tube study of Margitan, Kaufman and Anderson[17] obtained a result quite similar to the final results of Smith and Zellner[16]

from 270-470K. ($k_2 = 8.9 \times 10^{-14}$ cm^3 molecule^{-1}s^{-1}). However, the result at 272K ($k_2 = 1.12 \times 10^{-13}$ cm^3 molecule^{-1}s^{-1}) was discarded due to a large heterogeneous wall removal rate for HO and a small number of measurements. If one includes the 272K point, these these results may be expressed as $k_2 = 6.0 \times 10^{-14}$ exp(155/T) showing some negative temperature dependence. This result for the temperature dependence may be consistant with the possibility of some curvature in the Arrhenius plot noted here and in a later study by Margitan[25] where the plot appears to flatten out at higher temperatures. The lower rate constant measured here may also be the result of some of the gaseous HNO_3 expanded from a large pyrex bulb going to the walls where surface absorption may reduce the effective HNO_3 concentration.

The results of Nelson[31] reported in Nelson, Marinelli and Johnston[22] are difficult to reconcile with my results. The results were obtained in flowing FP/RF apparatus where HNO_3 and NO_2 were both measured using UV absorption. Nitrogen dioxide was less than or equal to a 0.15 percent impurity in the HNO_3 and the correction to the rate constant was less than 1.1 percent. The monitoring wavelength and absorption cross sections used were essentially the same as in this experiment. In flowing systems such as these, there is always a possibility of a pressure drop between the monitoring and photolysis cells resulting in an error in the measured rate constants. Early experiments done in his system did show a problem like this, however a series of monitoring cell vs <u>in situ</u> photolysis cell measurements of O_3 mixtures showed that measures taken to correct this problem were

successful. This would seem to be confirmed by experiments measuring the rate constant for the reaction of HO with H_2O_2, which agreed quite well with studies performed here and by other experimenters (see Table 3). It is possible that some wall catalyzed loss of HNO_3 may have occurred and not been detected, since no experiments were done to measure the rate constants with the monitor before and after the cell once the apparent pressure drop problem had been corrected.

The experiment of Wine et al.[21] also appears to be a careful study, very similar in technique and procedure to this work and that of Nelson.[31] A major difference between the studies was the use of a flash lamp for HNO_3 photolysis by Wine et al.[21] It is possible that the shorter wavelengths of light emitted by the photolysis lamp may produce excited states of HO having accelerated rates of reaction with HNO_3, however substitution of a KrF excimer laser similar to that used here and by Nelson[31] for the photolysis lamp had no effect on the results. Nitric acid was monitored in their study by UV absorption at 184.9 nm using an absorption cross section determined in the study that agrees with extrapolations of other reported results. It is not clear what differences between these three studies accounts for the differences in the final results, however studies by other groups are in progress and may shed further light on this problem.

The flash photolysis/laser absorption study of this reaction is difficult to evaluate. There appears to be a weak correlation between the measured values of k_2 and ϕ_{prod} and the experimental pressure and M gas identity. A somewhat stronger correlation exists between k_2 and ϕ_{prod} at varying degrees of pressure and laser fluence. The

magnitude of these effects appears to be a function of HNO_3 concentration. The general effect appears to be an elevation of rate constant and decrease in NO_3 product yield with increasing laser fluence. At higher pressures and HNO_3 concentrations the rate constant decreases and the NO_3 yield approaches one. Nitrogen appears to be a more efficient M gas than Ar in bringing about this pressure effect. At the high pressure/low fluence limits of these effects, an NO_3 product yield of one is obtained with a value of k_2 slightly higher than that obtained in the FP/RF experiments. The precision of k_2 is not very good as can be seen from the data tables.

The fact that an energy dependent effect is apparently diminished in systems having higher heat capacities or quenching efficiencies would suggest either significant heating of the sample or production of more reactive molecules producing NO_3 or other products in a reaction with HNO_3. In experiments using high energy lasers it is always necessary to ask what effects, if any, heating of the sample may produce. The FP/RF experiments employed fluences as high as 2.5×10^{16} photons cm^{-2}; however, at absorber concentrations less than 4×10^{15} molecules cm^{-3} heating of the sample is much less than 0.1K. The higher fluences and HNO_3 concentrations employed in the FP/LA experiments may result in sample heating as high as 8K in the beam. Using literature values[18,86] of the heat capacity at constant volume for Ar, N_2 and HNO_3, the magnitude of any temperature increase in the beam is assessed in Table 29 for all experimental conditions employed. Significant heating does occur at low pressures and high laser fluences and any resulting shock wave from this heating may have

Table 29. Estimated temperature increase in FP/LA experiment

Pressure (Torr)	Energy (photons cm^{-2})	Temperature Increase (K) Ar, $[HNO_3]$ (molecules cm^{-3}) $2x10^{16}$	Ar, $[HNO_3]$ (molecules cm^{-3}) $6x10^{15}$	N_2, $[HNO_3]$ (molecules cm^{-3}) $2x10^{16}$	N_2, $[HNO_3]$ (molecules cm^{-3}) $6x10^{15}$
10	$2x10^{17}$	8.1	2.7	5.7	1.7
	$5x10^{16}$	2.0	0.7	1.4	0.4
	$2x10^{16}$	0.8	0.3	0.6	0.2
30	$2x10^{17}$	3.0	0.9	1.9	0.6
	$5x10^{16}$	0.7	0.2	0.5	0.2
	$2x10^{16}$	0.3	0.1	0.2	0.1
50	$2x10^{17}$	1.8	0.6	1.1	0.3
	$5x10^{16}$	0.5	0.2	0.3	0.1
	$2x10^{16}$	0.2	—	-.1	—
745	$2x10^{17}$	—	—	—	—
	$5x10^{16}$	—	—	—	—
	$2x10^{16}$	—	—	—	—

some bearing on the results. However, these fluence effects have their greatest effect at lower HNO_3 concentrations where laser heating of the sample is less significant. To test for any thermal lensing that may cause deflection or attenuation of the beam, a high energy, high fluence, low pressure experiment was conducted in which the probe laser was tuned off the NO_3 absorption. Any thermal lensing of the beam should be independent of small displacements in wavelength, however no attenuation of the beam was detected. While it is clear that rotational thermalization of the HO and NO_2 translational and photoproducts occurs rapidly on the experimental time scale, rates of vibrational equilibration may occur in the same time regime as the reaction.

The notion of excited state chemistry being responsible for these effects is attractive but may not explain the fluence dependence. Simple one photon absorption is fluence independent; and while two photon absorptions would be fluence dependent, typical absorption cross sections for these types of processes are very small ($<10^{-50}$ cm^2 $molecule^{-1}$). No absorption cross sections for two photon absorption at the KrF laser wavelength have been measured for HNO_3 and therefore it is difficult to speculate about the magnitude of this process. Nitric acid photolysis at the KrF wavelength leaves approximately 23,500 cm^{-1} excess energy after bond breaking to be taken up in the translational and internal modes of the products. This would be sufficient to produce translationally or vibrationally hot HO. Resonance fluorescence detection only monitors HO ($v"=0$) and in a

situation where HO(v">0) reacts much faster than HO (v"=0) the appearance of NO_3 product may be faster than HO(v"=0) removal. The opening up of additional product channels or diffusion of HO out of the beam at lower pressures before reacting may account for the decreased product yield.

The observed NO_3 product yields and rise times are more than likely the weighted aggregate of some or all of the processes discussed here; however, little can be inferred about the actual mechanism of the reaction or possible experimental artifacts that give rise to these results from observation of these variables. The technique of flash photolysis/laser induced fluorescence has been used to probe the product states of HO radicals produced from a variety of precursors and excited state reactions. A similar study for HNO_3 photolysis is long overdue and would be welcomed. The main conclusion of this part of the study is that NO_3 is the primary product of the reaction of HO with HNO_3, having a low fluence product yield of 1.05 ± 0.26 (2σ).

B. The Reaction of HO with H_2O_2

The reaction of HO radicals with H_2O_2 has been extensively studied and these results are summarized in Table 30. Previous studies have been reviewed by Nelson[31] in his thesis, and the reader is referred there if more information is necessary. Subsequent review of Greiner[26] and Harris and Pitts[28] by Sridharan, Reiman and Kaufman[30] have shown problems with those experiments that when re-analyzed agree well with the most recently reported results. The results of Hack, Hoyermann and Wagner[27] have been called into question by the subsequent revision of the rate constant for the reaction

Table 30. Summary of reported rate constants for the reaction of HO with H_2O_2

Temperature Range(K)	k_{298}	k(T)[a,b]	Method	Reference
300-458	9.3×10^{-13}	$4.08 \times 10^{-13} \exp(-604/T)$	Flash photolysis/kinetic spectroscopy	26
298-670	8.4×10^{-13}	$7.97 \times 10^{-12} \exp(-670/T)$	Discharge flow/ESR	27
298	6.8×10^{-13}	-------	Flash photolysis/resonance fluorescence	28
245-423	1.64×10^{-12}	$2.51 \times 10^{-12} \exp(-126/T)$	Discharge flow/resonance fluorescence	29
250-459	1.69×10^{-12}	$2.96 \times 10^{-12} \exp(-164/T)$	Discharge flow/LIF	30
298	1.57×10^{-12}	-------	Flash photolysis/resonance fluorescence	31
298	1.81×10^{-12}	-------	Flash photolysis/resonance fluorescence	this work

[a] $cm^3\ molecule^{-1}s^{-1}$

[b] $k(T) = A \exp(-E/RT)$

$$HOO + NO \longrightarrow HO + NO_2 \qquad (54)$$

which was found to be 30 times faster than measured by them at the time. Hydroxyl radicals were prepared in that study by the reaction

$$H + NO_2 \longrightarrow HO + NO \qquad (55)$$

and subsequent reaction of HO and H_2O_2 produced HO_2. This HO_2 then fed back via reaction (54) with ambient NO to produce HO. Failure to adequately compensate for this back reaction resulted in the low rate constant measured in that system.

The result reported here of $(1.81 \pm 0.24) \times 10^{-12}$ cm^3 $molecule^{-1}s^{-1}$ agrees well with the 3 most recent flow tube and flash photolysis studies. The average of these reported values is $(1.68 \pm 0.20) \times 10^{-12}$ cm^3 $molecule^{-1}s^{-1}$ (2σ) at 298K. All values reported fall within 8 percent of the average. The agreement of this result with previously reported values is some confirmation that the experimental system was behaving properly.

C. The Reaction of Cl with HNO_3

The two previous studies of this reaction, using very similar techniques, came to different conclusions about the rate at 298K. The results of these studies and the present work are summarized in Table 31. Poulet, Le Bras, and Combourieu[33] were only able to place an upper limit of 2×10^{-17} cm^3 $molecule^{-1}s^{-1}$ on the rate constant, based on an extrapolation of high temperature data to 298K and detection limits. Leu and DeMore[32] reported a rate of $(6.8 \pm 3.4) \times$

Table 31. Summary of reported rate constants for the reaction of Cl with HNO_3

Temperature Range(K)	k_{298}	k(T)[a]	Method	Reference
298	6.8×10^{-15}	---	Discharge flow/mass spectroscopy	32
439-663	$<2 \times 19^{-17}$	$1.5 \times 10^{-11} \exp(-4394/T)$	Discharge flow/mass spectroscopy	33
298	6.48×10^{-15}	---	Flash photolysis/resonance fluorescence	this work

[a] $cm^3\ molecule^{-1} s^{-1}$

10^{-15} cm^3 $molecule^{-1}s^{-1}$ at 298K. Both studies used discharge flow/mass spectrometric techniques in which the attenuation of HNO_3 was measured in the presence of excess Cl atoms.

Poulet et al.[33] have sought to explain this discrepancy based on the concentrations of HNO_3 used in each experiment. The range of concentrations used in the Leu and DeMore experiment was estimated by them to be (0.6-0.9) x 10^{14} molecule cm^{-3}, as opposed to (1-15) x 10^{14} molecules cm^{-3} in their experiment. Margitan, Kaufman and Anderson[17] have shown that, for phosphoric acid poisoned flow tube walls of the type used in both experiments, saturation occurs only at HNO_3 concentrations greater than 4 x 10^{14} molecules cm^{-3}. Therefore, the Leu and DeMore experiment may have been conducted under unsaturated wall conditions where heterogeneous reactions or surface absorption may be the major mechanism for HNO_3 removal.

While this explanation is certaintly tenable, it does not explain the close agreement between this study and that of Leu and DeMore. The 298K rate constant of (6.48 ± 1.65) x 10^{-15} cm^3 $molecule^{-1}s^{-1}$, obtained by following the decay of Cl atoms in the presence of HNO_3 concentrations of ~10^{15} molcules cm^{-3}, is insensitive to any surface effects. One possible problem with this study may be that the Cl atoms are reacting with some impurity in the HNO_3 (carrier gas impurities are factored out in the first order plots). The major impurity in the HNO_3 is NO_2, which was never present in quantities greater than 0.2 percent. Removal of Cl atoms via the reaction

$$Cl + NO_2 + M \longrightarrow ClNO_2 + M \qquad (56)$$

was found to be negligible using a recommended rate constant of 2.0 x 10^{-13} cm^3 $molecule^{-1}s^{-1}$.[6] A calculation of NO_2 produced from HNO_3 photolysis by the Cl lamp found it to be insignificant compared to NO_2 already present as an impurity.

One problem with the study of Poulet et al.[33] may be the manner in which HNO_3 was monitored. Due to poor sensitivity at the molecular peak, HNO_3 was monitored at the NO_2^+ peak after correction for signal due to NO_2 present in the mixture. However, NO_2 was reported to be a major product of the reaction and, if improperly corrected, could be mistaken for HNO_3. If this were the case, the the attentuation of HNO_3 would appear much less and a smaller apparent rate constant would be calculated. Insufficient detail was presented in the paper to evaluate this hypothesis nor was any information on the details of HNO_3 detection outlined in Leu and DeMore. The closeness of this study and that of Leu and DeMore would seem to lend credence to a value of approximately 6.5 x 10^{-15} cm^3 $molecule^{-1}s^{-1}$ for the rate constant at 298K.

In addition to NO_2, Poulet et al.[33] observed HCl and ClO as major proucts of the reaction with traces of HOCl present. Leu and DeMore did not attempt to observe any products. From the large amount of HCl present, Poulet et al.[33] concluded that the major product channel was

$$Cl + HNO_3 \longrightarrow HCl + NO_3 \quad . \qquad (10a)$$

However, no NO_3 was observed as a product. To explain this they have postulated that the reaction

$$Cl + NO_3 \longrightarrow ClO + NO_2 \qquad (57)$$

occurs rapidly, consuming NO_3 and explaining the presence of large amounts of ClO and NO_2. The trace amounts of HOCl observed were thought to originate from the channel

$$Cl + HNO_3 \longrightarrow HOCl + NO_2 \quad . \qquad (10d)$$

The absence of any NO_3 production from the reaction, as determined in the FP/LA experiments, is not consistant with the mechanism of (10a) followed by (57). Even if (57) were fast ($\sim 10^{-11}$ cm^3 $molecule^{-1}s^{-1}$), the NO_3 lifetime in this second order process would still be on the order of 5 ms; this is much longer than the time scale of the experiment.

This discrepancy may be explained if one considers the fate of any HOCl produced via (10d). In the presence of excess Cl atoms, as in Poulet et al.,[33] HOCl may be consumed by the reaction

$$Cl + HOCL \longrightarrow HCl + ClO \quad . \qquad (58)$$

No studies of this reaction have been performed, however if one uses the rate constant for the analogous reaction (also determined in both these studies; $k \sim 5 \times 10^{-13}$ cm^3 $molecule^{-1}s^{-1}$)

$$Cl + H_2O_2 \longrightarrow HCl + HO_2 \qquad (59)$$

one obtains an HOCl lifetime of approximately 10^{-3} seconds for the average Cl atom concentration of $2x10^{15}$ molecule cm^{-3} of Poulet et al.[33] This is much less than the maximum reported reaction time of $2x10^{-2}$ seconds. If (10d) were the major product channel, then this mechanism would account for the observed major products HCl, ClO and NO_2 as well as the trace HOCl observed by Poulet et al.,[33] while explaining why no NO_3 was observed in the FP/LA experiments performed here. The relative exothermicities of reactions (10a) vs (10d), -1.8 vs -4.,5 kcal $mole^{-1}$, also lend credence to (10d) as the major product channel.

D. The Photochemistry of $ClONO_2$

The previous studies of $ClONO_2$ photolysis (see Table 32 for summary) can be classified into two categories. The experiments by Smith, Chou and Rowland[37] and by Adler-Golden and Wiesenfeld[39] have both concluded that a channel leading to the production of $O(^3P)$ atoms, possibly

$$ClONO_2 + h\nu \longrightarrow ClONO + O(^3P), \qquad (11c)$$

was the major channel. Neither study ws able to quantify the $O(^3P)$ yield for this channel. Chang, Parker, Davenport and Golden[38] were able to measure a Cl atom quantum yield of 1.0 ± 0.2, an NO_3 yield of $\geq$0.5 ± 0.3 and an $O(^3p)$ yield of 0.10 ± 0.02. Their conclusion was that the reaction channel

Table 32. Summary of reported results for $ClONO_2$ photolysis quantum yields.

Method	$\phi_{O(^3P)}$	ϕ_{Cl}	ϕ_{NO_3}	ϕ_{ClO}	Reference
Continuous photolysis/end product analysis	"major"	not detected	---	---	37
Very low pressure photolysis/mass spectroscopy	$\leq$ 0.1	1.0 ± 0.2	0.5 ± 0.3	$\leq$ 0.04	38
Flash photolysis/resonance absorption	"predominant"	$\leq$ 0.4	---	---	39
Flash photolysis/laser absorption	$\leq$ 0.1	not detected	0.55 ± 0.10	---	this work/31

$$ClONO_2 + h\nu \longrightarrow Cl + NO_3 \qquad (11b)$$

was predominant. Nelson[31] used XeF excimer laser photolysis of $ClONO_2$ at 350 nm coupled with O atom resonance fluorescence detection to show that the O atom channel was less than 0.10.

There are several possible serious complications involved in conducting these experiments. The most serious of these involves the purity of the $ClONO_2$. The paper of Smith et al.[37] describes neither the method of preparation nor the level of impurities present. Chang et al.[38] prepared $ClONO_2$ by reacting ClF with HNO_3. The major impurities were stated to be Cl_2 and NO_2 although no quantities or upper limits were specified. The study of Adler-Golden and Weisenfeld[37] did not describe the method of preparation of $ClONO_2$. Their analysis of the $ClONO_2$ found a 0.6 percent NO_2 impurity but no statement of any OClO or Cl_2O impurity levels were specified. This study used the reaction of Cl_2O with excess N_2O_5 to prepare $ClONO_2$. Analysis of the product by UV-visible absorption spectroscopy was able to put upper limits of 0.4 percent on Cl_2O, 0.8 percent on NO_2 and 0.07 percent on OClO impurities. An attempt to prepare $ClONO_2$ by the same method employed by Chang et al.[38] was abandoned after the ClF (supplied by the same supplier, Ozark Mahoning) was found to have sizable OClO impurities. Both OClO and Cl_2O are virtually impossible to separate from $ClONO_2$ without loss of a large fraction of the sample due to the parallel and very close vapor pressures of the three constituents. NO_2, Cl_2, and N_2O_5 are easily removed by vacuum distillation.

These impurity levels are important due to the somewhat broad band photolysis sources used in the Change and Adler-Golden experiments. The Xenon arc lamp filtered by a Corning 7-54 filtter used by Chang et al.[38] had a band width from 260-380 nm. Their deconvolution of the lamp intensity, filter transmission, and $ClONO_2$ absorption profiles showed that 50 percent of the photons absorbed have wavelengths below 300 nm. The unfiltered Xe flash lamp used by Adler-Golden and Weisenfeld[39] was characterized as having an emission profile of a 6500K blackbody, extending from 200 nm into the infrared, with a 20 μs pulse width. Chlorine monoxide, OClO and NO_2 are all potential O atom sources with strong absorption cross sections relative to $ClONO_2$ in the 250-400 nm range. Both Cl_2 and Cl_2O are good Cl atom sources with similar photolysis characteristics. Photolysis of any of these impurities could give the signals seen in these two experiments. Compounding this problem is the probable existance of two somewhat overlapping absorption continua in the range 300 to 350 nm as noted by Molia and Molina.[57] It is possible that these absorptions lead to different product channels.

A second problem with these experiments may be photolysis of the primary products of (11) to produce secondary products which are then detected. This could be particularly true for the results of Adler-Golden and Weisenfeld[37] where the unfiltered flash lamp may photolyse NO_3 to secondary products NO_2 + O. Their results show a linear dependence with photolysis energy for O atom production, from which they conclude that little secondary photolysis (which they claim would give a second order dependence for O atom appearance) occurs. This

conclusion is only true for small amounts of NO_3 photolysis. The rate of O atom production in this system is given by

$$\frac{d[O]}{dt} = j_1 [ClONO_2] (1-e^{-j_2 t}) \tag{60}$$

where j_1 and j_2 are the respective rates of $ClONO_2$ and NO_3 photolysis during the photolysis pulse. If j_2 is small, then $[o]_{pulse}$ is given by

$$[o]_{pulse} = \frac{j_1 j_2}{2} [ClONO_2] \tau^2_{pulse} \tag{61}$$

in agreement with their conclusions. However, if j_2 is large then (60) gives

$$[o]_{pulse} = j_1 [ClONO_2] \tau_{pulse} \tag{62}$$

which is linear with photolysis energy. While they claim less than 5 percent photolysis of NO_3, no photolysis energies were provided to substantiate this. This problem was avoided to a large extent by Chang et al. who filtered out radiation above 380 nm. Nitrate radical absorption cross sections in their photolysis region are small or non-existent.

The experiments performed in the study have the advantage of a short pulse width and well defined photolysis wavelength. The NO_3 product detected in these experiments is extremely unlikely as a result of secondary photolysis or from photolysis of any impurity present.

Its appearance was observed within 2μs following the photolysis pulse, thus it could not be the product of any chemical reaction with $ClONO_2$ (the most likely possibility) unless the rate constant for that process was greater than ~5 x 10^{-10} cm^3 $molecule^{-1}s^{-1}$. The only really puzzling aspect of the experiment is why the observed NO_3 quantum yield is 0.55 and not one. This result is in good agreement with that reported by Chang et al. of 0.5 ± 0.3 for NO_3 and 1.0 for Cl, suggesting channel (11b) as predominant. This low NO_3 quantum yield reported in both experiments would seem to suggest that this is not an experimental artifact.

One possible explanation which may explain the results of all experiments is the existence of two alternate reaction channels:

$$ClONO_2 + h\nu \longrightarrow Cl + NO + O_2 \qquad \lambda \leq 652 \text{ nm} \qquad (11e)$$

$$\longrightarrow Cl + NO_2 + O \qquad \lambda \leq 318 \text{ nm} \qquad (11f)$$

both of which are accessible using the wavelengths employed in these studies. If these two channels were operating in conjunction with (11b), then the diminished yield of NO_3 and the appearance of O atoms would be consistant with a Cl atom yield of one. However, this does not account for the inability of Adler-Golden and Weisenfeld[39] to see Cl atoms in their system. One possible explanation for this may be the presence of a fast Cl atom scavenger, such as OClO or Cl_2O, ($k(OClO) = 1.4 \times 10^{-10}$, $k(Cl_2O) = 9.8 \times 10^{-11}$ cm^3 $molecule^{-1}s^{-1}$) as an impurity. Since data was not recorded until 200μs following the

photolysis pulse in these experiments, it could be that Cl atoms were consumed before they could be detected.

The "slow" secondary rise of NO_3 noted in these experiments is also somewhat unexpected given the Cl atom scavenger present. One possible explanation of this may be a secondary reaction of O atoms (from a small O atom photolysis channel) with $ClONO_2$ to produce NO_3. These atoms would not react with CH_4. Another explanation may be the reaction of CH_3 radicals, produced in the Cl+ CH_4 reaction, with $ClONO_2$. A third, and perhaps more likely, possibility may be that not all of the NO_3 produced is born in ground vibrational states but rather in states having low absorption cross sections for the monitoring radiation. As the NO_3 is collisionally quenched to states having higher absorption cross sections, the apparent NO_3 concentration increases resulting in a signal like the one seen here. The magnitude of this secondary rise was always less than 20 percent of the initial production. The amount of excess energy available from photolysis (~26,000 cm^{-1}) makes it likely that some of this energy winds up in internal modes of NO_3.

It is difficult to critically evaluate the results of Smith, Chou and Rowland[37] due to the lack of experimental detail reported and the indirect method used to obtain the results. Their analysis hinges upon the existence of a fast heterogeneous reaction between HCl and $ClONO_2$. I cannot explain their results unless other unrecognized reactions interfered with their anticipated reaction sequence.

While the results reported here and those of Chang et al.[38] agree very well, I cannot definitively reconcile the differenes between these

results and those of Adler-Goldman and Weisenfeld.[39] Perhaps if these experiments were done with a better defined photolysis source then these discrepancies could be resolved.

In summary; the results reported here would indicate an NO_3 quantum yiled of $0.55^{+0.3}_{-0.1}$ (2σ). These results agree with those reported by Change et al.[38] and Nelson[31] but appear to disagree with rose of Smith, Chan, and Rowland[37] and Adler-Golden and Weisenfeld.[39] The major product channel appears to be

$$ClONO_2 + h\nu \longrightarrow Cl + NO_3 \quad . \tag{11b}$$

E. NO_3 Absorption Cross Sections and Lineshape

Ramsay[42] photographed the NO_3 spectrum between 665 and 500 nm using a Hilger E 1 spectrograph with glass optics. The NO_3 was prepared by mixing NO_2 and O_3, and the optical path length was several meters. Quantitative results were presented as the reproduction of a photographic plate with calibration lines from an iron hollow-cathode lamp superimposed on about 20 absorption bands. The locations of absorption bands are marked along the photographic plate, and the vacuum wavenumbers are printed with these marks. The resolution of this spectrograph appeared to be about one cm^{-1}. Also, Ramsay examined the NO_3 absorption bands at much higher resolution with a 21 foot concave grating instrument. These results were not presented, but it was stated that all the NO_3 bands were diffuse at this high resolution. By comparison with results that Ramsay has

obtained using the 21 foot grating instrument on other molecules,[87] its resolution appears to be about 0.001 nm.

For comparison with these results, Ramsay's vacuum frequencies are converted to those for one atmosphere air by adding 4 cm^{-1} to his values. Ramsay interpreted one progression as the symmetric stretching vibration in the excited electronic state. The 0–0 transition is the high intensity absorption presented in Fig. 40. Ramsay tentatively made the following assigments

Transition	ν cm^{-1}	$\Delta\nu$	$\Delta\Delta\nu$
0–0	15093		
		950	
1←0	16043		24
		926	
2←0	16969		5
		921	
3←0	17890		

This study observed the first two transitions, Fig. 43, but the results differ somewhat

Transition	ν	$\Delta\nu$
0–0	15109	
		935
1←0	16044	

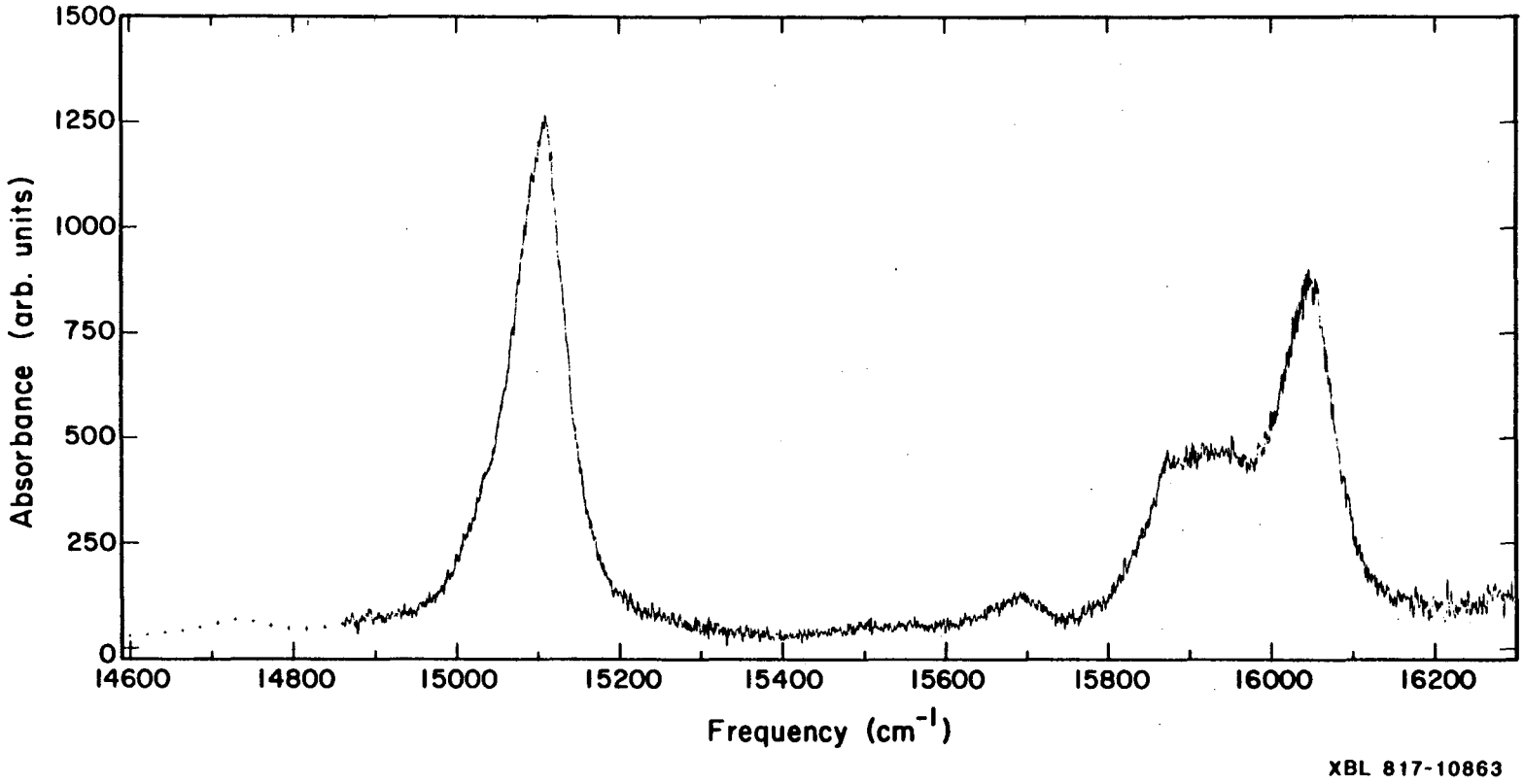

Figure 43. Relative absorption spectrum of NO_3 from 14900 cm^{-1} to 16200 cm^{-1} as observed here; + weak, presumably, hot band from Ref. 49.

Ramsay described his results as preliminary, and full details were not given. One possibility will be given here whereby the wavenumber of Ramsay's peak might be systematically low. The spectrographic plate for the 0–0 band showed a darkening due to NO_3 absorption that appears under a low-power microscope to be about 65 cm^{-1} wide, and the peak is accurately marked at the halfway point of the darkening. However, as can be seen from Fig. 40, the peak is not symmetrical; and the peak should not be centered in the opaque region of the photographic plate but displaced to higher energies. It is difficult to estimate how large this effect might be.

For the symmetric-stretch progression, Ramsay found successive $\Delta\nu$'s to be 950, 926, and 921 cm^{-1},, and the second differences are 24 and 5 cm^{-1}. Usually vibrational modes do not show such a large anharmonicity among the first four vibrational states. If Ramsay's peak of the 0–0 band is increased by 16 cm^{-1} to agree with the peak frequency found here, the successive $\Delta\nu$'s would be 934, 926, and 921 cm^{-1}, and the second differences would be 8 and 5 cm^{-1}, which seem more reasonable than the reported values.

Using a 21 foot grating spectrograph, Ramsay found all the NO_3 bands to be diffuse, which he interpreted as pre-disassociation. In this study, the width of the single mode laser appears to be about three-fold more narrow than the resolution of Ramsay's 21 foot grating. At this higher resolution, there is still no evidence of fine structure in the NO_3 spectrum, Fig. 42, and this study confirms and extends Ramsay's finding that the NO_3 spectrum is diffuse.

Ramsay did not determine absorption cross sections in his study. However, there are three other quantitative studies of the absorption cross section spectra of NO_3. One of these[43] depends on use of rate constants and equilibrium constant (K, k_{14}, k_{15}) to evaluate the concentration of NO_3, and two of these studies were direct, absolute methods.[44,45]

(1) Johnston and Graham[43] determined the absorption spectrum in a flowing system of N_2O_5 and O_3, measured the spectrum with a one-third meter (McPherson Model 218) monochrometer, and calculated the concentration of NO_3 from K, k_{14} and k_{15} on the basis of kinetic data obtained in the 1930's and 1950's. The article gives the experimental conditions used so that the NO_3 concentration can be recalculated using recent[44] values of K, k_{14} and K_{15}. The calculated concentrations of NO_3 is lowered by a factor of 3.68, and the published cross sections should be increased by the same factor. The concentration of nitric acid was not measured during the experiments, but it was noted that about 15 percent of the N_2O_5 was converted to HNO_3. This experiment is very similar in method to the present study except for the use of 1/3 meter monochromator then and use of a tunable laser here.

(2) Graham and Johnston[44] measured the NO_3 spectrum by a direct absolute method, and the results are negligibly dependent on values of rate constants. In a steady flowing system of N_2O_5 and O_3, NO_3 was photolyzed by on-off fluorescent light bulbs of green or gold color. The change in visible NO_3 absorption was measured at the flat topped peak at 627.0 nm. The associated change of N_2O_5 was

measured by infrared absorption at 8.028 μm, using an easily converted VIS/IR molecular modulation apparatus.[49] As the photolysis lamp flashed on-and-off, the molecular modulation of NO_3 and N_2O_5 were repeatedly, alternately measured. In this system, N_2O_5 and NO_3 are strongly coupled by reactions k_{12}, k_{13}, k_{14} and k_{15} and the situation may be abbreviated as

$$N_2O_5 \underset{k_{15}}{\overset{k_{12}}{\rightleftharpoons}} 2NO_3 \quad (k_{14}[O_3])$$

To a first approximation the stoichiometric factor between N_2O_5 and NO_3 is 2.00. However, as NO_3 is photolyzed to yield NO + O_2 or NO_2 + O, there are some secondary reactions involving NO and O. The system was computer modeled by a complete set of reactions, and these secondary reactions were found to have only a minor effect on the stoichiometric factor of two. The absolute cross section of NO_3 at 627.00 nm was measured at 24 different conditions: with varied O_2 (0.5 to 99 percent), O_3 (3.5 to 10.5 x 10^{15} molecules cm^{-3}), N_2O_5 (3.1 to 13.9 x 10^{14} molecules cm^{-3}), two reaction cells of different surface to volume ratios and two photolysis lamps (green or gold). The average stoichiometric factor was 2.07, the maximum value was 2.16. These data were reported[44] as the average cross section over 1 nm band width; for a nominal wavelength of 627, for example, the average reported is between 626 and 627 nm. This spectrum is presented as a bar graph, curve B, in Fig. 40. Graham[49] reported the maximum σ at 662.2 nm, and this point is indicated by the triangle in Fig. 40.

(3) Mitchell et al.[45] also determined the NO_3 absorption spectrum by a direct absolute method. By considering the rates of reactions, k_{12}, k_{13}, k_{14}, k_{15} and others, they found experimental conditions were essentially all NO_x (NO, NO_2, NO_3, N_2O_5) in the system would be in the form of NO_3. Thus, the measured NO_2 input was equal to NO_3 in the system. The required experimental conditions where that NO_x should be less than 10^{12} molecules cm^{-3} and ozone should be 5×10^{17} molecules cm^{-3} or more. These conditions yield an optical density ($\ln I_0/I$) for NO_3 of 3×10^{-4} in the 25 cm cell, and the superimposed optical density of O_3 at 662 nm is 2.5×10^{-2} or about 80-fold greater than that for NO_3. By a carefully designed double beam detector, they were able to overcome much of the difficulty posed by the weak NO_3 signal and the large overlapping O_3 signal. Their relative cross sections as a function of wavelength were tabulated in a laboratory publication,[19] these values were scaled by us to the published[45] value of 121×10^{-19} cm^2 $molecule^{-1}$ at the maximum, and their absorption spectrum of the strong peak around 662 nm is plotted as curve C in Fig. 40.

The four determinatons of the NO_3 absorption spectrum are compared in Table 33 in terms of 3 quantities: the value of the cross section at the peak at 662 nm, the ratio of peak cross section at 662 nm to that at 627 nm, and the integrated absorption spectrum over the range of Fig. 40.

$$I = \int_{14910}^{15290} \sigma d(1/\lambda) \qquad (63)$$

Table 33. Comparison of features of NO_3 absorption spectrum as found by different investigations.

Investigator	$\frac{\sigma_{max}}{10^{-19}\ cm^2}$ 662 nm	$\frac{\sigma(662)}{\sigma(627)}$	$\frac{I}{10^{-15}\ cm}$ Eq.(6)	Ref.
Johnston and Graham[a] (1974)	148	2.61	1.83	43
Graham and Johnston (1978)	186	2.65	1.99	44,49
Mitchell et al. (1980)	121	1.59	2.06	45
This work (ave)	161	2.61	1.73	

[a] corrected using current (ref. 44) values of K, k_{14} and k_{15}.

ratio is 1.6. The other three studies agree with each other, 2.61, 2.65, and 2.61, but disagree with Mitchell et al. From the shape of the three spectra in Fig. 40 and from these ratios, it appears that Mitchell et al. were correct in judging "that the breadth of our peaks is a result of the actual monochromator resolution being appreciably greater than that calculated." (Our experience with that model monochromator, Bausch and Lomb 33-86-79, shows that it has a large amount of scattered light that tends to degrade is resolution.)

It appears that the present study gives the best determination yet reported of the shape of the strong NO_3 absorption spectrum around 662 nm, but the absolute absorption is best obtained from the integrated absorption spectra of Graham and Johnston[44] or Mitchell et al.[45] Their two results are averaged to give an integrated absorption of 202×10^{-19} cm molecule^{-1} between 14910 cm^{-1} and 15290 cm^{-1}, and the average of the 12 curves observed here was scaled to give the same integrated absorption curve. These data are given for every 0.2 nm between 649 and 672 nm in Table 34. For spectroscopic studies of NO_3 in the atmosphere, these data are probably the best currently available. For photochemical models, the NO_3 cross sections integrated over 1 nm bands as given by Graham and Johnston are probably the most convenient form of the data.

Magnotta and Johnston[88] studied the wavelength-dependent quantum yileds for two channels of NO_3 photolysis, $NO_2 + O$ or $NO + O_2$. Using literature values for K and Graham and Johnston's values for σ, their results indicated a primary quantum yield of about 1.5 at 580 nm, which, of course, is impossible. They gave four, different, possible

Table 34. Average NO_3 cross sections in units of 10^{-19} cm^2 as measured here and scaled to give same integrated absorption between 14910 and 15290 cm^{-1} as those obtained from curves B and C in Fig. 40.

	0.0	0.2	0.4	0.6	0.8
648.					5.7
649.	3.7	5.7	4.3	4.8	3.4
650	3.5	4.7	4.1	3.9	4.5
651	5.1	4.9	5.1	5.3	6.7
562.	5.8	5.4	5.9	5.5	6.8
653	5.5	7.7	7.3	5.9	8.5
654.	7.1	7.5	8.4	7.9	8.3
655.	8.7	9.6	9.6	11.3	12.5
656.	11.4	12.2	11.8	12.4	12.7
657.	14.0	14.6	16.4	17.9	19.3
658.	19.4	20.6	23.7	25.7	27.9
659.	32.9	39.1	43.9	48.0	56.4
660.	65.4	75.6	86.2	106.7	119.6
661.	136.8	150.0	164.0	181.5	189.6
662.	185.5	178.7	171.9	166.8	154.0
663.	144.1	132.5	121.5	113.8	99.8
664.	93.2	86.0	78.2	70.9	66.5
665.	61.3	60.1	53.8	49.4	44.6
666.	42.2	39.6	35.0	31.7	27.9
667.	23.8	23.2	22.0	19.9	17.1
668.	16.2	16.7	14.5	14.4	12.7
669.	12.3	12.3	11.8	11.7	11.1
670.	10.4	11.6	11.1	9.1	9.1
671.	9.6	8.6	11.7	10.5	9.6
672	8.9	8.6	11.4	8.0	8.0

explanations for this apparent high quantum yield. One of these was that the cross section for NO_3 should be increased by about 50 percent. In view of the excellent agreement for the two absolute determinations of the integrated absorption spectrum,[44,45] it appears unlikely that their anomalous quantum yield is due to incorrect NO_3 cross sections. Some of their discrepancy could be explained by K being larger than the literature value, which is consistent with the low integrated absorptions observed here and in Ref. 43.

Our inability to observe fluorescence following excitation of any portion of the photochemically inactive region of the spectrum would suggest some fast internal conversion process to non-radiative or easily quenched states. Olsen and Burnelle[89] have estimated an oscillator strength for the transition (f = 0.013) from which a radiative lifetime of approximately 500 ns may be calculated. If this estimate of the lifetime is accurate, then strong visible fluorescence is expected under the experimental conditions employed.

A close examination of the band head shows that it appears to be a slightly distorted Lorentzian function, perhaps composed of two overlapping envelopes. We have been able to fit it (Fig. 45) to a pair of Lorentzian functions centered at 15066 cm^{-1} and 15109 cm^{-1} with linewidths (FWHM) of approximatey 96 cm^{-1} and 60 cm^{-1}, respectively. This finding is somewhat similar to that of Reddy, Bray, and Berry[91] who studied high vibrational overtone spectra in benzene. They found that many of the overtone bands assume Lorentzian lineshapes on the order of 80 cm^{-1} to 120 cm^{-1} linewidth. They attributed this to a coupling of the excited discrete states with the quasi-continuum of

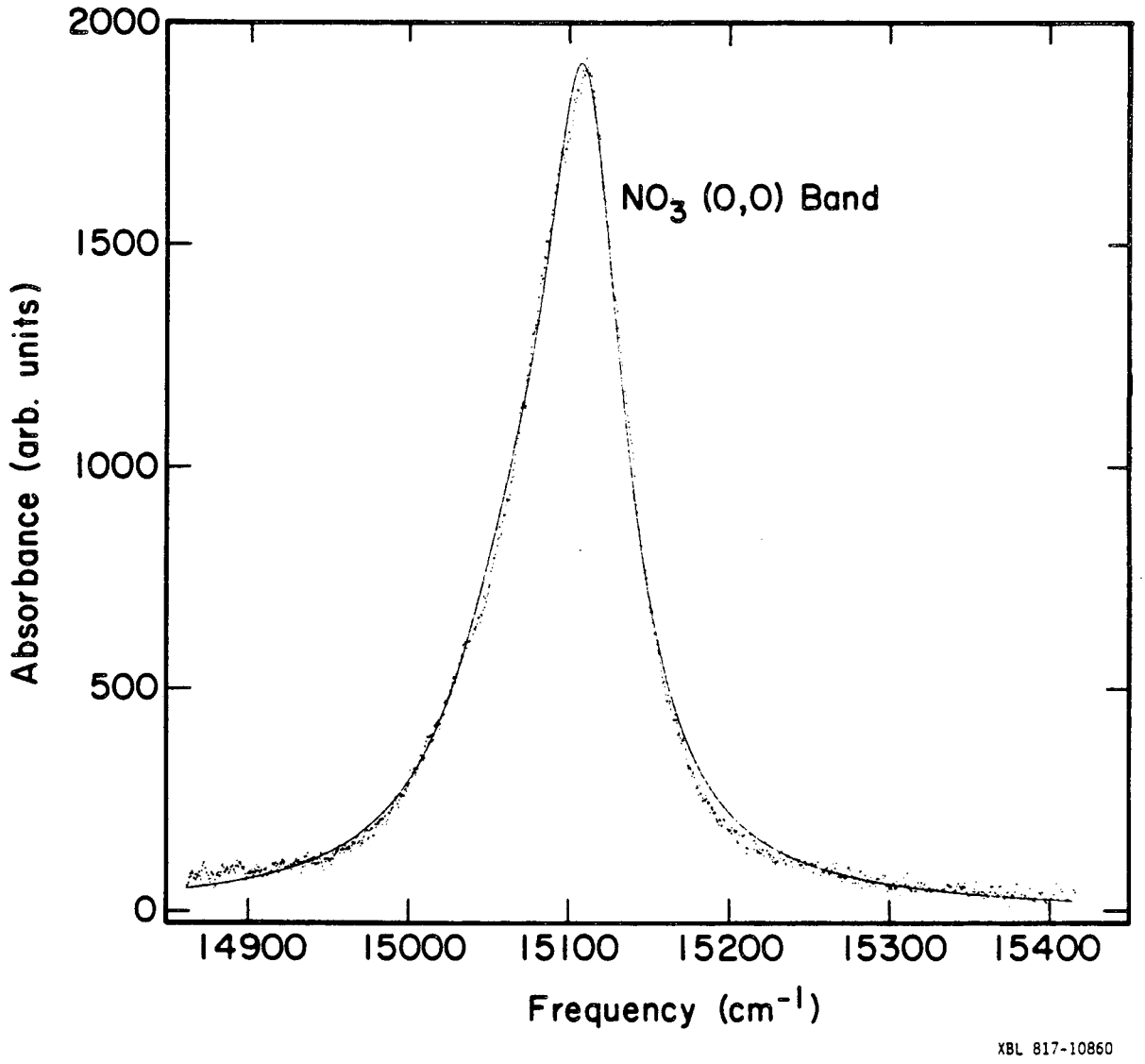

Figure 44. Average observed spectrum of the NO_3 (0,0) band, dots, and fitted line based on two superimposed Lorentzian functions.

background states available to produce an embedded state with a Lorentzian lineshape.

Coupling of discrete absorption to either metastable or ground state manifolds has been used by Douglas[91] to explain anomalously long radiative lifetimes for NO_2, SO_2 and CS_2. Radiationless transitions of this type have been discussed in an excellent review by Freed[92] and is illustrated in Fig. 45. The two parallel manifolds S° amd S' depict the excited and ground states. The transition $\phi_i^\circ - \phi_f^\circ$ in the S° manifold with dipole operator μ_{if}° is the only significant transition. After undergoing the transition $\langle \phi_f^\circ | \mu_{if}^\circ | \phi_i^\circ \rangle$ a molecule in state ϕ_f^o can either fluoresce or curve cross to isoenergetic levels ϕ_f' in the S' manifold due to higher order coupling between the two systems. The wavefunctions ψ_m corresponding to mixing of states ϕ_f° and ϕ_f' contain little ϕ_f° character due to the relative density of states and hence carry little oscillator strength relative to ϕ_f°. As long as the levels ϕ_f' are finite in number and external perturbations are negligable, the excitation energy may be multiply exchanged between the manifolds with an eventual fluorescence yield from ϕ_f^o of close to one. The levels ϕ_f' are metastable with respect to low vibrational levels of the ground state and are weak infrared radiators.

Jones, Zewail and Diestler[93] have treated this effect theoretically and showed that, for molecules where the width of the absorption lines is narrow compared to the separations between them and in the absence of collisions, a Lorentzian lineshape is expected with

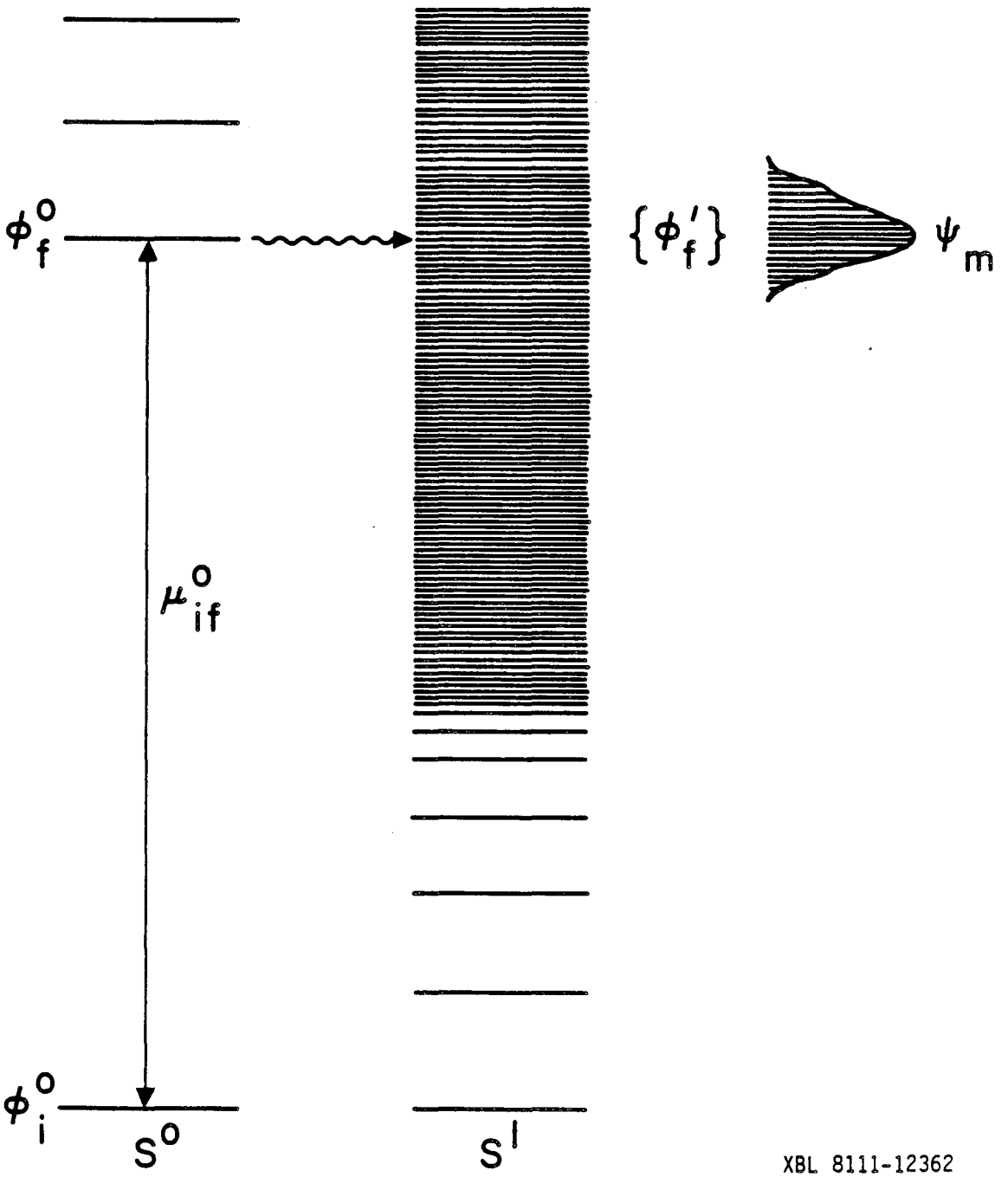

Figure 45. Schematic diagram of possible intramolecular energy transfer mechanism from NO_3 (0,0) band.

the inverse of the linewidth giving the lifetime of the discrete state. If the density of states is high or intermolecular processes are important, the line is inhomogeneously broadened, and the interpretation of the linewidth becomes less straightforward. In systems where the collisional decay times are less than or equal to the recurrence time for resonant transfer back to the excited state manifold, decay into the quasicontinuum is irreversible and the fluorescence yield is diminished.

A similar scheme can be constructed for NO_3 involving curve crossing from the excited electronic state to high vibrational evels of the ground state. The complications of curve crossing, collisions, and possibly a high density of states in the excited manifold may explain why a Lorentzian function is not observed. The linewidth observed here would indicate a lifetime of approximately 2 picoseconds for relaxation to the quasi-continuum in contrast to a lifetime of 500 ns for radiation of the excitation energy. The ratio of relaxation to radiation rates is approximately 2.5×10^5, and in this case little visible emission is expected. The relative density of states would favor maintaining the excitation energy in the quasi-continuum from which energy is lost primarily through quenching and infrared emission. Little or no fluorescence would be expected in the visible region and the apparent radiative lifetime is much longer than that calculated on the basis of the oscillator strength.

ACKNOWLEDGEMENTS

The successful conclusion of my graduate work at Berkeley would not have been possible without the help and support of many individuals. The guidance and encouragement provided by Professor Harold Johnston was deeply appreciated. His manner of direction allowed me a free hand in determining the course of my research and broadened the scope of my professional development.

The free exchange of scientific ideas and information as well as friendship provided by my fellow graduate students could not be more appreicated. Special thanks goes to Herb Nelson and Jim Podolske who introduced me to the laboratory and with whom I worked closely. Frank Magnotta and Herb were major contributors in the development of parts of the experimental apparatus while Jim was indispensable as group computer and electronics wizard. Peter Connell, John Girman and David Littlejohn were always available for discussions of science and life in general.

The support provided by the technical staff could not be surpassed. The help of Fred, Andy, Bob, Chuck, and George in the machine shop and especially Tom in the glass shop was always timely, patient and informative. These men were friends as well as co-workers.

The support and understanding of my wife, Karen, cannot be adequately described. When the work was the hardest, she often did much more than could be expected of most wives.

Finally, I would like to thank the Lawrence Berkeley Laboratories and the U.S. Department of Energy who provided the bountiful support for this work through the Materials and Molecular Research Division

under Contract No. W-7405-ENG-48. A testimonial is also due the San Francisco Laser Center which is supported by the National Science Foundation under Grant No. CHE79-16250 jointly awarded to the University of California, Berkeley and Stanford University. Innovative centers of this type promote broadening of scientific inquiry while minimizing costs and I feel their present success justifies their continued support.

APPENDIX A: Verification of Sweep Times for the Fabritek and Biomation Signal Averagers

Calibration of both devices was accomplished by setting up known pulse trains from a TTL pulse/delay generator verified by a calibrated Tektronics Model 464 oscilloscope. These pulse trains were fed into the device and the resulting sweeps compared with oscilloscope traces.

Fabritek 1074

A train of 10 ns pulses at 10 kHz was set up and the frequency was measured as 9952 Hz with a Heathkit frequency counter. This pulse train was sent into the signal averager and scanned 8192 times for each sweep speed. From the measured vs calculated counts recorded per channel, the channel "dead time" may be determined. These results are shown in the following Table 35.

Table 35. Fabritek 1074, Dead Time Measurements

Channel Width (μs)	Counts/Channel (calculated)	Counts/Channel (observed)	Δ Counts	Dead Time (μs)
1	81.5	76.6	5.9	72.4
2	163.1	156.9	6.2	76.0
5	407.6	404.3	3.3	40.5
10	815.6	809.3	6.0	73.6
20	1645.0	1637.7	7.2	88.2

The average dead time is 70.1 ns which is 7 percent at 1 μs channel width, however, at the minimum channel width of 5 μs used in these experiments this is only 1.4 percent.

A second test involved using the synchronous pulse of the pulse generator to trigger the signal averager and setting the 10 ms delay pulse to occur 750 channels into the sweep with the oscilloscope. This experiment is summarized in Table 36.

Table 36. Fabritek 1074 Sweep Time Calibrations

Channel Width	Measured Delay Pulse Channel
1	758
2	745
5	744
10	752
20	746

These results are well within the ability to set the delay using the oscillosocpe.

Biomation 805

Biomation 805 sweep times were calibrated in a simlar manner to the Fabritek 1074. The delay was set at 800 channels and the pulse width at 100 channels. These results are shown in Table 37.

Table 37. Biomation 805 Sweep Time Calibration

Channel Width (us)	Measured Delay Pulse Channel	Measured Pulse Width
2	813	101
5	809	103
10	810	102

These results are also well within the ability to set these time periods and show no significant error.

APPENDIX B. Corrections to Observed Rate Constants for Reaction of HO with NO_2.

The study of the reaction of HO with HNO_3

$$HO + HNO_3 \longrightarrow H_2O + NO_3 \qquad (2)$$

is complicated by the side reaction of HO radicals with NO_2

$$HO + NO_2 + M \longrightarrow HNO_3 + M \quad . \qquad (9)$$

Since the NO_2 impurity in the HNO_3 scales with the amount of HNO_3 used, the contribution of (9) to the measured first order rate constant is not separable using first order plots. To factor out the contribution of this reaction to the total rate, one must measure the amount of NO_2 impurity and, using accepted rate constants for reaction (9), calculate a first order rate constant to be subtracted from the total rate. The HNO_3 samples used in the FP/RF experiments had less than 0.05 percent NO_2 which, at the pressures used in those experiments, contributes negligably to the measured rate constants even at the lowest temperatures employed. The HNO_3 FP/LA experiments used a HNO_3 sample containing 0.15 percent NO_2, which does result in some contribution to the rate, especially at atmospheric pressures.

The third order rate constant for reaction (9) is calculated from the tabulated data of DeMore et al.[6] The rate constants are given in the form

$$k_o(T) = k_o^{300} (T/300)^{-n} \text{ cm}^6 \text{ molecule}^{-2} \quad (64)$$

with the specified values of k_o^{300} and n tabulated. Where pressure fall-off corrections are necessary, the limiting high pressure rate constant is given in a similar form

$$k_\infty(T) = k_\infty^{300} (T/300)^{-m} \text{ cm}^3\text{molecule}^{-1} \quad (65)$$

To obtain the effective second-order rate constant for a given condition of temperature and pressure the formula

$$k(M,T) = \left(\frac{k_o(T)[M]}{1+k_o(T)[M]/k_\infty(T)}\right) 0.6^{\left\{1+[\log_{10}(k_o(T)[M]/k_\infty(T))]^2\right\}^{-1}} \quad (66)$$

is used. The low pressure rate constants are described by the simple method developed by Troe.[80] The low pressure data is a combination of the results of Howard and Evenson,[81] Anderson,[82] Anastasi and Smith[83] and Wine, Kreutter, and Ravishankara.[62] The high pressure limit and temperature dependence come from the RRKM model of Smith and Golden.[84] The value of these parameters are: $k_o^{300} = 2.6 \pm 0.3 \times 10^{-30}$, $n = 2.9 \pm 0.7$, $k^{300} = 2.4 \pm 1.2 \times 10^{-11}$ and $m = 1.3 \pm 1.0$. The relative efficiencies of N_2 ($\beta = 1.0$) and Ar ($\beta = 0.42$) determined by Wine et a.[62] were applied as pressure corrections to [M].

The second order rate constants for reaction (9) are given in Table 38 for each of the experimental conditions used in the FP/LA experiments. The corrected first order rate constant is given by

$$k'_{corr} = k'_{meas} - 1.5 \times 10^{-3}\, k(M,T)\, [HNO_3] \qquad (67)$$

where the factor 1.5×10^{-3} is the fraction of NO_2 present in the HNO_3.

Table 38. Second Order Rate Constants for the Reaction HO + NO_2 + M at 295K.

Pressure (Torr)	k(M,T) cm^3 $molecule^{-1}s^{-1}$) Ar	N_2
10	3.27×10^{-13}	7.27×10^{-13}
30	8.92×10^{-13}	1.85×10^{-12}
50	1.38×10^{-12}	2.71×10^{-12}
744	7.87 xz 10^{-12}	1.60×10^{-11}

REFERENCES

1. H. S. Johnston, Science 173, 517 (1971).

2. M. J. Molina and F. S. Rowland, Nature 249, 810 (1974).

3. R. D. Hudson and E. I. Reed, NASA Ref. Publ. 1049, (1979).

4. F. M. Luther, J. S. Chang, W. H. Duewer, J. E. Penner, R. L. Tarp, and D. J. Wuebbles, U. S. Depart. of Trans. FAA-EE-79-23, (1979).

5. R. P. Turco, R. C. Whitten, O. B. Toon, E. C. Y. Inn, and P. Hamill, J. Geophys. Res., 86 (1981).

6. W. B. Demore et al., Chemical Kinetic and Photochemical Data for Use in Stratospheric Modeling, Evaluation Number 4, (NASA-JPL Publication 81-3, Pasadena, CA, January 1981).

7. R. Simonaitis and J. Heicklen, J. Phys. Chem. 78, 653 (1974).

8. H. Niki, P. D. Maker, C. M. Savage and L. P. Breitenback, Chem. Phys. Lett. 45, 564 (1977).

9. J. R. Barker, P. L. Trevor, R. A. Kenley, J. Chang, J. E. Davenport and B. Y. Lan., Stratospheric Reactions of Peroxynitric Acid, (Final Report U.S. DOT Contract No. DOT-FA78WA-4228, SRI International, Menlo Park, CA, 1980).

10. K. Glanzer and J. Troe, Ber. Bunsenges. Phys. Chem. 78, 71 (1974).

11. H. S. Johnston, L. Foering, and R. J. Thompson, J. Phys. Chem. 57, 390 (1953).

12. T. S. Godfrey, E. D. Hughes, and C. Ingold, J. Chem. Soc., 1063 (1965).

13. D. Husain and R. G. W. Norrish, Proc. Royal Soc. A. 273, 165 (1963).

14. C. Morley and I.W.M. Smith, J. Chem. Soc. Faraday Trans. II 68, 1016 (1972).

15. R. Zellner and I.W.M. Smith, Chem. Phys. Lett. 26, 72 (1974).

16. I.W.M. Smith and R. Zellner, Int. J. Chem. Kinet. Symposium 1, 341 (1975).

17. J. J. Margitan, F. Kaufman and J. G. Anderson, Int. J. Chem. Kinet. Symposium 1, 281 (1975).

18. R. F. Hampson and D. Garvin, Reaction Rate and Photochemical Data for Atmospheric Chemistry, U.S. Dept. of Com.-National Bureau of Standards, Washington, D.C., 1977).

19. W. B. DeMore et al., Chemical Kinetic and Photochemical Data for Use in Atmospheric Modeling, Evaluation Number 2, (NASA-JPL Publication 79-27, Pasadena, CA, April 1979).

20. D. L. Baulch et al., Evaluated Kinetic and Photochemical Data for Atmospheric Chemistry, J. Phys. Chem. Ref. Data 9, 295 (1980).

21. P. H. Wine, A. R. Ravishankara, N. M. Kreutter, R. C. Shah, J. M. Nicovich, R. L. Thompson and D. J. Wuebbles, J. Geophys. Res. 86, 1105 (1981).

22. H. H. Nelson, W. J. Marinelli and H. S. Johnston, Chem. Phys. Lett. 78, 495 (1981).

23. I. W. M. Smith, private communication.

24. C. J. Howard, 182nd ACS National Meeting, (New York, New York, 1981).

25. J. J. Margitan, 182nd ACS National Meeting, (New York, New York, 1981).

26. N. R. Greiner, J. Phys. Chem. 72, 406 (1968).

27. W. Hack, K. Hoyermann and H. G. Wagner, Int. J. Chem. Kinet. Symposium 1, 329 (1975).

28. G. W. Harris and J. N Pitts, J. Chem. Phys. 70, 2581 (1979).

29. L. F. Keyser, J. Phys. Chem. 84, 1659 (1980).

30. U. C. Sidharan, B. Reimann and F. Kaufman, J. Chem. Phys. 73, 1286 (1980).

31. H. H. Nelson, Ph.D. Thesis, University of California, Berkeley, and Lawrence Berkeley Laboratory Report LBL 11666, 1980.

32. M. T. Leu and W. B. DeMore, Chem. Phys. Lett. 41, 121 (1976).

33. G. Poulet, G. Le Bras and J. Combourieu, J. Chem. Phys. 69, 767 (1978).

34. M. J. Kurylo and R. G. Manning, Chem. Phys. Lett. 48, 279 (1977).

35. M. S. Zahniser, J. S. CHang and F. Kaufman, J. Chem. Phys. 67, 997 (1977).

36. L. T. Molina, J. E. Spencer and M. J. Molina, Chem. Phys. Lett. 45, 158 (1977).

37. W. S. Smith, C. C. Chou and F. S. Rowland, Geophys. Res. Lett. 4, 517 (1977).

38. J. S. Chang, J. R. Barker, J. E. Davenport and D. M. Golden, Chem. Phys. Lett. 60, 385 (1979).

39. S M. Adler-Golden and J. R. Wiesenfeld, Chen. Phys. Lett. 82, 281 (1981).

40. E. J. Jones and O. R. Wolf, J. Chem. Phys. 5, 873 (1937).

41. G. Schott and N. Davidson, J. Am. Chem. Soc. 80, 1841 (1958).

42. D. A. Ramsay, Proc. Colloq. Spectroscopy Int., 10th 583 (1962).

43. H. S. Johnston and R. A. Graham, Can. J. Chem. 52, 1415 (1974).

44. R. A. Grahan and H. S. Johnston, J. Phys. Chem. 82, 254 (1978).

45. D. N. Mitchel, R. P. Wayne, P. J. Allen, R. P. Harrison and R. J. Twin, J.C.S. Faraday II 76, 785 (1980).

46. A. D. Walsh, J. Chem. Soc., 2306 (1953).

47. F. Magnotta, Ph.D. Thesis, University of California, Berkeley, and Lawrence Berkeley Laboratory Report LBL-9981, 1979.

48. F. Magnotta and W. J. Marinelli, unpublished results.

49. R. A. Graham, Ph.D. Thesis, University of California, Berkeley, 1975.

50. R.G.W. Norrish and G. Porter, Nature 164, 568 (1949).

51. A. M. Bass, A. E. Ledford and a. H. Laufer, J. Res. Natl. Bur. Stand. 80A, 143 (1976).

52. M. O. Rodgers, K. Asai and D. D. Davis, Appl. Opt. 19, 3597 (1980).

53. J. P. Reilly, J. H. Clark, C B. Moore and G. C. Pimentel, J. Chem. Phys. 69, 4381 (1978).

54. K. Schofield, J. Quant. Spectrosc. Radiat. Trans. 17, 13 (1977).

55. J. G. Calvert and J. N. Pitts, Photochemistry (John Wiley and Sons, New York, 1966).

56. L. T. Molina and M. J. Molina, U.S. Dept. of Transportation Report FAA-EE-80-07, 1980.

57. L. T. Molina and M. J. Molina, J. Photochem 11, 139 (1979).

58. C. L. Lin, J. Chem. Eng. Data 21, 411 (1976).

59. R. T. Watson to F. Magnotta, private communication.

60. M.A.A. Clyne and H. W. Cruse, J. Chem. Soc. Farad Trans. II 68, 1281 (1972).

61. H. S. Johnston, S. G. Chang and G. Whitten, J. Phys. Chem. 78, 1 (1974).

62. P. H. Wine, N. M. Kreutter and A. R. Ravishankara, J. Phys. Chem. 83, 3191 (1979).

63. G. B. Kristiakowsky, J. Am. Chem. Soc. 52, 102 (1930).

64. N. M. Ballash and D. A. Armstrong, Spectrochim, Acta 30A, 941 (1974).

65. F. Paschen, Ann. Phys. 40, 27 (1919).

66. E. F. Zalewski, R. A. Keller and R. Engleman, J. Chem. Phys. 70, 1015 (1979).

67. K. C. Smyth, R. A. Keller and F. F. Crim, Chem. Phys. Lett. 55, 473 (1978).

68. D. S. King, P K. Schenk, K. C. Smyth and J. C. Travis, Appl. Opt. 16, 2617 (1977).

69. E. Vigroux, Ann. Phys. 8, 709 (1953).

70. L. T. Molina, S. D. Schinke, and M. J. Molina, Geophys. Res. Lett. 4, 580 (1977).

71. G. H. Cady, Inorg. Syn. 5, 156 (1957).

72. M. Schmeisser, Inorg. Syn. 9, 127 (1967).

73. J. V. White, J. Opt. Soc. Am. 32, 285 (1942).

74. P. R. Bevington, Data Reduction and Error Analysis for the Physical Sciences (McGraw-Hill, New York, 1969) Chapt. 9.

75. M. Braun, Differential Equations and Their Applications, (Springer-Verlag, New York, 1975), Chapt. 1.

76. G. Golub, V. Pereyra, and J. Bolsted, VARPRO: A Package for Weighted Least Squares Fitting to Data (Computer Science Dept., Stanford University, Palo Alto, CA, 1976).

77. K. Schofield, J. Phys. Chem. Ref. Data 8, 743 (1979).

78. G. Z Whitten and J. P. Meyer, CHEMK: A Computer Modeling Scheme for Chemical Kinetics (Systems Applications, Inc., 1979).

79. C. J. Howard and K. M. Evenson, Geophys. Res. Lett. 4, 437 (1977).

80. J. Troe, J. Chem. Phys. 66, 4745 (1977).

81. C. J. Howard and K. M. Evenson, J. Chem. Phys. 61, 1943 (1974).

82. J. G. Anderson, J. J. Margitan, and F. Kaufman, J. Chem. Phys. 60, 3310 (1974).

83. C. Anastasi and I.W.M. Smith, J. Chem. Soc. Faraday II 72, 1459 (1976).

84. G. P. Smith and D. M. Golden, Int. J. Chem. Kinet. 10, 489 (1978).

85. F. Biaume, J. Photochem. 2, 139 (1973/74).

86. W. J. Moore, Physical Chemistry (Prentice Hall, Englewood Cliffs, N.J., 1972).

87. K. Dressler and D. A. Ramsay, Philos. Trans. Roy. Soc. Lond. A251, 553 (1959).

88. F. Magnotta and H. S. Johnston, Geophys. Res. Lett. 7, 769 (1980).

89. J. F. Olsen and L. Burnelle, J. Am. Chem. Soc. 92, 3659 (1970).

90. K. V. Reddy, R. G. Bray and M. J. Berry, Advances in Laser Chemistry, (Springer Series in Chemical Physics Vol. 3, Springer-Verlag, New York, 1978), pp. 48-61.

91. A. E. Douglas, J. Chem. Phys. 45, 1007 (1966).

92. K. F. Freed, Accts. Chem. Res. 11, 74 (1978).

93. K. E. Jones, A. H. Zewail and D. J. Diestler, Advances in Laser Chemistry (Springer Series in Chemical Physics Vol. 3, Springer-Verlag, New York, 1978), pp. 258-270.

TECHNICAL INFORMATION DEPARTMENT
LAWRENCE BERKELEY LABORATORY
UNIVERSITY OF CALIFORNIA
BERKELEY, CALIFORNIA 94720